EFFICIENT COLLECTION AND STORAGE OF SOLAR ENERGY

By

Eng. ADEL ALY AHMED GHONEIM

A thesis Submitted for the degree of

Doctor Of Philosophy

In

Engineering Physics

at the

FACULTY OF ENGINEERING

UNIVERSITY OF ALEXANDRIA

1989

ABSTRACT

Since solar energy is available only during daylight hours of a certain periods of the year, a means of providing heat on a continuous bases from this intermittent source is required. This can be done by storing energy during daylight hours for later use. Energy storage provides a useful means of improving solar system performance. In this thesis, detailed theoretical models have been developed for both sensible and phase-change energy storage units. The present detailed models took all the assumptions made in earlier studies into account.

The transient simulation program (TRNSYS) developed at Solar Energy Laboratory, University of Wisconsin-Madison was used to determine the performance of the solar heating systems. A comparison was made between the solar system performance obtained using the present detailed models and the corresponding performance obtained using the assumptions made in earlier studies for both air and water-based active solar heating systems. The effects of varying the melting temperature and latent heat of the phase-change materials on the performance of air-based solar active heating systems were also examined. These effects were studied for different locations and different heating season months.

A sensible energy storage material called 'Abu-Siebera clay', which is found in Abu-Siebera, Egypt was investigated to test its performance as a sensible store medium. The thermal properties of this material were measured experimentally in the Faculty of

Engineering, University of Alexandria. The transient probe method was used to measure the thermal properties of the material. The performance of solar heating systems with Abu-Siebera clay using the weather data of Alexandria, Egypt was compared to the corresponding performance obtained with pebble bed energy storage. Also, the effects of varying system parameters were examined.

TRNSYS requires a high computer cost, and a lot of experience. An interesting alternative to the use of TRNSYS is the f-chart design method. The reliability of the f-chart design method in the Egyptian climate was investigated by comparing the performance of solar domestic hot water system (SDHW) obtained using f-chart design method and the corresponding performance obtained using TRNSYS.

Lastly, the performance of phase-change materials (PCMs) as a collector-storage walls was investigated. A comparison was made between the performance of collector-storage walls using PCMs and the corresponding performance with the sensible store materials (masonry and water). Also, the effects of varying the thermal properties of PCMs on the performance of collector-storage walls were studied.

ACKNOWLEDGEMENTS

After completing this thesis and writing about all the sophisticated physical and engineering problems, it is a pleasure to write about the people who contributed to this work. People without their help, and guidance this thesis would not be completed.

Professor J.A. Duffie, the previous director of the Solar Energy Laboratory at the University of Wisconsin-Madison, deserves much of the credit. He allowed me to use Solar Lab. facilities. His solar class introduced me to the Solar Energy field. He provided me during my weekly student-advisor meetings with many useful suggestions. His useful comments during the review of this thesis are deeply appreciated. Thank you, Jack, for showing that great interest in my research.

I would like to extend a special 'thank you' to Professor S.A. Klein, my external advisor, for his helpful ideas, guidance, and never ending supply of suggestions during this work, a better advisor I could never hoped for. It is a pleasure to pursue research under his guidance. Thank you Sandy for always being there to check over my work and solve my problems.

I have been fortunate to work and study under the supervision of these two great men, Jack and Sandy. My future will benefit from what they have taught me. I will be forever indebted to them.

I am deeply grateful and thankful to my advisors in Egypt for their support, help, guidance, and continuous encouragement. Professor A.A. Ammar gave me the guidance to get started the research work. Professor A.M. Okaz always provided me with help

and guidance. His advises, letters, phone calls during my stay in the United States are deeply appreciated. Useful suggestions and guidance of Professor M.M. Sorour are deeply acknowledged.

Many thanks also to Professor W.A. Beckman, the new director of the Solar Lab., for allowing use of Solar Lab. facilities. His questions during my seminar were helpful in understanding many important points in my research. Great help given by TRNSYS engineers Jim Kummer and Ruth Urban in solving TRNSYS problems is greatly acknowledged. The cooperation and friendship of all graduate students in the Solar Lab. are greatly appreciated. An added thanks to James Braun for his useful suggestions. Thanks to all the people in the Solar Lab. They made my stay here memorable and enjoyable. I am also deeply grateful to Moustafa Azab for his friendship, support and help during my stay in the United States. Moustafa, you have the amazing habit of often doing favors before they were even asked.

I am deeply grateful to all my colleagues in Laboratory of Physics at the Faculty of Engineering, University of Alexandria for their love, help, and friendship. They provided me by whatever I needed from my home department during my stay in the United States.

My wife and daughter deserve much of the credit : my wife for her understanding, patience, and selfless support, my daughter 'Menat Alaa' for always welcoming me home at the end of the day. Their moral support made the ups and downs more up and less down. Without their moral support the entire stay here in the United States would not have been possible.

Finally, but most important I would like to extend endless thanks and love to my wonderful parents. They have supported my college career with much prayers and love. The monthly letters from my father let me know what is going on in my home country. It was always a good feeling to know that things back home are going well.

TABLE OF CONTENTS

LIST OF FIGURES

LIST OF TABLES

NOMENCLATURE

A	cross sectional area of the storage material (m^2)
A_c	collector area (m^2)
A_f	fluid area (m^2)
A_g	cross sectional area of the gap (m^2)
A_t	inside surface area of the storage tank (m^2)
A_v	inlet (or outlet) wall vent area (m^2)
b	spacing between wall surface and first cover glazing (m)
Bi	Biot number, defined in pp. 36
c_f	specific heat of circulating fluid (kJ/kg K)
c_l	specific heat of PCM in liquid phase (kJ/kg K)
c_s	specific heat of PCM in solid phase (kJ/kg K)
d_s	thickness of PCM between channels, Figure 4.2 (m)
DD	heating degree days (°C days)
D_H	hydraulic diameter (m)
f	solar fraction
f_i	fraction of the collector irradiated by direct beam
F	annual solar fraction
F'	collector efficiency factor
F_{c-g}	collector radiation view factor of the ground

F_{c-s}	collector radiation view factor of the sky
Fo	Fourier number, defined in pp. 36
F_R	collector heat removal factor
F_R'	collector-heat exchanger efficiency factor
g	gravitational constant (m/s^2)
G	instantaneous total solar radiation on a horizontal surface per unit area (kJ/m^2)
G_b	instantaneous beam solar radiation on a horizontal surface per unit area (kJ/m^2)
G_d	instantaneous diffuse solar radiation on a horizontal surface per unit area (kJ/m^2)
G_s	mean solar radiation incident on a shaded collector per unit area (kJ/m^2)
h	specific enthalpy of PCM (kJ/kg)
h_c	convection heat transfer coefficient (kJ/h m^2 K)
h_{ce}	convection heat transfer coefficient between outer cover and environment (kJ/h m^2 K)
h_i	specific enthalpy of collector-storage wall node i per unit area (kJ/kg m^2)
h_r	radiation heat transfer coefficient (kJ/h m^2 K)
h_{re}	effective radiation heat transfer coefficient between cover and the environment (kJ/h m^2 K)
h_{sl}	solid-liquid transition latent heat (kJ/kg)
H	nondimensional enthalpy
H_{sl}	nondimensional liquid-solid transition latent heat

$\overline{H}_T$	is the monthly average daily radiation incident on the collector surface per unit area (kJ/m^2)
k	local thermal conductivity of the storage material (kJ/h m K)
k_f	thermal conductivity of the fluid (kJ/h m K)
k_l	thermal conductivity of PCM in liquid phase (kJ/h m K)
k_s	thermal conductivity of PCM in solid phase (kJ/h m K)
L	storage unit length in the flow direction (m), total heating load (kJ)
LCR	load collector ratio, defined in pp. 147 (kJ/h m^2 K)
L_s	monthly space heating load (kJ)
L_w	is the monthly water heating load (kJ)
m_i	mass of collector-storage wall node i per unit collector area (kg/m^2)
$\dot{m}$	fluid mass flow rate (kg/h)
M	number of radial elements
M_s	mass of the storage material (kg)
N	number of axial elements, number of days in the month
N_c	number of cylinder tubes, number of fluid channels
NTU	number of transfer units, defined in pp. 36
Nu	Nusselt number, defined in pp. 34
P	perimeter of the storage material (m)
P_f	perimeter of the circulating fluid (m)
Pr	Prandtl number, defined in pp. 35
$\dot{q}_b$	is the rate at which energy is convected and radiated from the inside surface of the wall into the room per unit area (kJ/h m^2)
$\dot{q}_l$	is the rate of energy loss through the glazing to the environment per unit area (kJ/h m^2)

$\dot{q}_s$	is the rate at which solar energy is absorbed on the wall surface per unit area (kJ/h m^2)
$\dot{q}_{st}$	is the rate of change of internal energy stored in the wall per unit area (kJ/h m^2)
$\dot{q}_v$	is the rate at which energy is carried away from the wall via airflow in the gap per unit area (kJ/h m^2)
Q_{aux}	auxiliary heating energy (kJ)
Q_b	energy transferred from the inside surface of the wall into the room (kJ)
Q_l	energy loss through the glazing to the environment (kJ)
Q_s	energy absorbed in the wall surface (kJ)
Q_v	energy vented from collector-storage wall to the building (kJ)
r	radial distance (m)
r_i	radius of the cylinder tube (m)
R	resistance to energy transfer through the gap per unit collector-storage wall area, nondimensional radial distance
R_b	ratio of incident beam radiation on the collector surface to incident beam radiation on the horizontal surface
Re	Renolds number, defined in pp. 34
SSF	solar savings fraction, defined in pp. 146
t	time (h)
T	storage material temperature (°C)
T_a	ambient air temperature (°C)
$\overline{T}_a$	is the monthly average ambient temperature (°C)
T_b	building temperature (°C)

T_{env}	environment temperature (°C)
T_f	fluid temperature (°C)
T_{fi}	inlet fluid temperature (°C)
T_{fo}	outlet fluid temperature (°C)
T_g	temperature of the inside glazing of the double glazed collector -storage wall (°C)
T_{in}	gap inlet air temperature (°C)
T_m	nominal melting temperature of the PCM (°C)
T_{main}	mains water supply temperature (°C)
T_{mg}	mean air temperature in the gap (°C)
T_{m1}	lower boundary temperature of the transition range (°C)
T_{m2}	upper boundary temperature of the transition range (°C)
T_N	temperature of the inside surface of the collector-storage wall (°C)
T_o	gap outlet air temperature (°C)
T_{ref}	arbitrary reference temperature (°C)
T_{set}	set point temperature of the hot water (°C)
T_u	minimum utilization temperature (°C)
T_1	outside surface temperature of the collector-storage wall (°C)
U	heat transfer coefficient between the PCM and the fluid (kJ/h m^2 K)
U'	heat loss coefficient from the storage unit to the surroundings (kJ/h m^2 K)
UA	loss coefficient-area product (kJ/h K)
$(UA)_{ns}$	thermal conductance of the house if the storage-collector wall is replaced by an adiabatic wall (kJ/h K)
U_b	the combined radiation and convection heat transfer coefficient between the inside wall surface and the room (kJ/h m^2 K)

U_L	collector overall loss coefficient (kJ/h m^2 K)
U_t	collector-storage wall top loss coefficient (kJ/h m^2 K)
v_f	fluid velocity (m/h)
V_t	the inside volume of the storage tank (m^3)
$\overline{V}$	mean air velocity in the gap (m/h)
V_w	wind speed (m/s)
w	collector-storage wall width (m)
x	collector-storage wall thickness (m)
X	nondimensional parameter for f-chart correlation, defined in pp. 116
Y	nondimensional parameter for f-chart correlation, defined in pp. 116
z	axial distance (m)
α	thermal diffusivity of the storage material (m^2/h)
α_w	collector-storage wall absorptance
χ	PCM quality or liquid fraction
Δt	is the total number of seconds in the month
$\Delta t'$	time step of component models using PCMs (h)
Δt_{TR}	TRNSYS time step (h)
ΔT_m	transition range bandwidth (°C)
ΔU	change in the internal energy of the storage material (kJ)
$\Delta\eta$	nondimensional time step
$\Delta\zeta$	nondimensional axial distance
ε_g	thermal emittance of the cover glazing
ε_w	thermal emittance of collector-storage wall
γ	control function

η_f	dynamic viscosity of the fluid (kg/h.m)
θ	nondimensional temperature of the storage material
θ_{env}	nondimensional environmental temperature
θ_f	nondimensional fluid temperature
θ_{m1}	nondimensional lower boundary temperature of the transition range
θ_{m2}	nondimensional upper boundary temperature of the transition range
ρ	ground reflectance, density of the storage material (kg/m^3)
ρ_f	fluid density (kg/m^3)
ρ_l	density of PCM in liquid phase (kg/m^3)
ρ_s	density of PCM in solid phase (kg/m^3)
σ	Stefan-Boltzman constant ($kJ/h\ m^2\ K^4$)
$(\overline{\tau\alpha})$	collector monthly average transmittance-absorptance product
$(\tau\alpha)_b$	transmittance-absorptance product for beam radiation
$(\tau\alpha)_{dr}$	transmittance-absorptance product for diffuse and ground reflected radiation
$(\tau\alpha)_n$	collector monthly average transmittance-absorptance product at normal incidence

CHAPTER 1
THERMAL ENERGY STORAGE

1.1 Introduction

Energy storage is used when there is a phase difference between heat supply and heat demand. Under these circumstances a heat storage system is needed to store the energy from the heat source for later use when there is a heat demand. The stored energy can make possible fuel savings, or fuel substitution in many application areas.

Energy storage can be for short-term duration or long-term duration. In solar thermal energy storage, short-term storage is carried-over from day to night or from sunny to cloudy days. On a long-term basis, energy is carried-over from one season to another. In solar terminology, long-term storage is always called annual or seasonal storage. Energy storage is usually in the form of sensible energy of a fluid or solid medium, energy associated with the phase-change of a material, or energy released from reversible chemical reactions.

1.2 Sensible Heat Storage

In sensible heat storage, energy is stored through a change in temperature of the storage medium. In this type of storage, the storage unit is charged and discharged by varying the temperature of a pebble bed in air-based systems or a water tank in water-based systems. The advantages of pebble bed system are availability, low cost, nontoxicity, no freezing or boiling, no corrosion problems, unlimited storage

temperature, and heat exchangers are not necessary. On the other hand, the main drawbacks of this system are large storage volume, charging and discharging can not be done simultaneously, and high pressure drop. The advantages of water heating system are availability, nontoxicity, high density, high specific heat, and low cost. The major drawbacks of this system are freezing or boiling of water, corrosion, and storage temperature effectively limited to 100 °C.

1.3 Latent Heat Storage

Latent heat storage utilizes the heat associated with a change in the phase of a material to store energy. Solid-liquid transition is the most interesting one since it is characterized by a relatively small volume change. The main advantages of phase-change energy storage are significant reduction in storage volume, and possibly better thermal performance due to the small temperature gradients in the storage material during charging and discharging.

On the other hand, phase-change energy storage (PCES) has two major drawbacks. Phase-change materials (PCMs) are more expensive than rock or water. In addition, the PCES unit must contain a heat exchanger since neither the circulating fluid is the same as the storage medium as the case in water-based system, nor the storage medium is always a solid as the case in the pebble bed storage system. Subsequently, a container must be provided to contain the phase-change material which provides additional thermal resistance. The PCM container must also provide a heat transfer surface for energy exchange between the circulating fluid and the storage medium. The PCM and its packaging should be chemically compatible to insure long-term durability of the containers.

1.3.1 Candidate Phase-Change Material

The candidate phase-change material must have several desired properties to be used as a storage medium [1,2] :

1. A melting temperature in the desired temperature range
2. High latent heat of fusion per unit mass
3. Small volume changes during phase transition so that a simple container and heat exchanger can be used
4. High density and high specific heat
6. High thermal conductivity, so that a small temperature gradients can be obtained during charging and discharging the storage unit
7. Congruent melting (i.e. the material should melt completely) and the liquid and solid phases are identical in composition
8. Little or no supercooling during freezing
9. Chemical stability
10 No corrosion
11. Nontoxicity, and non flammability
12. Low cost

1.3.2 Phase-Change Materials Selection

Solid or liquid to vapor transitions are always accompanied by a large volume change, so the materials which undergo solid or liquid to vapor transitions are of little interest in thermal energy storage. Most of the research on the area of selecting candidate phase-change materials for energy storage has been concentrated on the materials which undergo solid to liquid phase transition at a temperature range of 20-50 °C. This

transition is characterized by a small volume change during transition which allows the use of a much smaller volume of the storage unit in comparison with the volume used with sensible storage.

Many investigations have been done experimentally by researchers [3,4,5,6] to select candidate PCMs for energy storage. The results of these investigations suggest two general classes of PCMs to be used in thermal energy storage applications. These are the organic compounds, including paraffin waxes, and the inorganic salt hydrates. The general characteristics, advantages, and disadvantages of these materials are discussed below.

1.3.2.1 Paraffins

Paraffins have the general chemical formula $C_n H_{2n+2}$, and they are a family of saturated hydrocarbons. Paraffins have a very similar properties. The petroleum grade paraffins melt semicongruently, i.e., they melt over a finite temperature range. Chemically pure paraffins have a relatively high latent heat of fusion, on the order of 200 kJ/kg. The latent heat of petroleum grade paraffins is roughly 75% that of the pure paraffins [7,8]. There are many other organic compounds which have a melting temperature in the proper range for low temperature solar energy applications, however most of these compounds are unstable, corrosive, or toxic, which restrict their use as a storage media.

The major advantages of paraffins are high heat of fusion per unit mass, wide melting temperature range (-5-66 °C), low volume change on melting, no degradation with repeated cycling, no corrosion, and nontoxicity. The major drawbacks of paraffins are low density, flammability, and low thermal conductivity. The problem of low thermal conductivity can be reduced by using metallic fillers [9]. Also, the petroleum

grade paraffins have a significantly lower latent heat than pure paraffins and the chemical processes required to produce a chemically pure paraffins from petroleum grade paraffins result in a high material cost.

1.3.2.2 Salt Hydrates

Salt hydrates are represented by the general formula $C \cdot nH_2O$ where C is an anhydrous salt, and n is the number of water molecules associated with the salt molecule. Salt hydrates may melt congruently, semicongruently, or incongruently [7,10]. If at the melting temperature the anhydrous salt dissolves completely in its water of crystallization, a salt hydrate is said to melt congruently. Salt hydrates which exhibit congruent melting are preferable for thermal energy storage as they do not degrade with repeated cycling. However, they represent the lower end of the latent heat spectrum.

In semicongruent melting, a salt hydrate first transforms into a liquid and a lower hydrate (solid) at the transition temperature. The lower hydrate then melts at some higher temperature. The anhydrous salt is completely soluble at the higher temperature, and the solution has the composition of the original hydrate. The change of phase thus takes place with a finite temperature change. Some semicongruently melting salts are undesired for thermal energy storage, because of the separation of the lower hydrate out of the solution during cooling, which never fully rehydrates.

Most of salt hydrates melt incongruently, i.e. the water released does not dissolve all the present solid phase. In this case, there are two solid phases and a saturated aqueous phase at the transition temperature. Due to density difference, the lower hydrate (or the anhydrous salt) settles down at the bottom of the container. This change is generally irreversible, i.e. during cooling, the solid phase does not combine with the saturated solution to form the original salt hydrate. Incongruently melting salt hydrates

are thus unsuitable for thermal energy storage. However, the problem of incongruently melting can be avoided by mechanical means or by using a chemical agent. Telkes [11] reported the existence of a thixotropic agent which when used with sodium sulphate decahydrate (Glauber's salt, $Na_2SO_4 \cdot 10H_2O$) can prevent the precipitation of the anhydrous salt through 1000 cycles.

Salt hydrates also exhibit a strong tendency to supercool when the material is cooled in an enclosed container [10,12,13]. Supercooling can be defined as the process of cooling a liquid below the solid-liquid equilibrium temperature without the formation of the solid phase. This behavior results in a considerable decrease in the efficiency of the storage system. Supercooling can be eliminated or reduced by the use of a certain nucleating agents. Telkes showed that a 3-5% concentration of borax can prevent the supercooling of $Na_2SO_4 \cdot 10H_2O$. It is obvious that there are several problems produced with the use of salt hydrates in thermal energy storage application. However, progress has been achieved in these areas.

In general, the main advantages of salt hydrates are high heat of fusion per unit mass, small volume change during the transition, relatively higher thermal conductivity, high density, and low cost. The major drawbacks as stated above are incongruent melting, and supercooling.

1.4 Chemical Energy Storage

In chemical energy storage, energy can be stored in the form of the heat released from reversible chemical reactions. Such reactions are generally characterized by the relatively high energy accompanying the reversible destruction and reformation of chemical bonds. This makes chemical reactions generally offer large energy densities in

comparison with the storage densities provided by both sensible heat and latent heat storage materials. There are a number of reversible reactions which have been suggested for use in solar chemical systems [14,15,16]. For example, the dissociation of SO_3 into SO_2 and O_2, the dissociation of ammonia (NH_3) into N_2 and H_2, and the hydration of MgO to form $Mg(OH)_2$. On the other hand chemical technologies are more complex than sensible and latent heat systems, and as a result, they are less developed.

1.5 Solar Heating Systems

For solar heating systems, solar energy is first collected, then transferred directly to the heating load, or collected and then transferred to the storage unit for later use. There are three different types of solar heating systems which can deliver solar energy to a building : active systems, passive systems, and hybrid systems. A brief description of the mechanism of each type is given below.

1.5.1 Active Solar Heating Systems

Active solar heating systems use collectors, through which a fluid, either air or a liquid, is circulated by a fan or pump. The energy collected is then delivered to either the building directly, or to the storage unit which may be a pebble bed, water tank, or PCES.

1.5.2 Passive Solar Heating Systems

In passive solar heating systems, collection and storage of solar energy are done by natural means and there are no mechanical or electrical devices such as pumps and controllers. The energy storage unit for a passive system are the various elements of the building such as a south-facing window, collector-storage walls, roof, partitions, etc. There are several types of passive solar systems. In the following three classes are

briefly described.

1.5.2.1 Direct Gain

The direct gain concept is the most common passive solar system. The solar radiation is collected by a double glazing south facing window and then stored in a thermal storage mass which may be the floor and or the wall. Such floor and wall must be made of a massive construction to reduce the swings in room temperature, by storing the heat during day time and releasing it during night. The main advantages of direct gain are : the glazing serves multiple functions (solar collection, natural day lighting, and visual connection to the outside), and glazing is an inexpensive form of solar collectors. The main drawbacks of direct gain are : added expenses due to both the required storage mass to decrease room temperature fluctuations, and the required movable insulation systems over the glazing to reduce night heat losses.

1.5.2.2 Collector-Storage Wall

A collector-storage wall combines the functions of solar energy collection and storage into a single unit. A south wall, may be single or double glazed, is constructed from materials having large thermal capacities, such as masonry material or water tanks, painted black to absorb solar radiation. Solar radiation absorbed on the outside surface of the wall is transferred to the room by either or both of two paths. From the inside surface of the wall to the room by radiation and convection, or by forced or natural convection of air in the gap between glazing and wall. Air may enter the gap through a vent in the bottom of the wall and return to the room through a vent in the top of the wall. The major advantages of a collector-storage wall are : energy delivery to the space is more controllable than for a direct-gain system, and swings in room temperature are less than

in direct -gain system. The main drawbacks of collector-storage wall are : relatively large heat losses, and vents must be used to dump excess solar radiation during summer months to the environment.

1.5.2.3 Attached Sunspace

Sunspace attachment to building collects solar radiation in a secondary space which is separate from the occupied area, and stores heat in walls, and floor for later use. Thus, a sunspace is midway between a direct-gain system, in which the space collects heat, and a collector-storage wall system, which collects heat indirectly for the building. Sunspace provides a relatively inexpensive additional living space to the building. However, in cold climates, energy losses from the sunspace attachment can exceed the absorbed gains.

1.5.3 Hybrid Solar Heating Systems

Hybrid solar heating systems are a combination of active and passive solar heating systems. There are three types of hybrid solar heating systems. First, active system-passive system hybrid which has both active and passive collectors, and uses both the building mass and a storage tank, or a pebble bed for energy storage. Each of the two subsystems is relatively independent of the other. The second type is active collection-passive storage systems which are a combination of active collectors and passive storage. The use of this type eliminates the cost of an active storage units. Also, there is no need to use night insulation, since the fluid circulation can be turned off at night. The problem of building overheating during the summer months due to excess solar gains can be avoided. In the third type, active plus passive collection-passive storage hybrid, there is a variation on the active collection-passive storage system, using both active collectors

and direct gain, with passive energy storage. Figure 1.1 shows the different classifications of the solar systems.

1.6 Analysis of Solar Heating Systems

There are two basic methods to calculate the performance of the solar heating systems, i.e. the fraction of the load met by solar energy system. The first is to use a detailed simulation programs, such as the transient simulation program TRNSYS [17], to simulate solar energy systems. TRNSYS needs a lot of experience, and a large computational time, but at the same time it provides a flexible mean to simulate almost all the different solar systems. The experimental tests conducted at the Colorado State University Houses, have shown the reliability of TRNSYS simulations [18].

An interesting alternative to detailed simulation methods are the simplified design methods generally based on monthly calculations. Design methods are based on empirical correlations which give the solar fraction as a function of several system parameters and weather data. In general, there is a limitation on the range of parameters which can be used with the simplified design methods. This leads to a number of design methods for different solar systems. The most widely design methods are the f-chart design method [19,20] for both active and passive solar systems, the solar load ratio (SLR) method [21,22] for passive solar systems, and the direct-gain and collector-storage wall Un-utilizability methods [23,24].

Active

	Natural	Forced
Collector/storage		•
Storage/space		•

Passive

	Natural	Forced
Collector/storage	•	
Storage/space	•	

Hybrid

	Natural	Forced
Collector/storage	•	
Storage/space		•

Hybrid

	Natural	Forced
Collector/storage		•
Storage/space	•	

Figure 1.1 Classifying Active, Passive, and Hybrid Solar Systems

1.7 Literature Review

The use of phase-change materials for thermal energy storage in solar heating and cooling systems has received considerable attention. The motivation for using PCES is the reduction in storage volume which can be achieved compared to sensible heat storage. A brief discussion of the most important work done in this area is given below.

1.7.1 Active Solar Heating Systems

Using a one-dimensional model with an infinite heat transfer coefficient between the air and storage medium, Morrison, et al. [25,26] have shown that air-based solar systems utilizing sodium sulphate decahydrate ($Na_2SO_4 \cdot 10H_2O$) as a storage medium require roughly one-fourth the storage volume of a pebble bed. For paraffin wax, the required volume increases to approximately one-half the storage volume of a pebble bed. Their results are based on a seven month heating season from October 1 to May 1 for Madison (Wisconsin) and Albuquerque (New Mexico).

For liquid-based systems, their results showed that a system utilizing paraffin wax may require a slightly larger storage volume than a system of comparable performance with a water tank. On the other hand, systems utilizing $Na_2SO_4 \cdot 10H_2O$ require roughly one-half the storage volume of a conventional water tank system.

The model used by Morrison et al. to describe the performance of PCES unit is based on the following assumptions :

1) the PCM behaves ideally, i.e. such phenomena as property degradation, supercooling and crystallization are not accounted for, and the phase-change material is assumed to have definite melting temperature.
2) infinite thermal conductivity for the PCM in the direction normal to the flow (radial direction); this assumption requires that Biot number is sufficiently

low such that the temperature gradients in the storage material normal to the flow direction can be ignored.

3) heat losses from the storage unit to the surroundings are negligible.
4) zero thermal conductivity for the PCM in the direction parallel to the flow (axial direction)
5) the number of transfer units of the storage unit, NTU, is sufficiently large so that the local film temperature difference between the fluid and the PCM can be ignored.

Visser [27] developed a two-dimensional model for phase-change materials. He made a parametric study only on the storage unit using water as a circulating fluid. He did not study the effect of different theoretical models on the thermal performance of both air and water-based solar heating systems. At the same time the equations which give the relations between the specific enthalpy and the temperature for different phase ranges are not correct.

The effect of phase-change material melting temperature and latent heat has been studied by Jurinak et al. [28,29]. Their results are based on a heating season simulation from October 1-May 1 in Madison (Wisconsin). Their main conclusion was that it is important to select the PCM on the basis of its melting temperature, rather than its latent heat, i.e., the melting temperature has a significant effect on system performance.

There are many factors which affect system performance such as, the average temperature of the storage unit, the fraction of time that the storage unit is charged (collector to store mode), the fraction of time that the storage unit is discharged (store to load mode), the fraction of time that the storage unit is isolated (collector to load mode),

and the fraction of total time that the storage unit operates in the liquid phase mode. These factors depend primarily on the amount of incident solar energy relative to the heating load. To conclusively determine the effect of thermal properties on system performance, a simulation study must be conducted for different ratios of incident solar energy to heating load and a variety of climate types.

1.7.2 Passive Solar Heating Systems

The idea of using phase-change materials to replace masonry in a Trombe wall has been previously suggested by Telkes [30] and others. Experimental and theoretical tests have been done to investigate the reliability of PCMs as a Trombe walls. Chahroudi [31] developed methods of sealing porous concrete blocks and infusing them with calcium chloride hexahydrate. Thermal and mechanical performance were good, but chemical incompatibility with the cement caused cracking.

Benard et al. [32] have determined experimentally the behavior of three different thermal walls. The first two walls were hard paraffin melting between 40-50 °C, and a soft paraffin which has a wide melting temperature range (15-50 °C). The third wall was a concrete wall. The behavior of each wall was examined for one year. A paraffin wall of a total weight (including container) approximately equal to one-twelfth of the concrete wall, gave average efficiencies, and average comfort conditions similar to those of the concrete wall.

Christensen [33] used a computer simulations to predict the performance of collector-storage walls using solid state phase-change materials. A solid state phase-change material is any material that absorbs or releases energy when changing from one solid phase to another solid phase. Computer results showed that the performance of solid state PCM is better than the performance obtained with concrete wall four times

thicker.

Bourdeau [34] reported tests of two identical vented Trombe walls. One using water and the other using chliarolithe (a mixture of strontium chloride hexahydrate and diatomaceous earth). He estimated that water-filled tubes must have 2.5 times the diameter of PCM tubes for equal storage and collection efficiency. Bourdeau [35] tested unvented masonry wall and two types of passive storage collector walls using PCM. He concluded that an 8.1 cm thick PCM wall has slightly better thermal performance than 40 cm thick masonry wall. In addition, less swings in the room air temperature were obtained in the cases of PCM walls.

Askew [36] used a sandwich panel made of a thin slab of paraffin contained in a suitable envelope and packed by a layer of insulation mounted behind the double glazing of a wall or roof surface such as south facing surface to investigate solar energy collection, storage, and space heating. In the energy collection and storage mode, the paraffin side of the panel is exposed to solar radiation. A part of solar gains is absorbed and stored in the paraffin during the solid-liquid phase transition, and the remaining part is lost to the environment. When solar radiation is not available for collection and there is a heat demand (storage to load mode), the panels are rotated about their longitudinal axes to allow the release of the stored energy in the slab to the building, during the liquid-solid phase transition. No overheating during energy collection was observed, since energy released to the building in a controlled manner and thermal efficiencies comparable to conventional flat-plate collectors were predicted.

Collier et al. [37] showed that a macro-encapsulated PCM material cemented within masonry building blocks results in significant increase in the system performance over an equivalent volume of concrete.

1.8 Objectives

The main objectives of this thesis are :

1) To develop a theoretical model for both PCES and sensible heat storage which considers the assumptions made in earlier studies.
2) To study the effect of assumptions in the models of earlier studies on both the solar fraction and the required storage capacities for both air and water-based active solar heating systems.
3) To study the effect of melting temperature and latent heat for different storage masses on active solar system performance for different ratios of incident solar energy to heating load and different climates.
4) To investigate the possibility of using a building material called Abu-Siebera clay which is found in Abu-Siebera, Egypt, as a sensible storage medium.
5) To recommend system parameters, based on solar system performance, for both air and water-based active solar heating systems using Abu-Siebera clay in the Egyptian climate.
6) to compare the thermal performance of solar domestic hot water (SDHW) system obtained using TRNSYS and the corresponding performance obtained using the f- chart design method to examine the reliability of the f-chart design method in the Egyptian climate. Also, the effects of varying SDHW system parameters on system performance were studied.
7) To develop a computer program compatible with TRNSYS to allow the use of PCMs as a collector-storage wall, and compare the performance of collector-storage walls using masonry and PCMs.
8) to study the effect of the thermal properties of phase-change materials on the performance of collector-storage walls.

1.9 Organization

The remainder of this thesis is arranged as follows. Chapter 2 presents a brief description of the transient simulation program (TRNSYS) and its different components. Chapter 3 discusses the present theoretical model for PCES unit and gives the results of the comparison made between the present model and the earlier models based on the system performance. The comparison was conducted for both air and water-based active solar heating systems. Chapter 4 examines the effect of both melting temperature and latent heat on system performance for different climates and different heating season months (January, and March). Chapter 5 presents the comparison between the different theoretical models for sensible energy storage and investigates the possibility of using Abu-Siebera clay as a sensible storage medium by comparing the performance of solar heating system uses Abu-Siebera clay and the corresponding one uses rock. Chapter 6 compares the thermal performance of solar domestic hot water system obtained using TRNSYS and the corresponding performance obtained using the f-chart design method to examine the reliability of the f-chart design method in the Egyptian climate. Chapter 7 presents the analysis of the theoretical model developed to allow the use of phase-change materials as a collector-storage walls. The effects of the thermal properties of phase-change materials on the performance of collector-storage walls were also studied. Chapter 8 states the general conclusions of the present study and gives recommendations for future work.

CHAPTER 2
TRANSIENT SIMULATION PROGRAM (TRNSYS)

2.1 Introduction

If time is a variable to any of the components of the solar system, the simulation of the system is defined to be a transient simulation. Time is variable to most of the solar system components used in the present study. So, TRNSYS[17] is used to determine the performance of different solar heating systems simulated in the present work. TRNSYS is a transient simulation program developed at the University of Wisconsin Solar Energy Laboratory.

TRNSYS consists of a main program and a set of subroutines. These subroutines model the different components in a solar energy system such as the collectors, storage units, heat exchangers, domestic water heating load, space heating load, pumps or fans, pipes or ducts, valves, and temperature controllers. Solar energy system components are described by individual FORTRAN subroutines. All these subroutines are contained in TRNSYS library. If a particular component is not available in TRNSYS library, the user can develop his own component in a manner compatible with other TRNSYS subroutine components (Appendix A describes one of the components developed in this study).

A solar system consists of a set of interconnected components. For example, a typical solar air-based heating system may consist of a solar collector, an energy storage unit, an auxiliary energy heater, a fan, and temperature controllers. It is possible to simulate the performance of the system by simulating the performance of the interconnected components.

The performance of a system component depends on fixed parameters, the outputs of other components, and time dependent forcing functions. For a solar air-based heating system, knowledge of the weather data (i.e., solar radiation, ambient temperature, humidity ratio, wind speed, etc.), the hot water load demand, and space heating load demand as a function of time are necessary in order to determine the transient system performance. The modular simulation technique greatly reduces the process of system simulation because it reduces the large problem into a number of more easily solved problems. Many components such as solar collectors, heat exchangers, pumps, pipes, controllers etc. are common to different solar systems, so they can be used in many different systems configurations with little modifications which make the simulation process much easier.

TRNSYS includes two interactive programs. DEBUG program tests user-written TRNSYS component. DEBUG provides a useful ways of performing parametric studies on any TRNSYS component. PREP program generates transfer function coefficients for heating or cooling load calculations of exterior walls, internal partitions, floors, and roofs. PREP uses the z-transfer function program developed by Mitalas and Arsenault [38]. The user can provide PREP with material properties from Table 8, Chapter 25, of the 1977 ASHRAE Handbook of Fundamentals [39] or Table 8, Chapter 26 of the 1981 ASHRAE Handbook of Fundamentals [40]. The wall description begins at the outside surface of the wall and proceeds to the inside surface of the wall.

In addition, TRNSYS includes a number of subroutines which perform general mathematical and algebraic operations. For example, subroutine TYPECK to perform checks on the user input component configuration. It terminates the simulation after compilation of the component with error messages if errors are found. Subroutine DATA

reads user supplied data from FORTRAN logical units and if necessary interpolates this data during the simulation. Function subroutine TALF calculates the transmittance-absorptance product ($\tau\alpha$) of a solar collector as a function of angle of incidence of radiation and collector construction.

Subroutine DIFFEQ utilizes a modified Euler or improved polygon method for solving first-order ordinary differential equations. The modified Euler method consider the derivative to be constant over any time step. Checking the convergence of the solutions to differential equations is done by comparing successive values of the dependent variables. Subroutine TABLE assigns transfer function coefficients corresponding to the standard walls, partitions, floors, and ceiling from the 1977 and 1981 ASHRAE Handbook of Fundamentals. It reads the transfer function coefficients values from a FORTRAN logical unit. After reading the coefficients, the coefficients are stored internally for later use on subsequent calls to TABLE. Subroutine ENCL calculates the view factors between continuous rectangular surfaces in building simulation. Subroutines FIT and DFIT use linear least-squares regression to calculate coefficients of a user specified correlation. FIT uses single precision, and DFIT uses double precision.

2.2 Utility Subroutines

Transient simulation program (TRNSYS) contains a number of useful utility subroutines. The user can make use of one or more of these subroutines as needed in his own simulations. In the following a brief description of the most important utility subroutines.

2.2.1 Data Reader (TYPE 9)

The purpose of this subroutine is reading data at regular time intervals from a data card, converting it to the desired system of units, then these data can be supplied to other TRNSYS units as time varying forcing functions. TYPE 9 can be used in either of two reading modes a free or a formatted reading. In free reading the user specifies the number of each value on the data card he desires to use in the simulation. In formatted reading all data cards will be read in a formatting manner significantly reducing TRNSYS run time. Radiation data should not be interpolated since that is done in the radiation processor component. The time in the first data card must correspond to the starting time of the simulation.

2.2.2 Time Dependent Forcing Function (TYPE 14)

Some components in the solar heating system, such as the hot water load, can be represented as a time dependent forcing function which is characterized by a repeated pattern. The user provides TYPE 14 with a set of discrete data points for the values of the function at different times in one cycle. TYPE 14 uses linear interpolation to generate a continuous forcing function from these discrete data.

2.2.3 Solar Radiation Processor (TYPE 16)

Weather data (i.e. insolation, ambient temperature, humidity ratio etc.) usually available at one hour intervals and on a horizontal surface. Some TRNSYS simulations need estimates of radiation on a tilted surface or the values of the weather data at an intervals smaller than one hour. TYPE 16 can provide such desired information.

The solar radiation processor has a five different modes for obtaining beam and diffuse radiation from total radiation data. The first mode uses the relationship of Liu and

Jordan [41] to estimate beam and diffuse radiation from total radiation. The second mode uses the work made by Boes et al. [42] for estimating the beam and diffuse components of total radiation. In mode 3 the relationship developed by Erbs [43] is used to estimate the diffuse fraction of total horizontal radiation. In mode 4, beam and diffuse radiation are inputs directly, and total and direct normal radiation are inputs in mode 5.

2.2.4 Quantity Integrator (TYPE 24)

This component performs integration over any period of time for any desired quantity before printing the results. For example, the collector component subroutine outputs the rate of energy gain from the collector. The user can use TYPE 24 to calculate the total energy gain from the collector over the simulation period. The integrated quantities can be printed directly or after making one or more algebraic operations (multiplication, division, addition, subtraction, or negation etc.) with the use of EQUATIONS card which is recently added to the TRNSYS library.

2.2.5 Psychrometrics (TYPE 33)

This component calculates various moist air properties from ASHRAE correlations and ideal gas laws. It takes as input a dry bulb temperature or humidity ratio and one of the following properties : wet bulb temperature, relative humidity, humidity ratio, dew point temperature, or enthalpy. The outputs of this subroutine are humidity ratio (or relative humidity when the humidity ratio is an input), wet bulb temperature, enthalpy (or relative humidity when enthalpy is an input), mixture density, and dry air density. This component is useful for cases where various moist air properties at ambient conditions are required. With this component, the required properties are added to the weather data

file. This is generally more efficient than repeating the calculations for each simulation.

2.2.6 Weather Data Generator (TYPE 54)

This component is useful when hourly weather data are not available. TYPE 54 generates hourly weather data given the monthly average values of solar radiation, ambient temperature, humidity ratio, and wind speed. The data are statistically generated in a manner approximately equal to the long-term statistics at the specified location. This component generates a single year of typical data, similar to a Typical Meteorological Year (TMY) data. TYPE 54 is based on algorithms developed by Knight [44], and Degelman [45]. The weather data file of Alexandria, Egypt [46] contains the monthly average values of solar radiation, ambient temperature, humidity ratio, and wind speed. Since TRNSYS simulations needs hourly values of these parameters, the weather data generator was used in all the simulations using the weather data of Alexandria, Egypt.

2.3 Information Flow Diagram

After specifying each system component and mathematically describing each component, it is necessary to construct an information flow diagram for the system which is a schematic representation of the direction of information into and out of each of the system components. Each component is represented as a box. The user must differentiate between information flowing into and that flowing out of the component. As an example, Figure 2.1 shows the flow diagram of one of the collector modes contained in TRNSYS library (Appendix A contains the information flow diagram of the PCES unit developed in this study). In this mode, the collector efficiency is obtained from the Hottel-Whillier equation [47]. In the following a complete description of this subroutine component.

INPUTS - 5

OUTPUTS - 3

PARAMETERS - 11

DERIVATIVES - 0

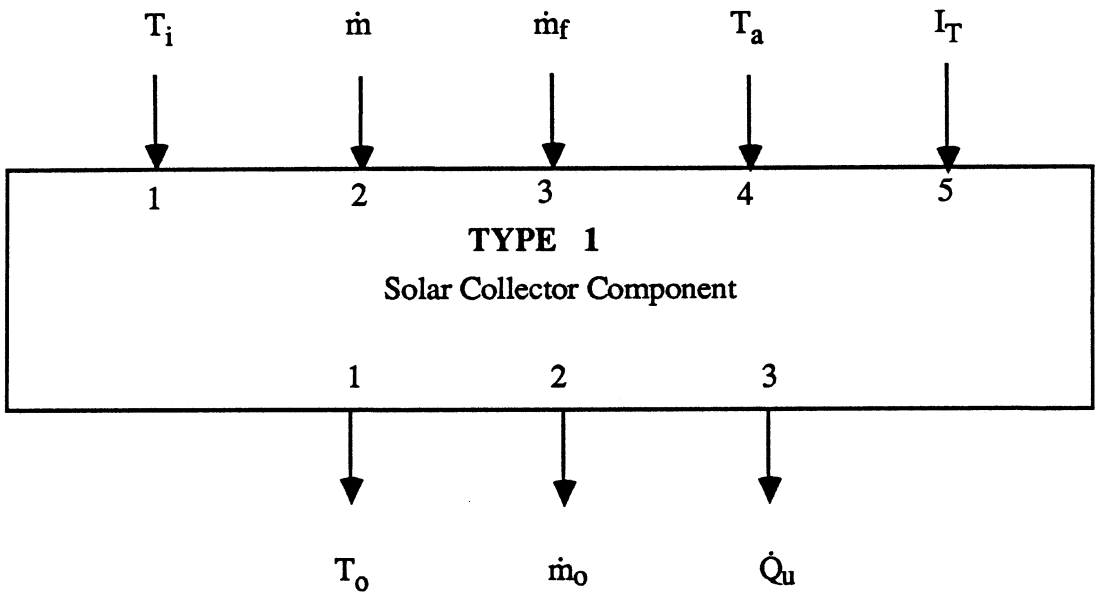

PARAMETERS

1. Collector mode (1)
2. N_s
3. A_c
4. c_f
5. Efficiency mode (1)
6. G_{ts}
7. a
8. b
9. ε
10. c_f
11. Optical mode (0)

Figure 2.1 Solar Collector Component Flow Diagram

The information for any component of the system can be of three types :

1. Information which are always constant throughout the simulation. These are the PARAMETERS of the component. The PARAMETERS of the collector component are :

PARAMETERS No.	DESCRIPTION
1	Collector mode : specify 1
2	N_s - Number of collectors in series
3	A_c - Total collector area
4	c_f - Specific heat of collector fluid
5	Efficiency mode :
	1- η vs. $(T_i - T_a) / I_T$
6	$\dot{m}_{ts}$ - Mass flow rate per unit area at test conditions
7	a - Intercept efficiency $[F_R (\tau\alpha)_n]$
8	b - Negative of the slope of the efficiency curve $(F_R U_L)$
9	ε - Effectiveness of the collector loop heat exchanger (if ≤ 0, then no heat exchanger)
10	c_f - Specific heat of fluid entering the cold side of the heat exchanger
11	Optical mode (0 for no incident angle modifier)

2. Information flowing into a component represented by inwardly directed arrows which are variables from other components in the system which is defined as the

INPUTS variables to the component. For a transient system, the INPUTS variables may vary with time. In general, an INPUT to a component must be an OUTPUT variable from one of the other components of the system. The INPUTS variables of the collector component are :

INPUT No.	DESCRIPTION
1	T_i - Temperature of fluid entering cold side of heat exchanger or collector inlet if no heat exchanger
2	$\dot{m}$ - Collector fluid mass flow rate
3	$\dot{m}_f$ - Heat exchanger cold side fluid mass flow rate
4	T_a - Ambient temperature
5	I_T - Incident radiation

3. The number of time dependent differential equations involved in the mathematical model of a system component, and the initial values of the dependent variables are specified by the DERIVATIVES control card. For the collector component no DERIVATIVES card used. OUTPUTS variables are the outputs of special interest for the user. The desired OUTPUTS from TYPE 1 are :

OUTPUT No	DESCRIPTION
1	T_o - Outlet fluid temperature
2	$\dot{m}_o$ - Outlet fluid mass flow rate
3	$\dot{Q}_u$ - Rate of useful energy gain from the collector

2.4 TRNSYS Deck

The final step in the simulation process is preparing a TRNSYS deck for each solar heating system. The TRNSYS deck consists of the control cards and data cards required to simulate the desired solar system. TRNSYS control cards divided into four categories, component control cards, simulation control cards, listing control cards, and the end control card. Component control cards define the components of the solar system to be simulated and their interconnection. Simulation control cards determine the simulation time (i.e. one day, a month, a year etc.), simulation time step, and error tolerances. Listing control cards affect the outputs of the TRNSYS simulation. The end control card signals the end of the TRNSYS deck, it must be the last card in the TRNSYS deck. Appendix B contains two of the TRNSYS decks written for the simulation of both air and water-based solar heating system.

TRNSYS time step is fixed throughout the simulation at a value specified by the user on the SIMULATION control card. The time step must be chosen small enough such that the numerical integration algorithm remains stable during the simulation process. The incorporation of phase-change energy storage (PCES) models into TRNSYS produces a major problem. The time step required for the stability of PCES models is too small for economic use of TRNSYS. According to PCM properties, number of the nodes used in the numerical technique, and the size of PCES unit in active solar heating system or PCM wall thickness in passive solar heating system, the time step required by PCES models is much smaller than that required by the other TRNSYS subroutines.

This problem was solved by running TRNSYS at the default time step (0.25 h), which is shown to be small enough to ensure the stability of TRNSYS subroutines, and subdividing it within the time step required to meet the stability condition of PCES

models. For every TRNSYS time step, the PCES subroutines equations only are solved several times. This method reduces TRNSYS run time in comparison with the time needed if one chooses to use the time step of PCES for all other TRNSYS subroutines.

2.5 Simulation Output

The TRNSYS library contains built in output devices which provide a means of outputting results of the simulation process. The TYPE 25 printer prints values of inputs at specified intervals of time. TYPE 25 can also print the integrated outputs of TYPE 24 integrator. The TYPE 26 component produces a plot of one or more inputs versus time. TYPE 27 component prints tabulated time or frequency distributions and plots histograms for a detailed representation of the same information.

Simulation summary (TYPE 28) integrates its inputs over the summary interval, performs a specified algebraic operations on the integrals, and prints the results. The relative accuracy of the simulation can be estimated by checking energy balance on the system and or subsystem boundary. TYPE 28 includes an energy balance checking routine. If an energy balance does not close within the value specified by the user, the simulation will be terminated. This means that the system components have not been specified correctly. TYPE 29 performs a life cycle cost analysis based on the results of simulation and cost data. It compares the capital and back-up fuel costs of a solar system to the fuel cost of a conventional non-solar system.

CHAPTER 3
COMPARISON OF THEORETICAL MODELS OF PHASE-CHANGE HEAT STORAGE FOR AIR AND WATER-BASED SOLAR HEATING SYSTEMS

Section 3.1 describes the configuration of the storage unit studied. Section 3.2 discusses the theoretical model developed in this investigation to study the thermal performance of both air and water-based solar heating systems. Section 3.3 contains the configurations and control strategies for both air and water-based solar heating systems. Section 3.4 compares the results of the present detailed model and the corresponding results obtained using the assumptions made in the model developed by Morrison et al. [26] for phase-change energy storage unit.

3.1 Configuration of the Storage Unit

Figure 3.1 shows the configuration chosen for the storage unit. It consists of a vessel packed in the vertical direction with cylindrical tubes. The storage material is inside the tubes and the heat transfer fluid flows parallel to it. To have as much phase-change material as possible, the vessel must be closely packed. The void fraction (the ratio between the fluid volume and the storage tank volume) is assumed to be equal to 0.3. The inside volume and inside surface area of the tank are respectively given by V_t and A_t. The number of cylinders inside the vessel is N_c. The radius of the cylinder tubes is r_i, the length of the cylinders as well as the inside height of the vessel is given by L.

The ratio r_i / L is set to 0.01 which is small enough to minimize radial heat conduction in the storage material. The fluid is contained in the annulus (r_o - r_i).

3.2 Theoretical Model

The thermal energy storage in the PCM makes use of the latent heat of the material. The change of state results in a moving boundary : On one side of the interface the material is solid, while on the other side it is liquid. This class of problem is known as "Stefan" problems. The problem of tracing the interface can be eliminated by using the specific enthalpy "h" rather than the temperature as the dependent variable. An energy balance for the PCM, considering the radial and axial conduction, yields

$$\frac{\partial h}{\partial t} = \frac{k}{\rho}\frac{\partial^2 T}{\partial r^2} + \frac{k}{r\rho}\frac{\partial T}{\partial r} + \frac{k}{\rho}\frac{\partial^2 T}{\partial z^2} \tag{3.1}$$

An energy balance for the circulating fluid yields

$$\frac{\partial T_f}{\partial t} + \frac{\dot{m}}{\rho_f A_f}\frac{\partial T_f}{\partial z} = \frac{U P}{\rho_f A_f c_f}(T - T_f) + \frac{U' P_f}{\rho_f A_f c_f}(T_{env} - T_f) \tag{3.2}$$

T, ρ, and k are respectively, the temperature, the density, and the thermal conductivity of the PCM. The local thermal conductivity of PCM can be approximated as

$$k = \chi k_l + (1 - \chi) k_s \tag{3.3}$$

k_s, and k_l are the thermal conductivity of the phase-change material in the solid and liquid phases, respectively. U is the heat transfer coefficient between the PCM and the fluid. The correlations used to determine U are given in section 3.2.1.

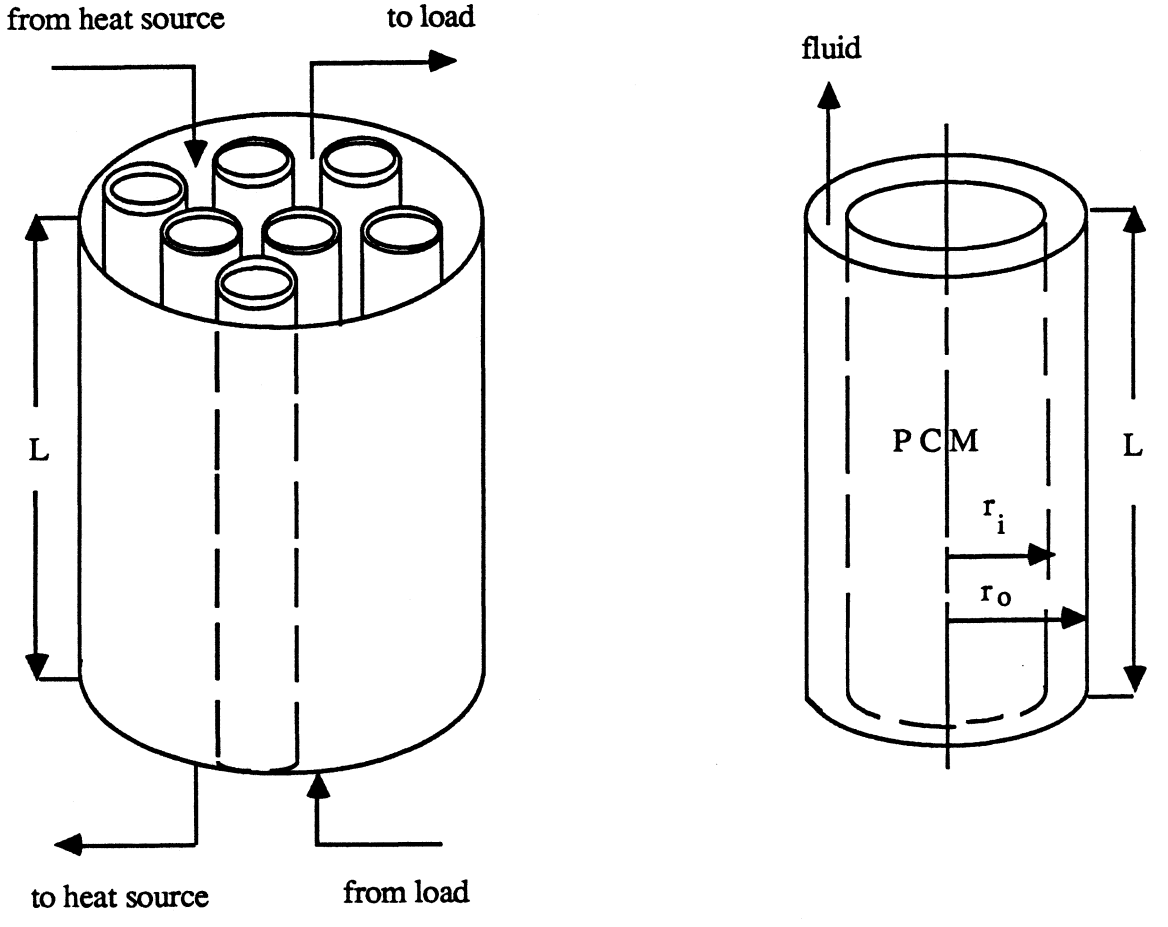

a) The Cylinder-Packed Vessel

b) The Model for One Cylinder

Figure 3.1 Configuration of the Storage Unit

T_f, $\dot{m}$, and c_f are respectively, the temperature, mass flow rate, density, and specific heat of the circulating fluid. A_f, fluid area, is given by

$$A_f = \pi N_c (r_o^2 - r_i^2) \tag{3.4}$$

T_{env} is the temperature of the environment. U', the heat loss coefficient from the storage unit to the surrounding, is assumed to to be equal to 1.5 kJ/h m^2 K. P and P_f are respectively, the perimeter of the the PCM and the perimeter of the circulating fluid, and they can be expressed as

$$P = 2 \pi r_i N_c \tag{3.5}$$

$$P_f = 2 \pi r_o N_c \tag{3.6}$$

Assuming adiabatic boundary conditions at the bottom and the top of the storage unit, i.e. the heat flow through the upper and lower surfaces is equal to zero, and there is no heat flow through the axis of the cylinder, these give the following boundary conditions :

$$z=0 \qquad \frac{\partial T}{\partial z} = 0 \tag{3.7a}$$

$$z=L \qquad \frac{\partial T}{\partial z} = 0 \tag{3.7b}$$

$$r=0 \qquad \frac{\partial T}{\partial r} = 0 \tag{3.7c}$$

$$r=r_i \qquad k \frac{\partial T}{\partial r} = U (T_f - T) \tag{3.7d}$$

The relations between the specific enthalpy "h" and the temperature "T" for different transition ranges are as follow :

$$h = c_s (T - T_{ref}) \qquad \text{for } T < T_{m1} \qquad (3.8a)$$

$$h = c_s (T_{m1} - T_{ref}) + h_{sl} \chi \qquad \text{for } T_{m1} < T < T_{m2} \qquad (3.8b)$$

and

$$h (T) = c_s (T_{m1} - T_{ref}) + h_{sl} + c_l (T - T_{m2}) \qquad \text{for } T > T_{m2} \qquad (3.8c)$$

where T_{m1} and T_{m2} are respectively, the lower and upper boundary of the transition range, T_{ref} is an arbitrary temperature, h_{sl} is the latent heat of the phase- change material, c_s is the specific heat in the solid range, c_l is the specific heat in the liquid range, and χ is the liquid fraction which is given by the following relations :

$$\chi = 0 \qquad \text{for } T < T_{m1} \qquad (3.9a)$$

$$\chi = \frac{T - T_{m1}}{T_{m2} - T_{m1}} \qquad \text{for } T_{m1} < T < T_{m2} \qquad (3.9b)$$

$$\chi = 1 \qquad \text{for } T > T_{m2} \qquad (3.9c)$$

3.2.1 Heat Transfer Coefficient Calculation

The heat transfer coefficient, U, describing the energy flow between the circulating fluid and the PCM is calculated internally in the PCES subroutine. The value of the heat transfer coefficient depends on the type of the flow, i.e. laminar ($Re \leq 2200$) or turbulent

flow (Re >2200). The Reynolds number, Re, is given by

$$Re = \frac{\rho_f v_f D_h}{\eta_f} \tag{3.10}$$

ρ_f, v_f, and η_f are respectively the density, the velocity, and the dynamic viscosity of the fluid. D_h, the hydraulic diameter, is given by

$$D_h = 2 (r_o - r_i) \tag{3.11}$$

and v_f is given by

$$v_f = \frac{\dot{m}}{\pi N_c \rho_f (r_o^2 - r_i^2)} \tag{3.12}$$

The heat transfer coefficient can be described in terms of the Nusselt number :

$$Nu = \frac{U D_h}{k_f} \tag{3.13}$$

where k_f is the thermal conductivity of the fluid. Nu, the Nusselt number, can be calculated from the empirical relations given by Rohsenow et al. [48] assuming a constant surface temperature. For laminar flow, the Nusselt number can be expressed as

$$Nu = 3.66 + 4.12 \left(\frac{D_h}{r_i} - 0.205 \right)^{0.569} \qquad \text{for } Re \leq 2200 \tag{3.14}$$

The term $\frac{D_h}{r_i}$ indicates the density of the packing of the cylinders. For turbulent flow,

the Nusselt number can be calculated from the following empirical correlation :

$$\frac{Nu}{Nu'} = 1.08 - 0.794 \exp\left[-\frac{1.62\, D_h}{r_i}\right] \qquad \text{for} \quad Re > 2200 \qquad (3.15)$$

Nu' is the Nusselt number for the corresponding configuration (i.e. the configuration in which the circulating fluid passes inside the tubes and the PCM surrounds the fluid), and it can be calculated from the correlation given by Dittus and Boelter [49] :

$$Nu' = 0.023\, Re^{0.8}\, Pr^{0.4} \qquad \text{for} \quad Re > 2200 \qquad (3.16)$$

Pr, the Prandtl number, is given by

$$Pr = \frac{\eta_f\, c_f}{k_f} \qquad (3.17)$$

3.2.2 Solution Method

The numerical analysis and the computer program can be simplified by writing the governing equations [equations (3.1), and (3.2)] and the boundary conditions [equations (3.7)] in a nondimensional form. The following nondimensional groups can be used :

$$H = \frac{h}{c\,(T^* - T_{ref})}, \qquad H_{sl} = \frac{h_{sl}}{c\,(T^* - T_{ref})},$$

$$\theta = \frac{(T - T_{ref})}{(T^* - T_{ref})}, \qquad \theta_f = \frac{(T_f - T_{ref})}{(T^* - T_{ref})},$$

$$\theta_{m1} = \frac{(T_{m1} - T_{ref})}{(T^* - T_{ref})}, \qquad \theta_{m2} = \frac{(T_{m2} - T_{ref})}{(T^* - T_{ref})},$$

$$\theta_{env} = \frac{(T_{env} - T_{ref})}{(T^* - T_{ref})} \quad , \qquad V = \frac{r_i}{L} \quad ,$$

$$C = \frac{c_s}{c_l} \quad , \qquad W = \frac{\rho_f A_f c_f}{\rho A c} \quad ,$$

$$Y = \frac{U' P_f}{U P} \quad , \qquad R = \frac{r}{r_i} \quad ,$$

$$\zeta = \frac{U P}{\dot{m} c_f} z \quad , \qquad Bi = \frac{U r_i}{k} \quad ,$$

$$Fo = \frac{k}{\rho c r_i^2} t \quad , \text{ and} \quad NTU = \frac{U P L}{\dot{m} c_f}$$

where T* is an arbitrary temperature, and A, the PCM cross sectional area, is given by :

$$A = \pi N_c r_i^2 \tag{3.18}$$

B_i, Fo, and NTU are Biot number, Fourier number, and the number of transfer units, respectively. Substitution of these nondimensional quantities into equations (3.1), (3.2), and (3.7) gives the following nondimensional equations :

<u>For the storage material</u>

$$\frac{\partial H}{\partial Fo} = \left[\frac{\partial^2 \theta}{\partial R^2} + \frac{1}{R} \frac{\partial \theta}{\partial R} \right] + V^2 (NTU)^2 \frac{\partial^2 \theta}{\partial \zeta^2} \tag{3.19}$$

For the circulating fluid

$$\frac{\partial \theta_f}{\partial Fo} = \frac{2\,Bi}{W}\left[(\theta - \theta_f) + Y(\theta_{env} - \theta_f) - \frac{\partial \theta_f}{\partial \zeta}\right] \tag{3.20}$$

For the boundary conditions

$$\zeta = 0 \qquad \frac{\partial \theta}{\partial \zeta} = 0 \tag{3.21a}$$

$$\zeta = \frac{U\,P}{\dot{m}\,c_f} L \qquad \frac{\partial \theta}{\partial \zeta} = 0 \tag{3.21b}$$

$$R = 0 \qquad \frac{\partial \theta}{\partial R} = 0 \tag{3.21c}$$

$$R = 1 \qquad \frac{\partial \theta}{\partial R} = Bi\,(\theta_f - \theta) \tag{3.21d}$$

where H, and θ are the nondimensional enthalpy and the nondimensional temperature of the PCM, respectively. θ_f is the nondimensional fluid temperature. R, and ζ are the nondimensional radial and axial distances, respectively.

The relations between the nondimensional enthalpy and the nondimensional temperature of the PCM become :

$$H = \theta \qquad \text{for } \theta < \theta_{m1} \tag{3.22a}$$

$$H = \theta_{m1} + H_{sl}\,\chi \qquad \text{for } \theta_{m1} < \theta < \theta_{m2} \tag{3.22b}$$

$$H = C\,\theta_{m1} + H_{sl} + (\theta - \theta_{m2}) \qquad \text{for } \theta > \theta_{m2} \tag{3.22c}$$

Finite difference techniques were used to solve the governing equations for both the storage material and the circulating fluid. The storage unit was divided into N nodes in the axial direction (i.e. the direction parallel to the fluid flow), and M nodes in the radial direction (i.e. the direction normal to the fluid flow). The fluid was divided into N elements in the axial direction. Figure 3.2 shows the nodal representation of the phase-change energy storage unit. Using forward differencing techniques, equations (3.19) and (3.20) can be rewritten as follow :

$$\frac{H_{i,j}^{\nu+1} - H_{i,j}^{\nu}}{\Delta Fo} = \left[\frac{\theta_{i+1,j}^{\nu} + \theta_{i-1,j}^{\nu} - 2\,\theta_{i,j}^{\nu}}{(\Delta R)^2} + \frac{1}{R} \frac{\theta_{i+1,j}^{\nu} - \theta_{i,j}^{\nu}}{\Delta R} \right]$$

$$+ \; V^2 (NTU)^2 \left[\frac{\theta_{i,j+1}^{\nu} + \theta_{i,j-1}^{\nu} - 2\,\theta_{i,j}^{\nu}}{(\Delta \zeta)^2} \right] \tag{3.23}$$

and

$$\frac{\theta_{f_i}^{\nu+1} - \theta_{f_i}^{\nu}}{\Delta Fo} = \frac{2\,Bi}{W} \left[(\theta_{i,J}^{\nu} - \theta_{f_i}^{\nu}) + Y (\theta_{env} - \theta_{f_i}^{\nu}) - \frac{(\theta_{f_{i+1}}^{\nu} - \theta_{f_i}^{\nu})}{\Delta \zeta} \right] \tag{3.24}$$

i, j represent the nodal position, and ν and $\nu+1$ refer to the values at the old and new time step. ΔFo is the nondimensional time step, ΔR, and $\Delta \zeta$ are the nondimensional nodal spacings.

Equations (3.23) and (3.24) can be rearranged as follow :

$$H_{i,j}^{\nu+1} = H_{i,j}^{\nu} + \Delta Fo \left[\frac{\theta_{i+1,j}^{\nu} + \theta_{i-1,j}^{\nu} - 2\,\theta_{i,j}^{\nu}}{(\Delta R)^2} + \frac{1}{R} \frac{\theta_{i+1,j}^{\nu} - \theta_{i,j}^{\nu}}{\Delta R} \right]$$

$$+ \; \Delta Fo\, V^2 (NTU)^2 \left[\frac{\theta_{i,j+1}^{\nu} + \theta_{i,j-1}^{\nu} - 2\,\theta_{i,j}^{\nu}}{(\Delta \zeta)^2} \right] \tag{3.25}$$

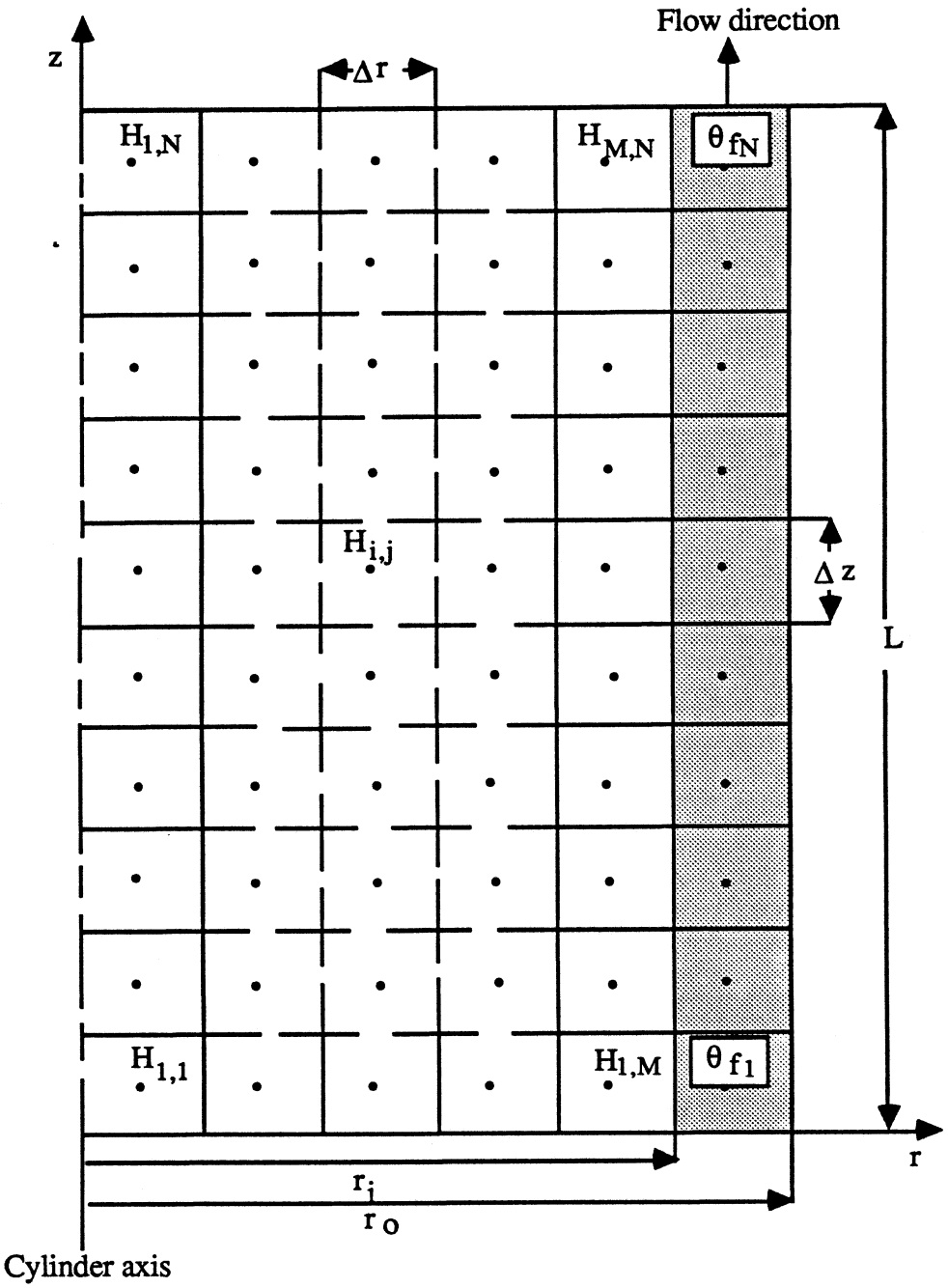

Figure 3.2 Nodal Representation of PCES Unit

and

$$\theta_{f_i}^{\nu+1} = \theta_{f_i}^{\nu} + \frac{2\,Bi\,\Delta\,Fo}{W}\left[(\theta_{i,J}^{\nu} - \theta_{f_i}^{\nu}) + Y\ (\theta_{env} - \theta_{f_i}^{\nu}) - \frac{(\theta_{f_{i+1}}^{\nu} - \theta_{f_i}^{\nu})}{\Delta\,\zeta} \right] \qquad (3.26)$$

At every time step an implicit set of N x (M+1) simultaneous equations has to be solved. N x M for the phase-change material, and N for the circulating fluid. This set of equations can be solved either by matrix inversion or iteration methods. At any time level, ν, the phase-change material may change phase which results in different thermal properties. This makes the use of the matrix inversion methods impractical. Therefore, in this study, the Gauss-Seidel iterative method was used to solve this set of equations. At a specific time level, ν, the entire problem is defined by the nondimensional quantities H and θ values of the phase-change material and θ_f values of the fluid. At the next time level, $\nu+1$, the values of H and θ_f are then updated from equations (3.25) and (3.26). The value of θ, the nondimensional temperature of the PCM, can be now updated using equations (3.22). Then a convergence test was done, if a convergence criterion is achieved the time level is increased. Otherwise another iteration is performed at the same time level. The convergence criterion ε for both the nondimensional enthalpy of the phase-change material and the nondimensional temperature of the circulating fluid can be expressed as

$$2.\left| \frac{H_{j,k}^{\nu,n} - H_{j,k}^{\nu,n-1}}{H_{j,k}^{\nu,n} + H_{j,k}^{\nu,n-1}} \right| < \varepsilon \qquad (3.27)$$

and

$$2.\left| \frac{\theta_{f_i}^{\nu,n} - \theta_{f_i}^{\nu,n-1}}{\theta_{f_i}^{\nu,n} + \theta_{f_i}^{\nu,n-1}} \right| < \varepsilon \qquad (3.28)$$

where n is the number of the iteration at a time level v. The value of ε determines the accuracy of the solution method. The convergence criterion were set to 0.01 for air-based systems, and 0.00001 for water based-systems. These values were found to be small enough to achieve a reasonable accuracy in the solution method.

3.2.3 Model Stability and Accuracy

The stability and accuracy of the present numerical solution depend upon the nondimensional time step ΔFo and both the nondimensional spacings ΔR and $\Delta\zeta$ (i.e. the number of the nodes in both the radial and axial directions). For each simulation, a sensitivity parametric study was performed first to determine the effect of the number of the axial and radial nodes and time step on the accuracy of the results. The variation of the heat stored in the PCM with time during the heating mode only using constant inlet fluid temperature was calculated using different values of ΔR, $\Delta\zeta$, and ΔFo. There is no significant variation in the stored energy with increasing the number of radial points above 5 (i.e. M=5) or with increasing the number of axial points above 10 (i.e. N=10). Also, stability and acceptable accuracy conditions were achieved for ΔFo less than or equal to 0.1.

Another sensitivity study was performed after incorporating the PCES subroutine into TRNSYS. The optimum values of ΔFo, M, and N predicted from the parametric study gave excellent stability and accuracy results for the performance of the complete solar heating systems. An energy balance for both the PCES subroutine and the complete solar heating systems was conducted for each simulation. The present results showed a closure of 0.3-1.5%. The closure of a simulation energy balance may be defined as the absolute value of the difference between the energy flows into and out of the system divided by the energy flow into the system.

3.2.4 Incorporation into TRNSYS

The incorporation of the PCES model into TRNSYS subroutines resulted in a major problem. The time step required for the stability of PCES unit, Δt, was several times smaller than the time step required for other TRNSYS subroutines (Δt_{TR}).This problem can be solved by running TRNSYS at the optimum time step (usually 0.25 h) and subdividing it within the PCES time step. In general Δt_{TR} does not exactly equal an integer number of Δt. By introducing a number , N_s, which is the first integer greater than $\frac{\Delta t_{TR}}{\Delta t}$, the time step of PCES subroutine can now be recalculated from the following equation :

$$\Delta t' = \frac{\Delta t_{TR}}{N_s} \tag{3.29}$$

For every TRNSYS time step, the equations in the phase-change energy storage subroutine are solved N_s times using the PCES time step ($\Delta t'$). This method saves a great deal of computational time in comparison with the other option of running TRNSYS subroutines at the time step of PCES subroutine (Appendix A describes this component).

3.3 Systems Description and Control Strategy

Both air and water-based heating systems are used in the present simulations. There are several advantages of solar air-based heating systems over the water-based heating systems. The most important one is that the same medium (air) is used for collectors and space heating, eliminating the need of a heat exchanger. In solar air-based systems, the storage medium acts as a heat storage and heat exchanger. Air systems are characterized by a high degree of stratification in the storage unit, i.e. lower inlet collector temperature and higher outlet collector temperature, resulting in higher collector efficiency. No corrosion, freezing or boiling problems in air systems. The main

drawbacks of solar air-based systems are high pumping cost due to the large volume of air to be used, and relatively large volume of storage size.

The main advantages of water-based solar heating systems in comparison with air-based systems are that they are less expensive and widely used in commercial building. For the same collector inlet temperatures, water-based systems operate at a higher efficiencies and they can also provide domestic hot water at a higher efficiency compared to air systems. The disadvantages of water-based systems are freezing, corrosion, leakage, high cost due to additional heat exchangers.

3.3.1 Air-Based System

TRNSYS is used to determine the performance of the standard solar air space and domestic water system shown in Figure 3.3. The parameters selected for the system components are listed in Table 3.1. The system shown in Figure 3.3, has three modes of operation. The first mode occurs when solar energy is available for collection and the space heating load is non-zero. During this mode, the fluid is circulated between the collectors and the load while the storage unit is isolated. The second mode occurs when solar energy is available for collection and the space heating load is zero. In this case, air is circulated between the collectors and the storage unit. The final mode occurs when solar energy is not available for collection and there is a space heating load. In this case, air is circulated between the storage unit and the load. The system operation is controlled by a series of thermostats, fans, and flow diverters. Air flow to the space heating load and auxiliary heat is governed by a two stage thermostat which monitors room temperature. It commands first stage (solar source) heating when the room temperature drops below 20 °C, and second stage (auxiliary source) heating when the room temperature drops below 18.5 °

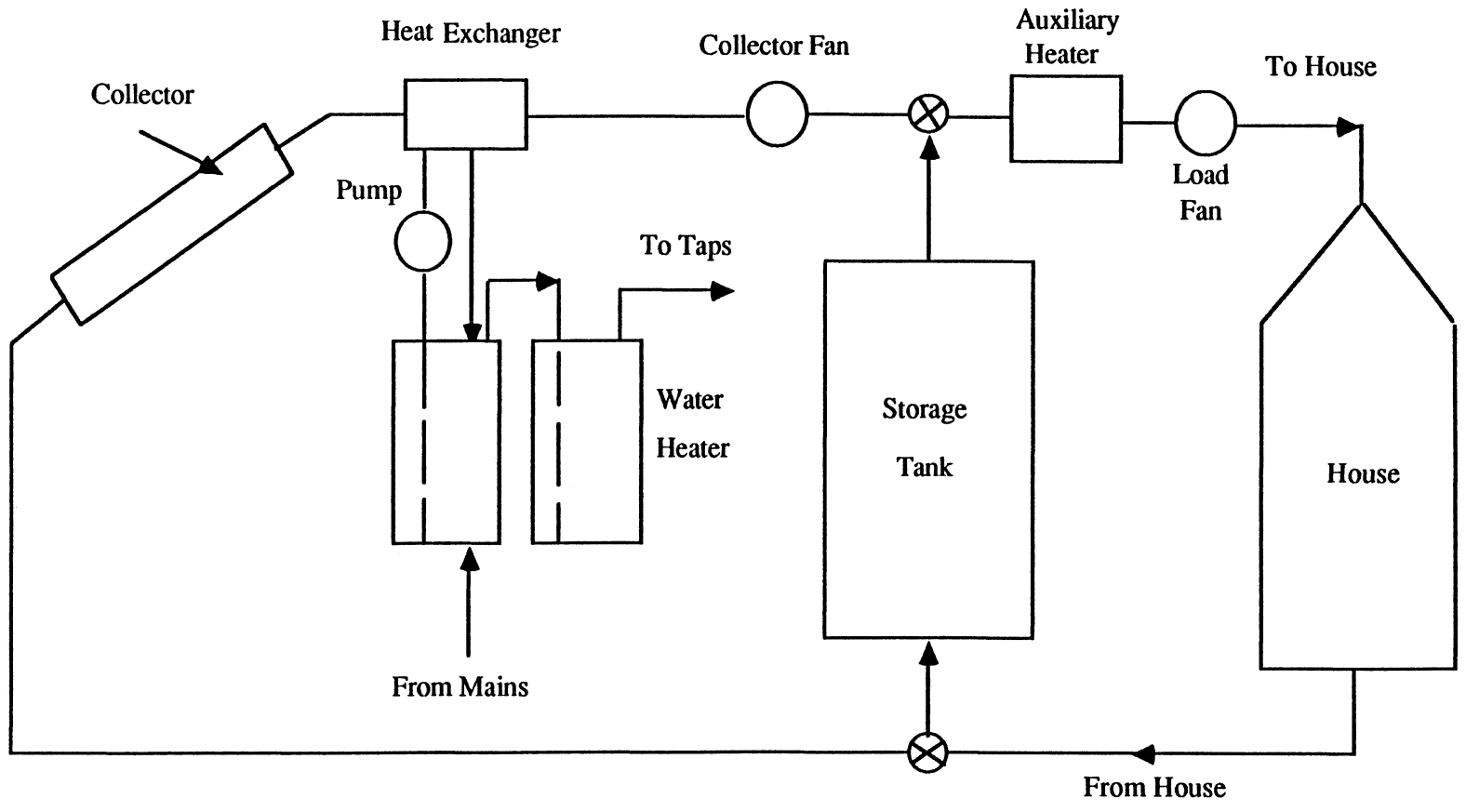

Figure 3.3 Schematic Representation of the Standard Solar Air Heating System.

Table 3.1 Air-Based System Parameters

Collector	
Number of glass covers	2
Product of extinction coefficient and thickness of each glass cover	0.037
Refractive index	1.526
Collector plate absorptance (α)	0.95
Collector emittance (ε)	0.9
Collector efficiency factor (F')	0.7
Back and side losses	1.5 kJ/h m^2 K
Mass flow rate per unit collector area	44 kg/h m^2
Glazing spacing	0.04 m
Ducts	
The collector circuit pipings and the heating circuit piping are divided into a cold and a hot side , and the following data are the same for both sides.	
Collector circuit pipe (each side)	
Length	20 m
Diameter	0.04 m
Heat loss	20 kJ/h K
Fluid density	1.204 kg/m^3
Fluid specific heat	1.012 kJ/kg K
Ambient temperature	20 °C
Diameter	0.04 m

Table 3.1 (continued)

Heating circuit pipe (each side)	
Length	15 m
Heat loss	15 kJ/h-K
Fluid density	1.204 kg/m^3
Fluid specific heat	1.012 kJ/kg K
Ambient temperature	20 °C
Load	
Load capacitance (MC_P)	20,000 kJ/K
Nominal space heating load (UA)	1000 kJ/h K
Water preheat tank volume	0.35 m^3
Air to water heat exchange effectiveness	0.75
Cold water inlet	15 °C
Set point for hot water	60 °C

3.3.2 Water-Based System

The water-based system simulated in this study is shown in Figure 3.4, and system parameters are listed in Table 3.2. This system differs from air-based system in that the storage unit can be charged and discharged simultaneously. This system consists of three independently operating subsystems, i.e. the collector loop, the load, and the domestic hot water system. Whenever solar energy is available, it is collected and transferred to the storage unit. Whenever a space heating load is present, it is met by the storage unit and the auxiliary energy source. The domestic hot water system takes energy from the storage unit when it is necessary. Relief valves are shown for dumping excess energy.

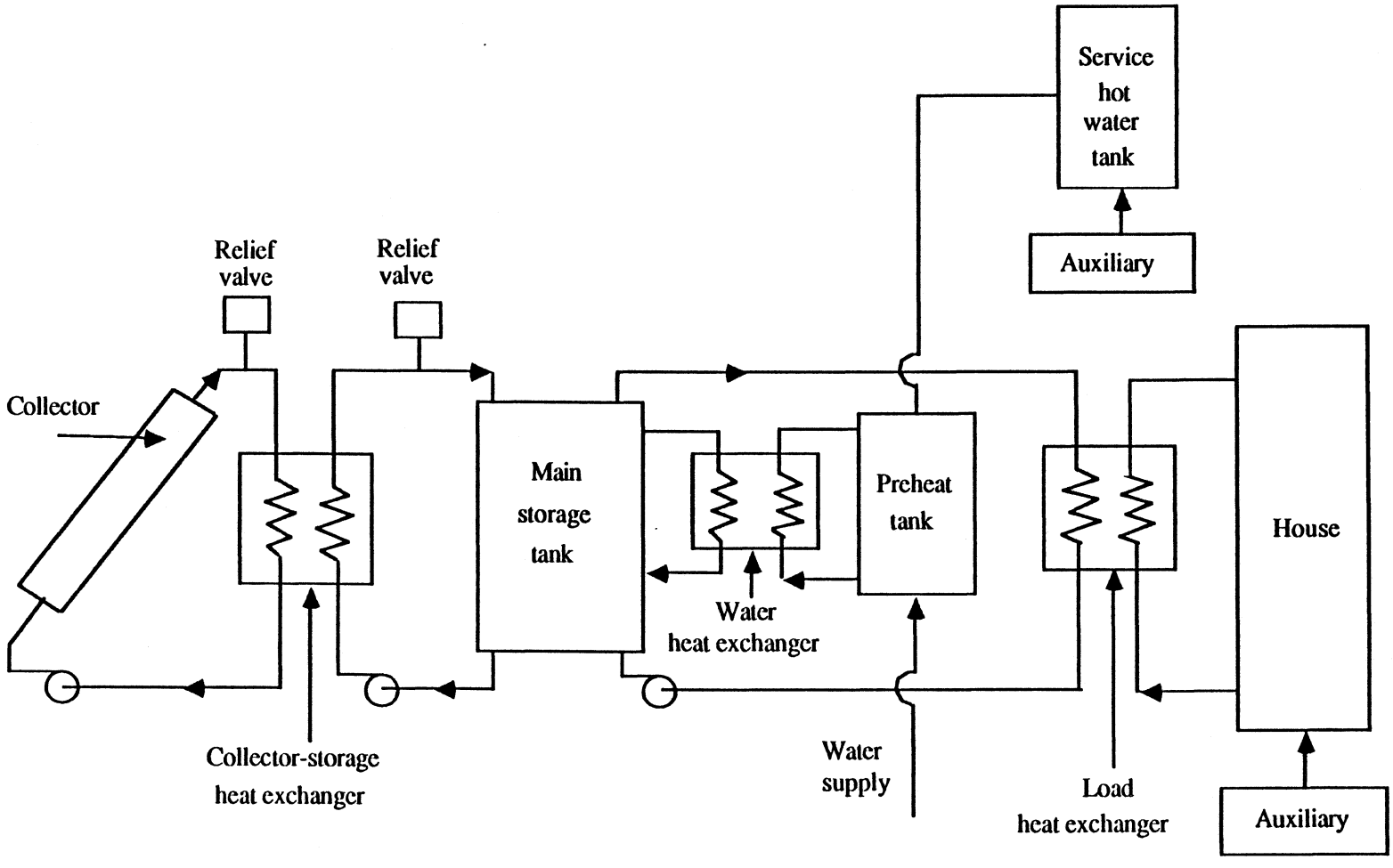

Figure 3.4 Schematic Representation of Solar Water Heating System.

Table 3.2 Water-Based System Parameters

Collector	
Number of glass covers	2
Product of extinction coefficient and thickness of each glass cover	0.037
Refractive index	1.526
Collector plate absorptance (α)	0.95
Collector emittance (ε)	0.9
Collector efficiency factor (F')	0.9
Back and side losses	1.5 kJ/h m^2 K
Mass flow rate	50 kg/h m^2
Piping	
The collector circuit piping and heating circuit piping are divided into a cold side and a hot side, and the following data are the same for both sides.	
Collector circuit pipe (each side)	
Length	20 m
Diameter	0.05 m
Heat loss	18 kJ/h K
Fluid density	1000 kg/m^3
Fluid specific heat	4.197 kJ/kg K
Ambient temperature	20 °C
Heating circuit pipe (each side)	
Length	15 m
Diameter	0.05 m
Heat loss	10.8 kJ/h K
Fluid density	1000 kg/m^3
Fluid density	1000 kg/m^3

Table 3.2 (continued)

Fluid specific heat	4.197 kJ/kg K
Ambient temperature	20 °C
Preheat tank	
Volume	0.35 m^3
Thermal loss	1.5 kJ/h m^2 K
Shape	H/D = 1
Cold water inlet temperature	15 °C
Ambient temperature	20 °C
Set point for hot water	60 °C

3.4 Results and Discussion

In the following a discussion of the results obtained using the present detailed model. Also, a comparison was made between these results and the corresponding results obtained using the infinite NTU model of Morrison et al. [26]. In the following analysis, when axial conduction is considered it will be called the one-dimensional (1D) finite NTU model, and when both axial and radial conduction are considered, it will be called the two-dimensional (2D) finite NTU model. Air and water-based solar heating systems utilizing three different PCMs were investigated. Sodium sulphate decahydrate ($Na_2SO_4 \cdot 10H_2O$), Sunoco's P116 paraffin wax, and medicinal paraffin were selected for this study. The first material represents salt hydrates and the other two materials represent waxes. The first two materials were studied by Morrison et al. [26]. The third was chosen because it has a semi-congruent melting behavior over a finite temperature range [40 - 44 °C]. The thermal properties of the storage media used in the present work are given in Table 3.3.

Table 3.3 Thermal Properties of the Storage Media [1]

Properties	P116 Wax	Medicinal Paraffin	$Na_2SO_4 \cdot 10H_2O$	Rock
c_s (kJ/kg K)	2.89	2.3	1.92	0.84
c_l (kJ/kg K)	+++	2.2	3.26	---
k_s (kJ/m h K)	0.5	0.5	1.85	0.45
k_l (kJ/m h K)	+++	2.1	+++	---
T_{m1} (°C)	46.7	40	32	---
T_{m2} (°C)	+++	44	+++	---
h_{sl} (kJ/kg)	209	146	251	---
ρ_s (kg/m^3)	786	830	1460	2400
ρ_l (kg/m^3)	+++	+++	1330	---

+++ assumed equal to corresponding value for solid phase

3.4.1 Air-Based System

The effect of storage capacity on system performance for air-based system using P116 wax is shown in Figure 3.5. These results were obtained from one week of simulation starting January 1 in Albuquerque (New Mexico). Figure 3.5 shows the difference between the present finite NTU model, and the infinite NTU model used by Morrison et al. [26] for the parameters values investigated.

As seen from Figure 3.5, almost the same results were obtained for both one and two-dimensional finite NTU models. Also, there is a little difference between the finite

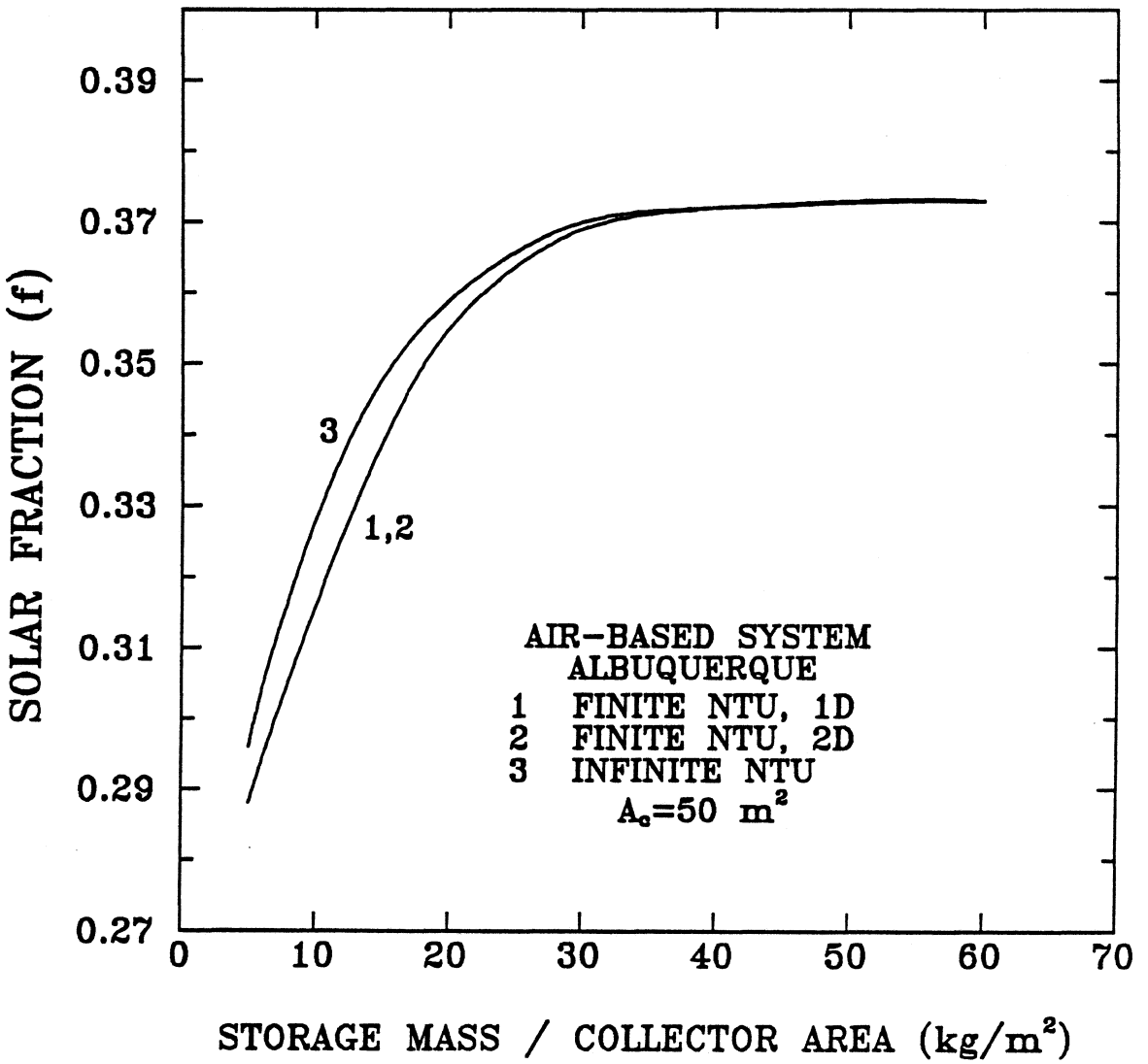

Figure 3.5 Variation of Solar Fraction with Storage Mass for P116 Wax (One Week Simulation Starting January 1).

and infinite NTU results. This difference is not more than 2% of the load at the smallest storage mass used 5 kg/m^2 (corresponding to NTU=1). As storage capacity increases (which increases the value of NTU for the finite NTU model), this difference becomes smaller and approximately disappears completely at storage capacities above 40 kg/m^2 (corresponding to NTU=8). These results indicate that, for air-based systems, the infinite NTU can be used with a very small error taking advantage of its huge decrease in computational cost in comparison with the finite NTU model. Further results were obtained for air-based system using the infinite NTU model. The pebble bed used the same computer program as used for PCES by setting the material melting temperature arbitrarily high, so that all energy stored is in the form of sensible heat. For sensible heat storage with the infinite NTU assumption, the model reduces to that developed by Hughes et al. [50]. The following results are generated using one year simulation in Albuquerque.

Figures 3.6, and 3.7 show the variation of solar fraction with storage mass and storage volume for sodium sulphate decahydrate, P116 wax, and medicinal paraffin. At a solar fraction equal to 0.85, Morrison et al. recommend storage capacities of 12 kg/m^2, 16 kg/m^2, 118 kg/m^2 for $Na_2SO_4 \cdot 10H_2O$, paraffin wax, and pebble bed storage, respectively. A system using sodium sulphate and wax will require only 17% and 41% of the storage volume of a pebble bed system to achieve the same system performance.

At the same solar fraction (0.85), the values resulting from the more detailed model in this study are 14 kg/m^2, 17 kg/m^2, 23 kg/m^2, and 125 kg/m^2 for sodium sulphate decahydrate, P116 wax, medicinal paraffin, and pebble bed, respectively. The present storage capacities are higher than those indicated by Morrison et al. for sodium sulphate and paraffin wax due to the effect of energy losses from the storage unit which had been taken into consideration in the present model. The storage volume required for medicinal

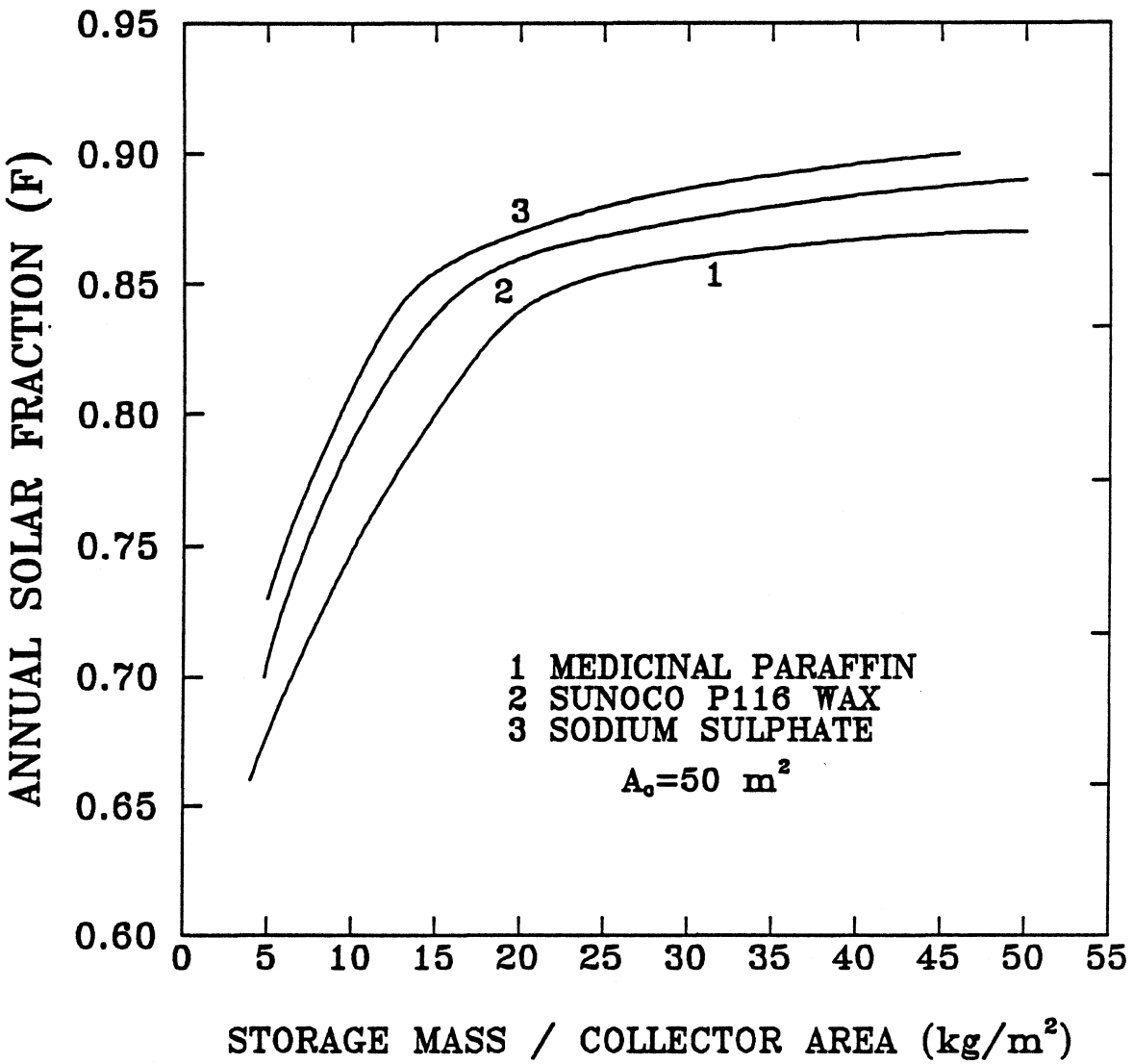

Figure 3.6 Variation of Annual Solar Fraction with Storage Mass for Air-Based System in Albuquerque.

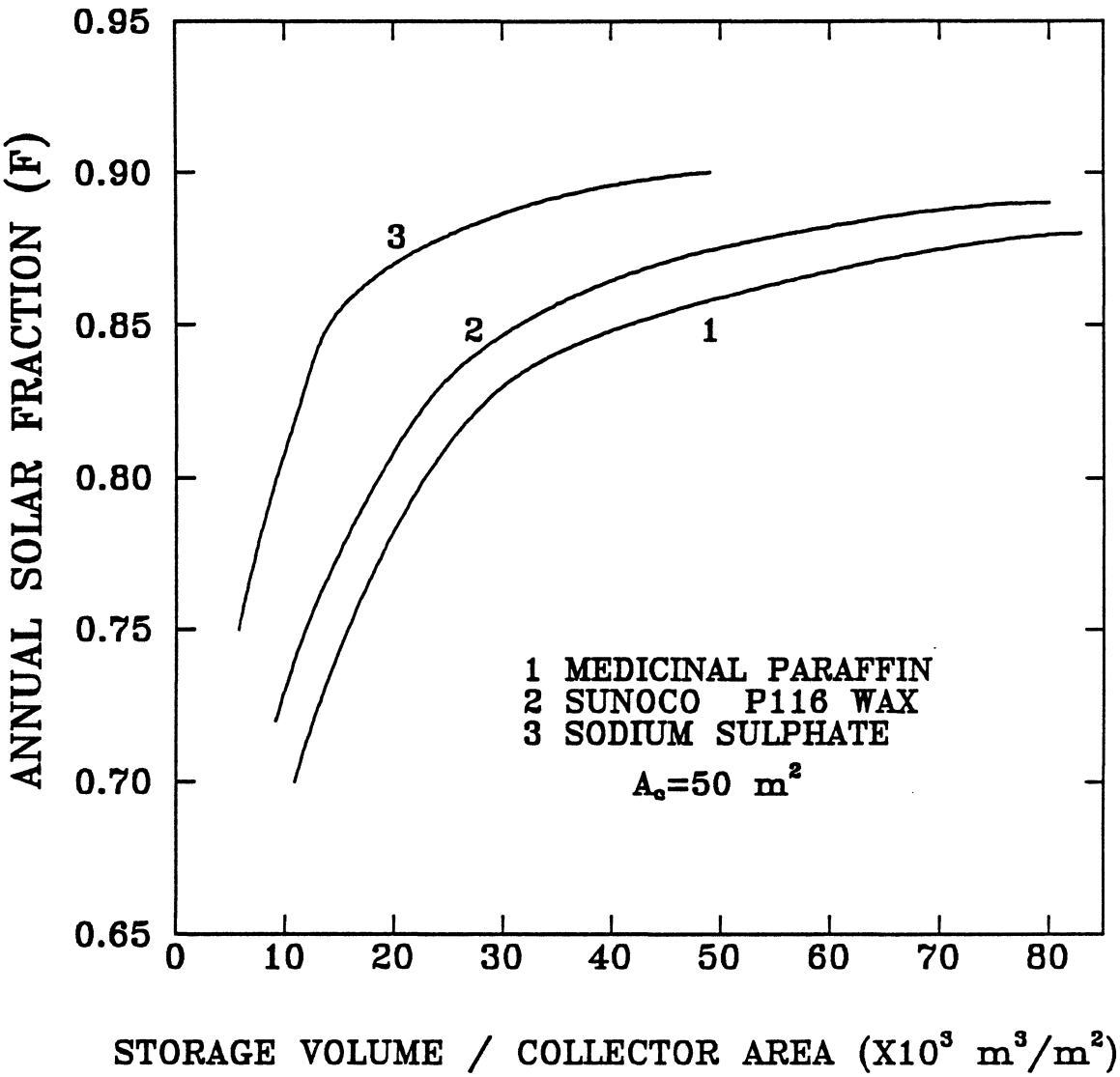

Figure 3.7 Variation of Annual Solar Fraction with Storage Volume for Air-Based System Utilizing Sensible and Latent Heat in Albuquerque.

paraffin is larger than the storage volumes required for sodium sulphate and paraffin wax because it has the lowest latent heat (146 kJ/kg) and a relatively high melting temperature(40-44 °C). Systems using sodium sulphate, P116 wax, and medicinal paraffin will require roughly 19 %, 42 %, and 53 % of the storage volume of sensible heat system using pebbles in order to achieve the same system performance. These results indicate the advantage of using phase-change materials as energy storage media. The results presented here are based on ideal behavior of the PCM, because such phenomena as property degradation, supercooling, and crystallization are not accounted for.

3.4.2 Water-Based System

For water-based system, a parametric study for energy stored was conducted first because significant differences between the finite and infinite NTU models were expected due to the relatively large heat capacity of water. Figure 3.8 shows the variation of fluid outlet temperature with time for P116 wax at different values of NTU. This figure had been generated during the heating mode only assuming constant inlet fluid temperature (T_{fi}) of 80 °C. As NTU increases at a given time, the outlet fluid temperature becomes smaller i.e. more heat is removed from the fluid and consequently more heat will be stored in the material. This figure shows that there is a significant difference between the finite and infinite NTU model.

Figure 3.9 shows the variation of stored energy with time for P116 wax. There is little difference between the finite NTU model 1D, and the finite NTU model, 2D but still there is a significant difference between the values of stored energy obtained using the infinite NTU model and the finite NTU model (about 36 %).

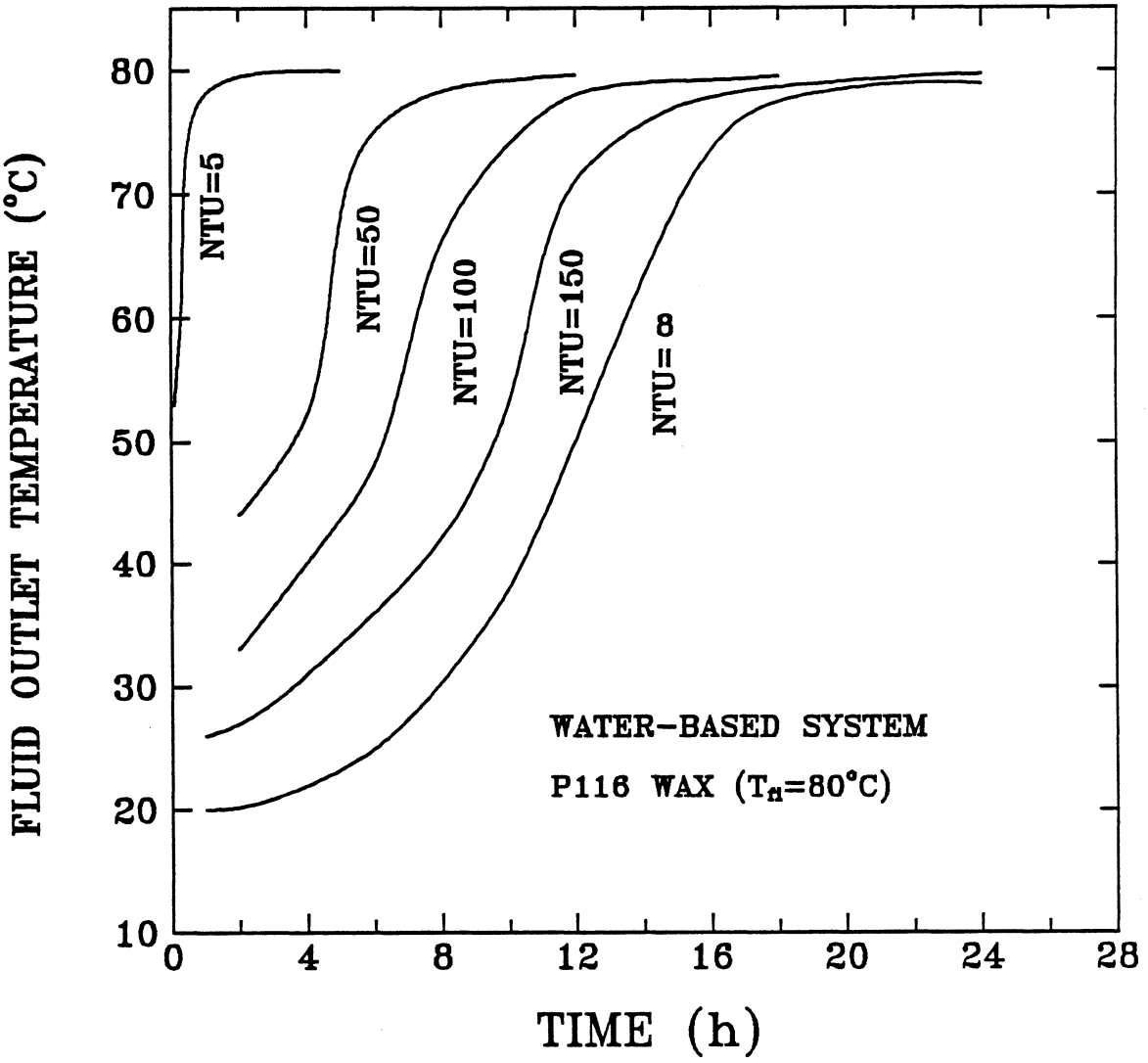

Figure 3.8 Variation of Outlet Fluid Temperature with Different Values of NTU for P116 Wax.

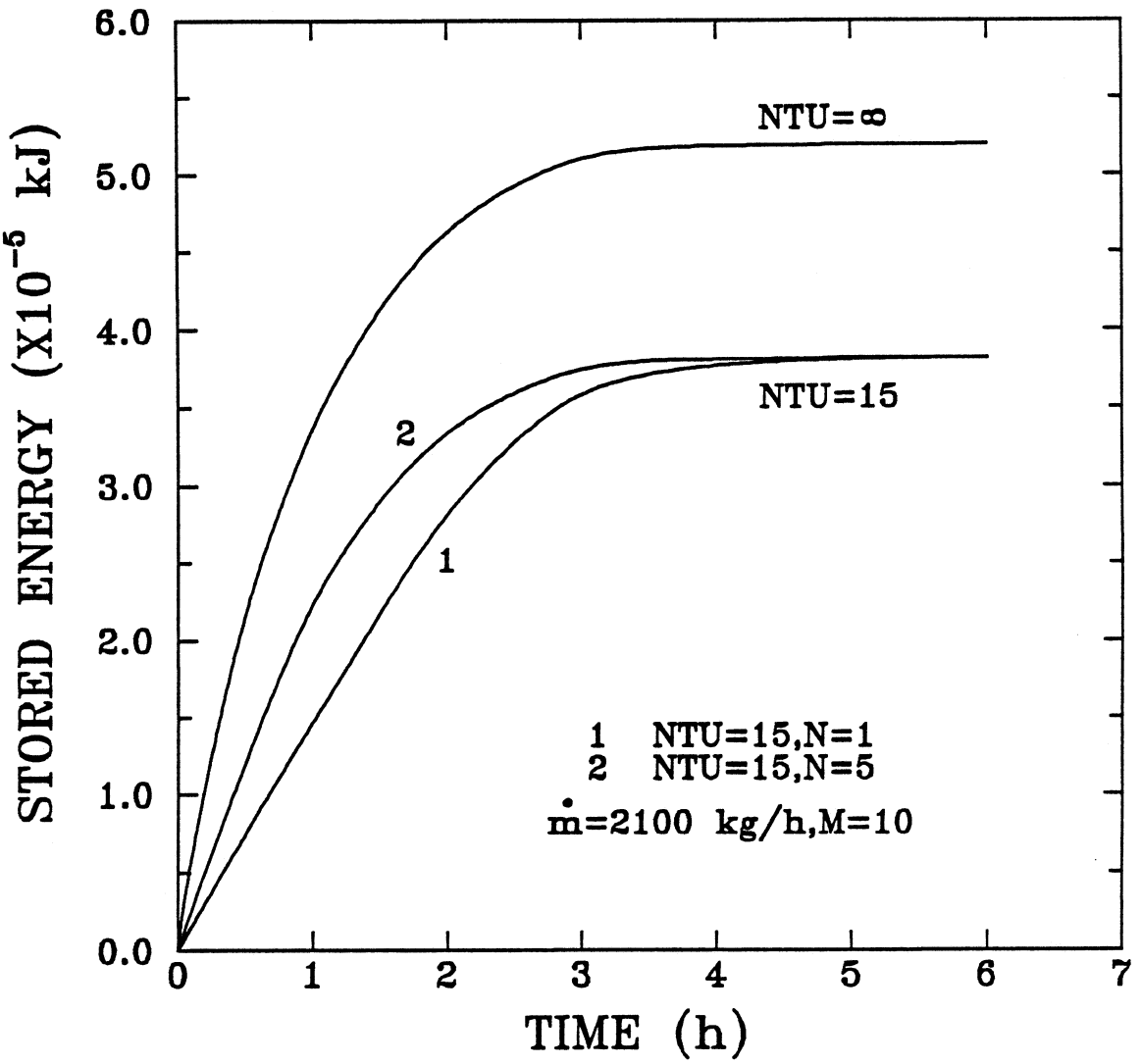

Figure 3.9 Variation of Stored Energy with Time for P116 Wax (Water-Based System).

A comparison was made between using finite NTU, 1D, and finite NTU, 2D in Figure 3.10 for P116 wax. As seen from the figure, the 2D model gives slightly better results and the difference between the two models becomes smaller as NTU increases, and disappears for NTU values above 300. This behavior is due to many factors such as the mass flow rate, system size, inlet fluid temperature, heat transfer coefficient between the fluid and material surface, fluid temperature distribution, and storage material temperature distribution. Since the stored energy in the material depends on the area under the temperature vs. distance curve, the result for the more accurate 2D case is due to the increase in this area when considering temperature gradients in the storage material.

Figure 3.11 shows the variation of the storage material temperature with the radial distance for P116 wax for different times of heating the storage unit [T_{fi}=80 °C, and $\dot{m}$=2100 kg/h]. This figure shows that the area under the curves is larger for the 2D case.

To study the effect of different models on the values of storage masses, the standard water-based system shown in Figure 3.4 was simulated, using both PCES and a stratified conventional water tank (5 nodes) for the main storage tank. The simulations were run for one week starting January 1, in Albuquerque. To examine this effect, consider a solar fraction of 0.65. From Figure 3.12, the recommended storage masses per unit collector area are 13.6 (0.025), 16 (0.029), and 16.8 kg/m^2 (0.031 m^3/m^2) for infinite NTU model, finite NTU (2D), and finite NTU model (1D), respectively. So, the use of infinite NTU model of Morrison et al. will give an error in the recommended storage mass value of about 15%, whereas the difference between finite 1D, 2D models values is roughly 5 %. An accurate examination of the water-based system can be obtained only using the detailed solution, i.e. the finite NTU (2D) model. The approximation of infinite NTU model (unlike in the air-based system) gives a significant error in the determination of the recommended storage masses.

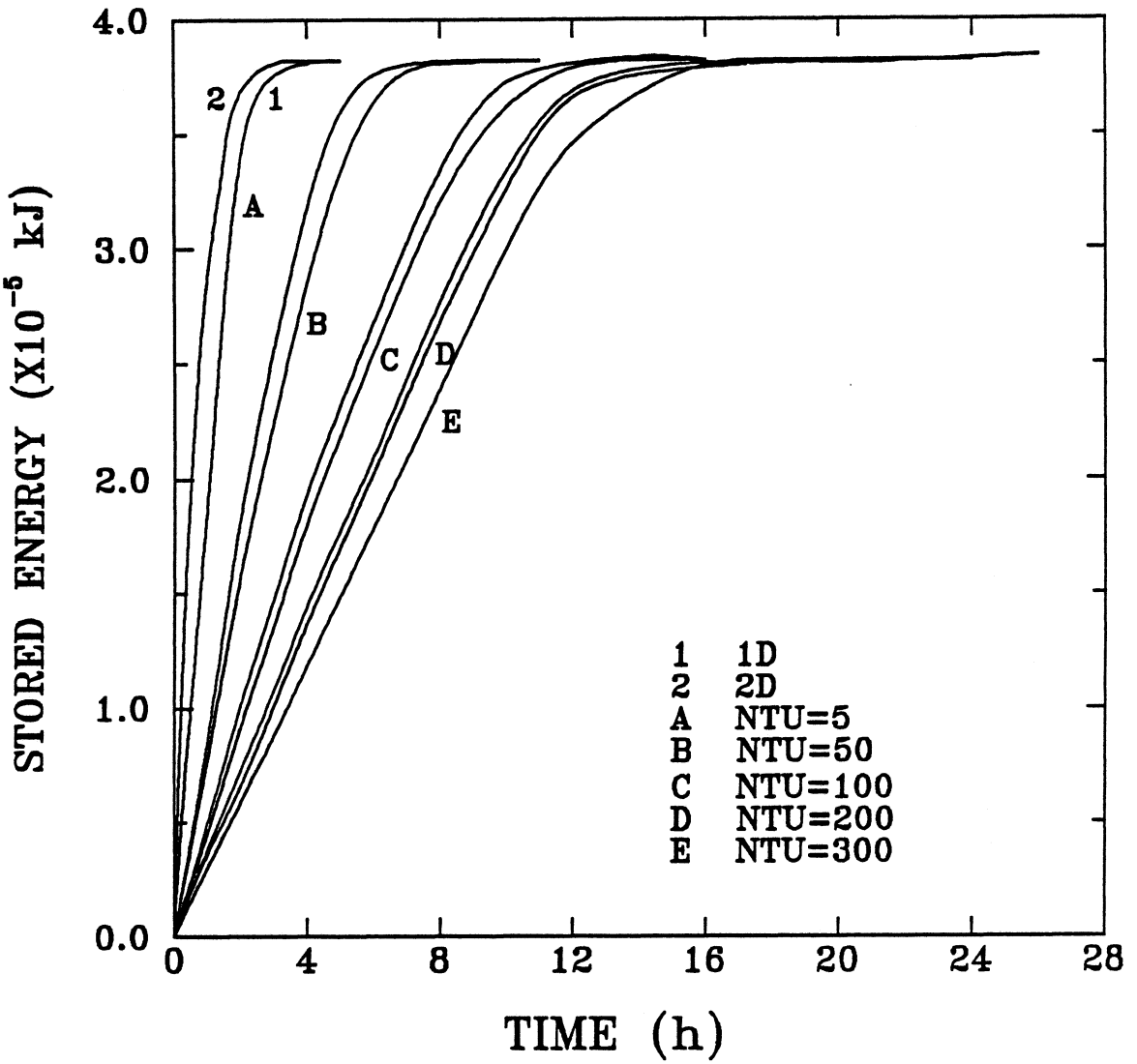

Figure 3.10 Comparison Between 1D, 2D for P116 Wax (Latent Heat Storage) with Water-Based System.

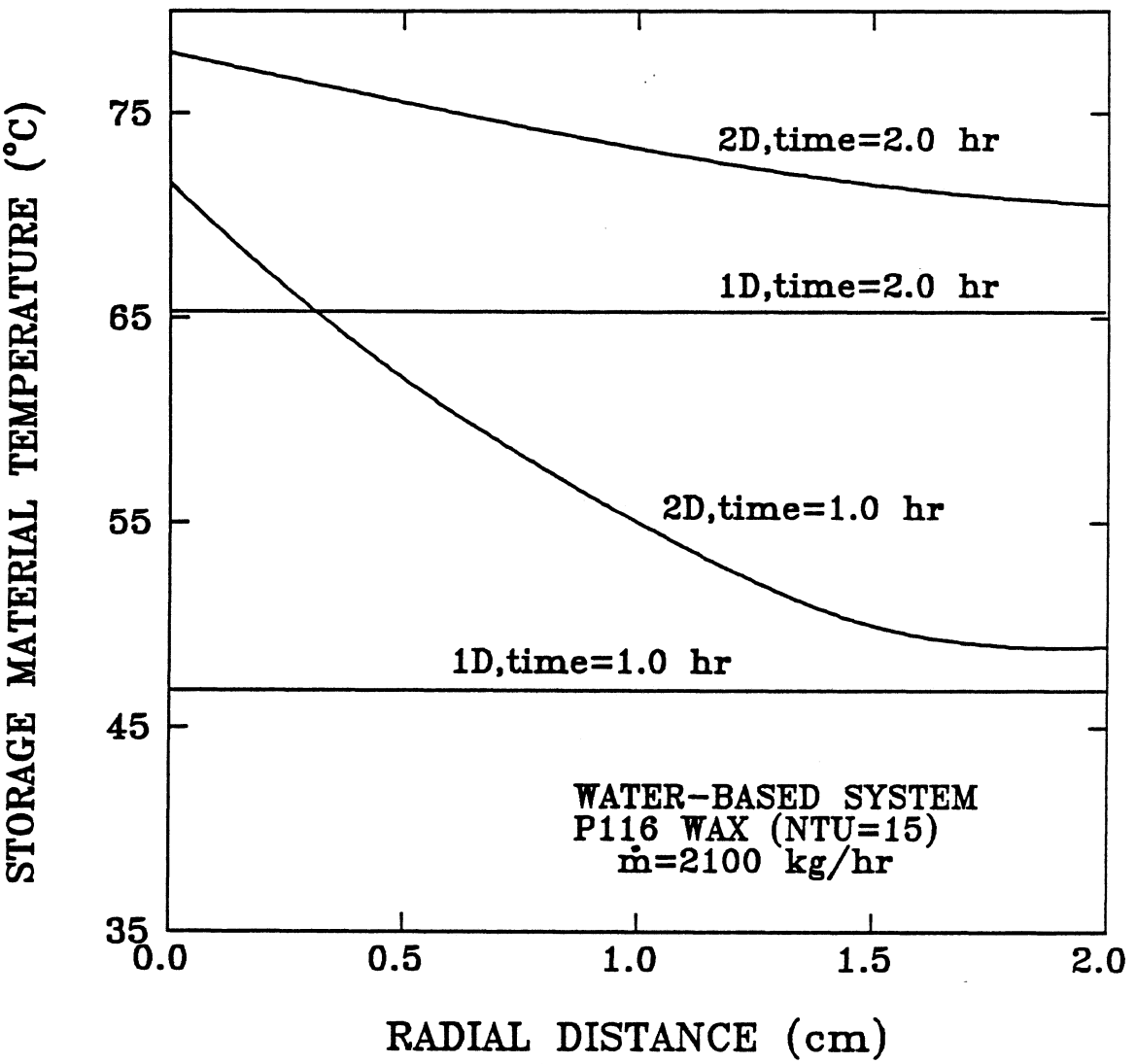

Figure 3.11 Variation of Storage Material Temperature with Radial Distance (Measured from Material Surface).

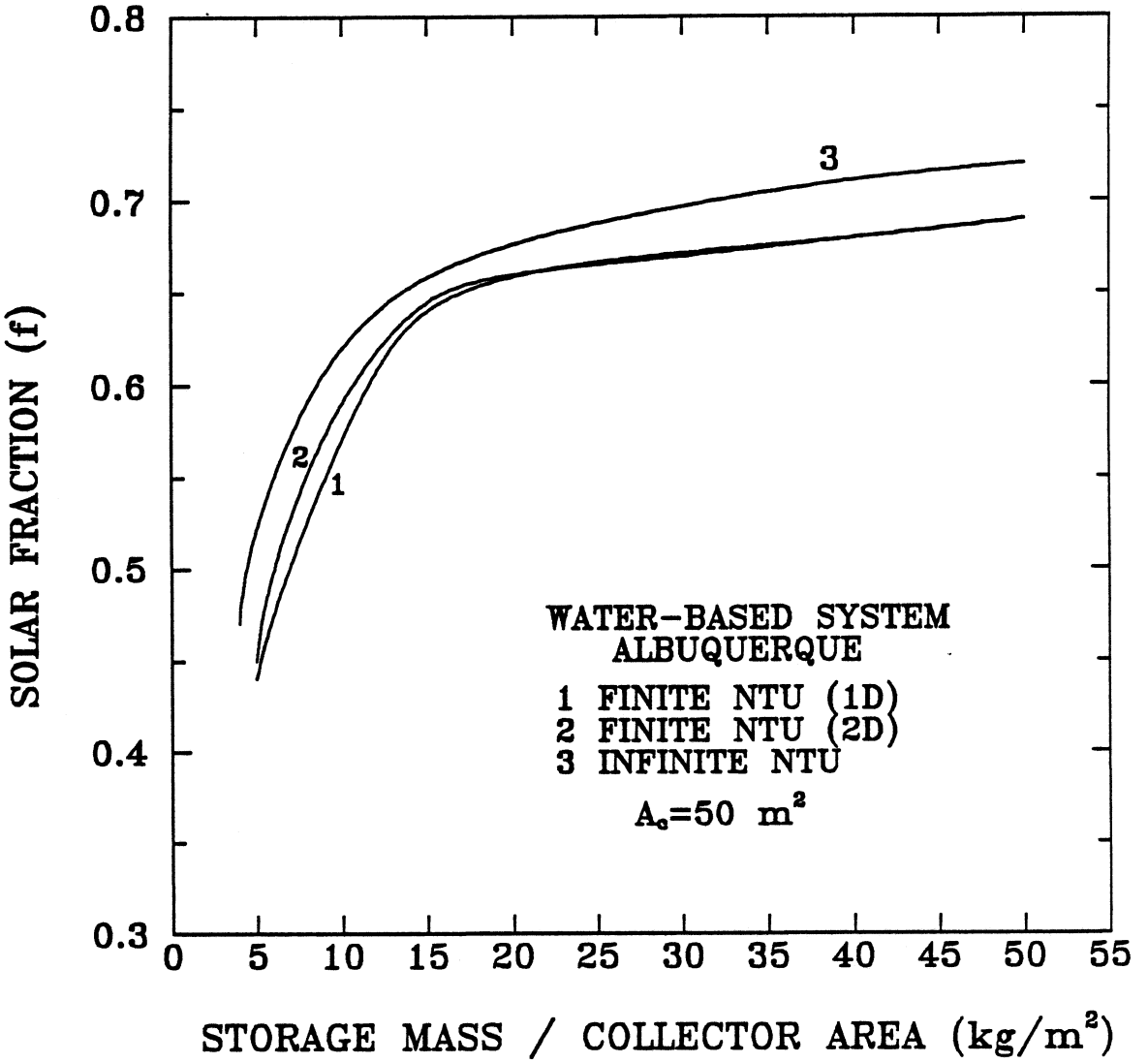

Figure 3.12 Variation of Solar Fraction with Storage Mass for P116 Wax (One Week Simulation Starting January 1).

Figure 3.13 shows the variation of solar fraction with storage volume for water tank, P116 wax, and sodium sulphate decahydrate. Here, the reduction in storage volume is not so pronounced as the case of air-based system. For example a solar fraction of 0.65 can be realized by using a sodium sulphate with a storage volume of 0.014 m^3/m^2 (14 kg/m^2) or a paraffin wax with a storage volume of 0.029 m^3/m^2 (16 kg/m^2) or a conventional water tank with a storage volume of 0.029 m^3/m^2 (29 kg/m^2) i. e., the required storage volume of sodium sulphate is roughly 50 % of the storage volume required by a conventional water tank to realize the same system performance. For paraffin wax, the storage volume required is approximately the same as required by a conventional water tank. So even with liquid-based system, the use of phase-change material can result in a decrease in the storage volume but not nearly as large as in the air-based system. The recommended value for the storage volume for P116 wax (i.e., the value of the storage volume above which there is no significant increase in system performance) which is equal to 0.03 m^3/m^2 for air-based system is approximately equal to the recommended value for water-based system (0.029 m^3/m^2). The recommended storage volume does not depend on system configuration (i. e., air or water-based system) for any of the materials studied.

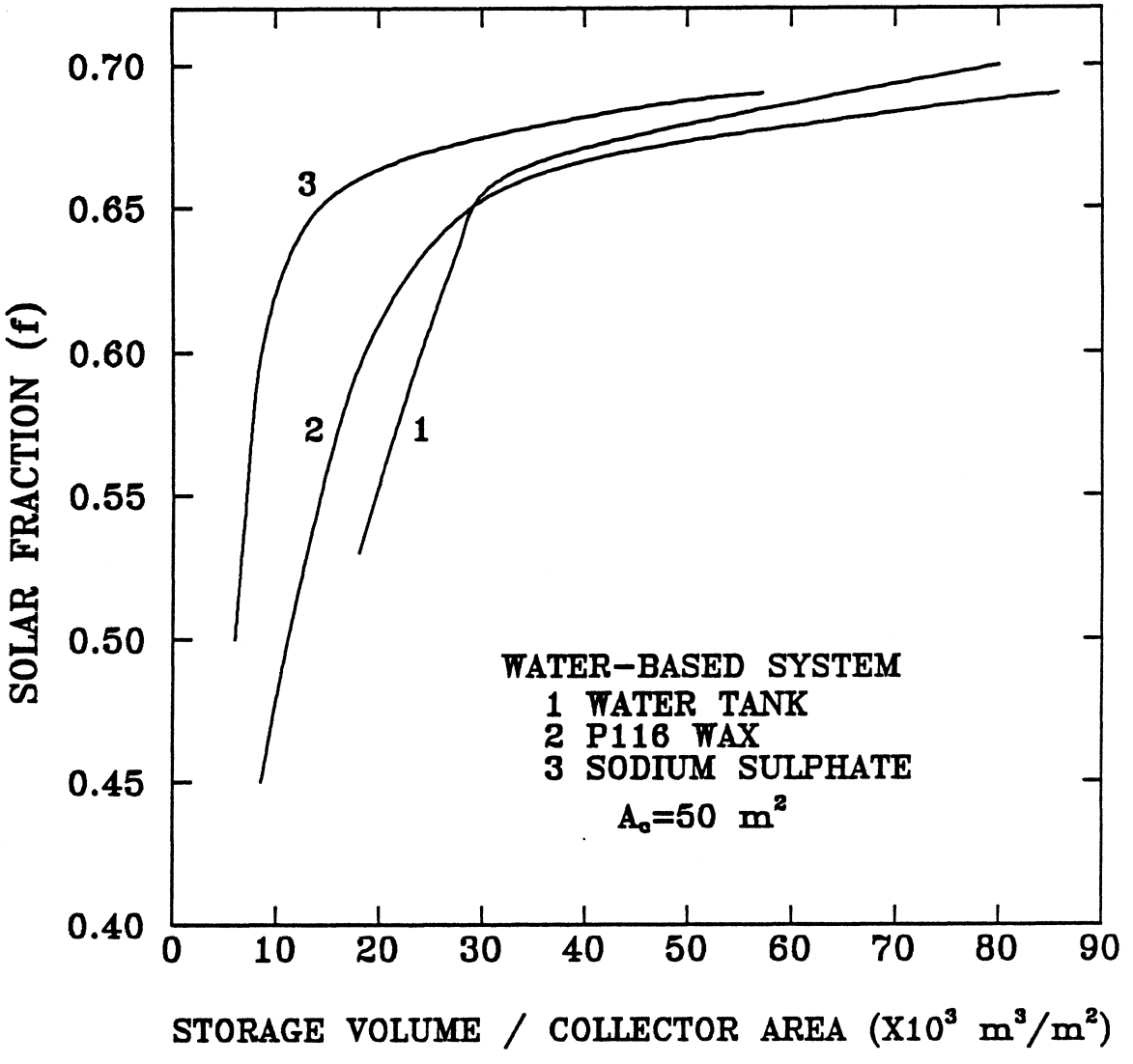

Figure 3.13 Variation of Solar Fraction with Storage Volume for Sensible and Latent Heat Storage Media in Albuquerque, NM.

CHAPTER 4
THE EFFECT OF PHASE-CHANGE MATERIAL PROPERTIES ON THE PERFORMANCE OF SOLAR AIR-BASED HEATING SYSTEMS

4.1 Introduction

Considerable attention has been devoted to the development of phase-change energy storage (PCES) units for solar heating and cooling systems. This work has been motivated by the significant reduction in storage volume which can be achieved with phase-change energy storage (PCES) compared to sensible heat storage, especially with air-based systems. The melting temperature and latent heat of the phase-change material (PCM) characterize the PCES substance. The effects of phase-change material melting temperature and latent heat have been studied by Jurinak et al. [28,29]. Their results are based on a heating season simulation from October 1-May 1 in Madison (Wisconsin). Their main conclusion was that it is important to select the PCM on the basis of its melting temperature, rather than its latent heat, i.e., the melting temperature has a significant effect on system performance.

There are many factors which affect system performance such as, the average temperature of the storage unit, the fraction of time that the storage unit is charged (collector to store mode), the fraction of time that the storage unit is discharged (store to load mode), the fraction of time that the storage unit is isolated (collector to load mode), and the fraction of total time that the storage unit operates in the liquid phase mode. These factors depend primarily on the amount of incident solar energy relative to the

heating load. To determine the effect of thermal properties on system performance, a simulation study must be conducted for different ratios of incident solar energy to heating load and a variety of climate types.

In this chapter the effect of melting temperature and latent heat for different storage masses on solar system performance for different ratios of incident solar energy to heating load was studied for seven different locations. Finally, a comparison between the performance of solar heating systems utilizing industrial grade and pure paraffins was conducted.

The effect of PCES on the performance of water-based systems was examined in Chapter 3. It was found that, compared to sensible heat storage with water, there were no significant gains in using PCES with water-based systems. The effect of using different theoretical models on the performance of solar heating systems was also examined before [51]. It was found that, with air-based systems, little error in the calculated system performance results from the use of the simplified infinite NTU model of Morrison et al. [26] after taking heat losses from the storage unit into consideration. The analysis in this chapter will be limited to air-based systems utilizing PCES with the infinite NTU model. Also, the heat losses from the storage unit were not considered since the study in this chapter is a parametric one.

4.2 System Configuration and Control Strategy

The transient simulation program, TRNSYS, is used to determine the performance of the standard solar air space heating system shown in Figure 4.1. The parameters selected for the system components are listed in Table 4.1 The system shown in Figure 4.1 has the same three modes of operation as the standard solar air heating system (Figure 3.3) described in detail in Chapter 3.

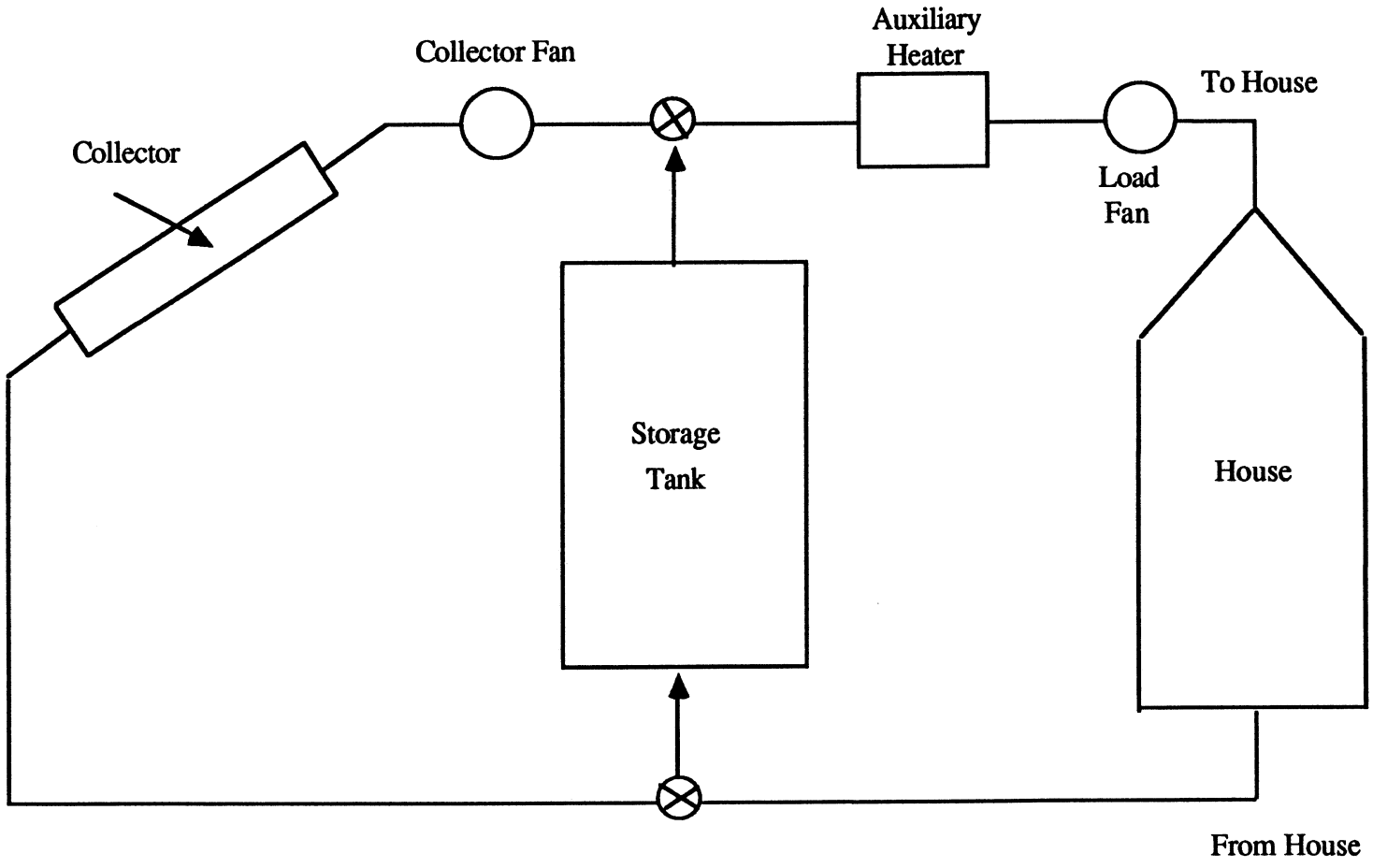

Figure 4.1 Schematic Representation of the Standard Solar Air Space Heating System

Table 4.1 Air-Based Space Heating System Parameters

Collector	
Number of glass covers	2
Product of extinction coefficient and thickness of each glass cover	0.037
Refractive index	1.526
Collector plate absorptance (α)	0.95
Collector emittance (ε)	0.9
$F_R (\tau\alpha)_n$	0.6
$F_R U_L$	12 kJ/h m^2 K
Mass flow rate per unit collector area	44 kg/h m^2
Glazing spacing	0.04 m
Ducts	
The collector circuit pipings and the heating circuit piping are divided into a cold and a hot side, and the following data are the same for both sides.	
Collector circuit pipe (each side)	
Length	20 m
Diameter	0.04 m
Heat loss	20 kJ/h K
Fluid density	1.204 kg/m^3
Fluid specific heat	1.012 kJ/kg K
Ambient temperature	20 °C
Heating circuit pipe (each side)	
Length	15 m
Diameter	0.04 m
Heat loss	15 kJ/h K
Fluid density	1.204 kg/m^3
Fluid specific heat	1.012 kJ/kg K
Ambient temperature	20 °C

4.3 Analysis

A schematic representation of the PCES unit chosen for the present study is shown in Figure 4.2. The storage unit composed of a number of rectangular cross-sectioned channels for the flowing fluid, connected in parallel and separated by the phase-change material (PCM). L and w are the length and the wide of the storage unit, respectively. d_s is the thickness of the storage material between channels.

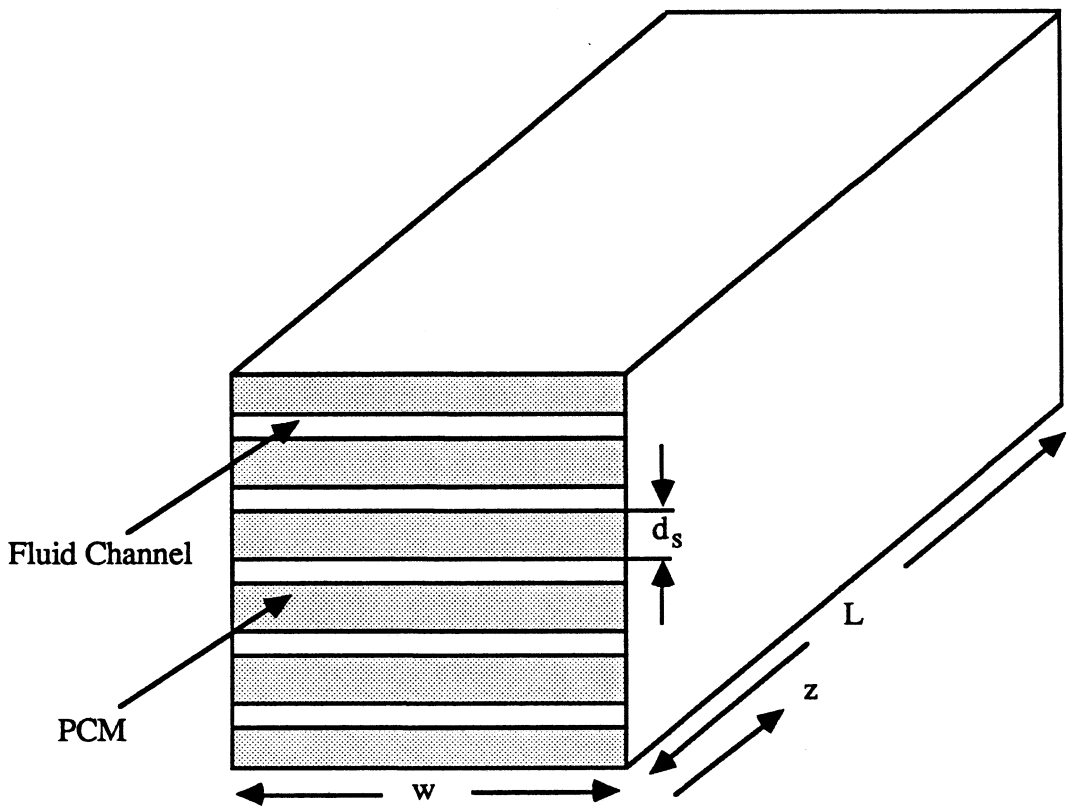

Figure 4.2 Schematic Representation of PCES Unit

Using the approximations made in the infinite NTU model of Morrison et al. for air-based solar heating system, the governing equations for the PCM and the circulating fluid reduce to [26] :

$$\frac{\partial h}{\partial t} = - \frac{\dot{m} c_f}{\rho A} \frac{\partial T}{\partial z} \tag{4.1}$$

and

$$T_f = T \tag{4.2}$$

where T, h, and ρ are the temperature, the specific enthalpy, and the density of the PCM, respectively. A, the cross sectional area of the PCM, is given by

$$A = N_c \, w \, d_s \tag{4.3}$$

where N_c is the number of the fluid channels.

T_f, $\dot{m}$, and c_f are the temperature, the mass flow rate, and the specific heat of the circulating fluid, respectively. t is the time, and z is the direction parallel to the air flow. The relations between the specific enthalpy 'h' and the temperature 'T' are given by equations (3.8). A finite difference technique is used to solve equation (4.1).

4.4 Results and Discussion

Simulations of air-based PCES systems were conducted for Albuquerque (New Mexico), Charleston (South Carolina), Columbia (Missouri), Great Falls (Montana), Madison (Wisconsin), Alexandria (Egypt), Marsa-Matrouh (Egypt), and for two different heating season months (January and March).

The mass flow rate per unit collector area, collector area, heat removal factor-

collector overall loss coefficient product, and system control strategy are assumed to be the same for all the simulations carried out in this study. Simulation results are presented as a function of Y, where

$$Y = A_c F_R (\overline{\tau \alpha}) \overline{H}_T N / L_s \tag{4.4}$$

A_c	is the area of the solar collector (m^2)
F_R	is the collector heat removal factor
$(\overline{\tau \alpha})$	is the collector monthly average transmittance-absorptance product
$\overline{H}_T$	is the monthly average daily radiation incident on the collector surface per unit collector area (kJ/m^2)
N	is the number of days in the month
L_s	is the monthly space heating load (kJ)

The equation for Y can be rewritten in a more convenient form for calculations [19] :

$$Y = F_R (\tau \alpha)_n \cdot \frac{(\overline{\tau \alpha})}{(\tau \alpha)_n} \cdot \overline{H}_T A_c N / L_s \tag{4.5}$$

where, $(\tau\alpha)_n$ is the collector monthly average transmittance-absorptance product at normal incidence. The monthly average daily radiation incident on the collector surface per unit collector area ($\overline{H}_T$) could be calculated from monthly global horizontal data as described in [52], but in this work, $\overline{H}_T$ was calculated by hourly TRNSYS simulations using typical meteorological year (TMY) data for the first five locations. For Alexandria and Marsa-Matrouh, the weather data generator (TYPE 54) included in TRNSYS library

was used to generate the hourly weather data from the monthly weather data available for these two locations [46]. The value of $F_R\ (\tau\alpha)_n$ can be calculated from standard ASHRAE collector tests [53]. The ratio $\frac{(\overline{\tau\alpha})}{(\tau\alpha)_n}$ is approximately 0.94 for a two-cover collector for most of the heating season months when the collector is tilted within 15° of the latitude [19]. The space heating load, for a small thermal capacitance building, is approximately equal to (UA*DD). The loss coefficient-area product (UA) of the building was varied in this study. The number of degree-days in the month, DD, in ° C-days, is calculated in a 18.3 ° C base.

The density, specific heat, and thermal conductivity of the PCM are assumed to be equal to the corresponding values for paraffin wax. A wax was chosen because a member of the paraffin family can be found which melts at any desired temperature. In addition, paraffins do not supercool, do not degrade with repeated cycling, and are generally stable which offsets their disadvantage of having a much lower density than salt hydrates. For space heating applications, the melting temperature is bounded by the room temperature (20 °C) and approximately 50 °C. In the present study melting temperature is varied from 30 °C to 50 °C. The variation of the PCM melting temperature at constant latent heat can be closely approximated by substituting various paraffins. The latent heat of candidate phase-change material varies between 129-289 kJ/kg [7].

Figure 4.3 shows the variation of the solar fraction with melting temperature at different storage masses (10, 20, and 40 kg/m^2) for different values of Y (0.7, 1.0, and 2.0). For values of Y up to 0.6, the melting temperature and latent heat have no effect on the solar fraction. At these low values of Y, the average temperature of the storage unit does not exceed 25 °C for the melting temperature range (30-50 °C) and latent heat range

(129-289 kJ/kg) used in this study, i.e., the PCES unit can be approximated as a sensible store. For values of Y greater than 0.6, the solar fraction decreases with increasing melting temperature because the average temperature of the storage unit increases, increasing the average collector inlet temperature, which decreases the collector efficiency. As seen from Figure 4.3, the optimum melting temperature does not depend on the storage mass and it is equal to the minimum utilization temperature. The minimum utilization temperature of the solar system represents a constraint on the temperature of the airstream supplied to meet the space heating load in order to assure comfort. The minimum solar source airstream temperature must be larger than the minimum utilization temperature to an extent dependent on heat exchanger size.

Changing the melting temperature from 30-50 °C at the nominal latent heat (209 kJ/kg) for the different storage masses used, results in decreasing the solar fraction. This decrease is more pronounced for the values of Y up to 1.0. For example, changing the melting temperature from 30-50 °C at the nominal latent heat, and using a storage mass of 20 kg/m^2 results in decreasing the solar fraction by approximately 2.0, and 2.9% of the load for values of Y equal to 0.7, and 1.0 respectively. These changes represent approximately 5.0% of solar fraction range for each case. At values of Y equal to or greater than 2.0, the effect of melting temperature becomes small. For example, changing the melting temperature from 30-50 °C at the nominal latent heat decreases the solar fraction by 1% of the load for storage mass equal to 20 kg/m^2 (1.2% of the scale).

These results indicate that the melting temperature has a significant effect on the thermal performance of the solar system for values of Y between 0.6 and about 1.0 only. As the value of Y increases above 1.0, the effect of melting temperature becomes smaller. For values of Y equal to or greater than 2.0, the effect of melting temperature on the performance of solar systems can be neglected.

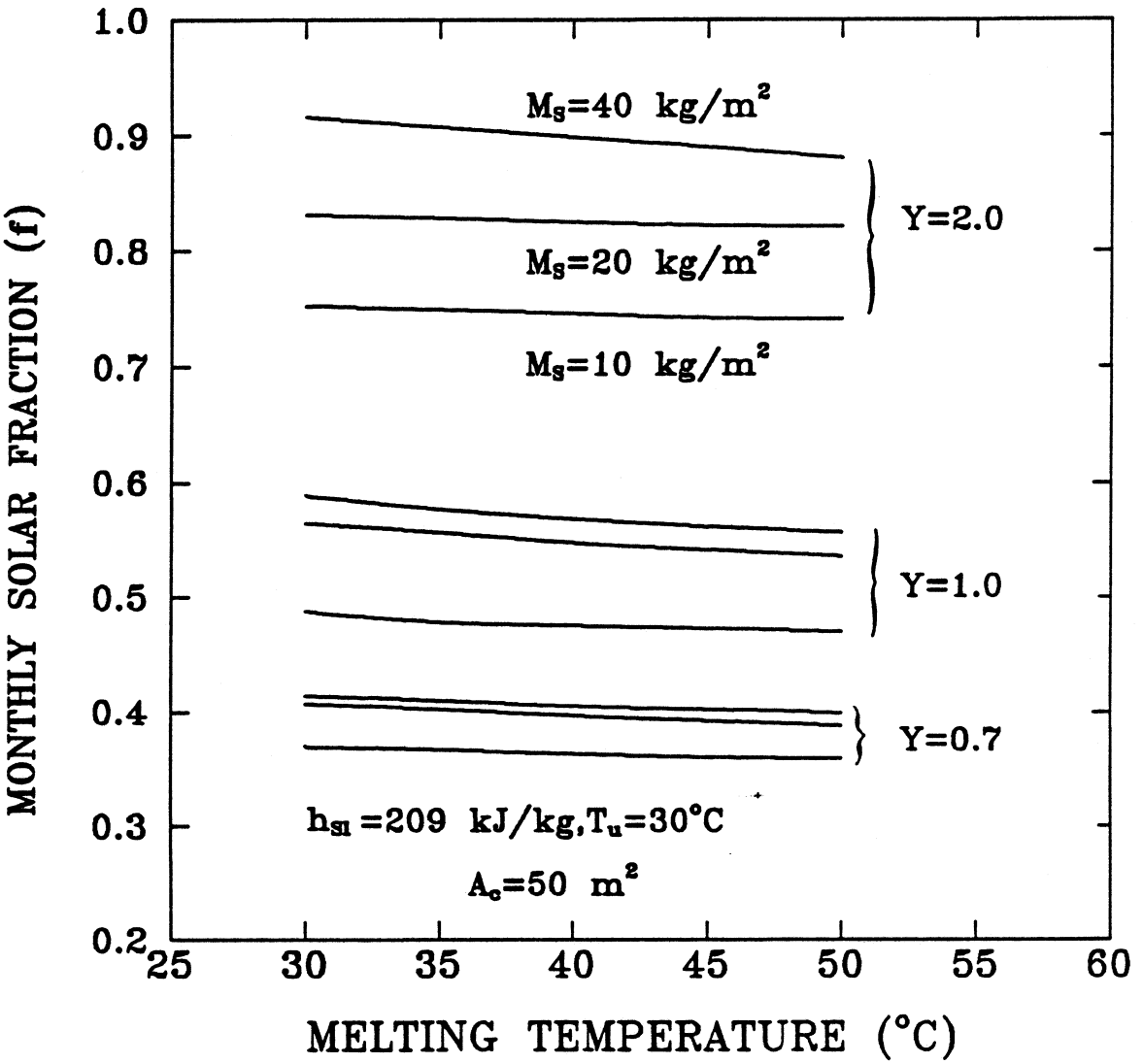

Figure 4.3 Variation of Monthly Solar Fraction with Melting Temperature and Storage Mass.

Figure 4.4 shows the variation of solar fraction with latent heat at different storage masses for different values of Y (0.7, 1.0, and 2.0). As the latent heat increases, the amount of energy stored in the material increases and this subsequently increases the solar fraction. At the smallest storage mass used (10 kg/m^2), the latent heat has a significant effect on the performance of the solar system for all values of Y. For example, at storage mass equal to 10 kg/m^2, and melting temperature equal to the minimum utilization temperature (T_m=T_u=30 °C), increasing the latent heat from its lowest value (129 kJ/kg) to its highest value (289 kJ/kg), increases the solar fraction by 3.2, 4.5, and 7.2% of the load for values of Y equal to 0.7, 1.0, and 2.0, respectively (8.3, 8.9, and 9.2% of the range, respectively). The latent heat has a larger effect on the performance of the solar systems with smaller storage masses. As the storage mass increases, this change becomes less important for values of Y up to 1.0. For values of Y equal to or greater than 2.0, the latent heat becomes significantly important for all storage masses.

To confirm the previous results, the effect of the average temperature of the storage unit, and the fraction of time that the storage unit operates in the liquid phase mode, were studied. At values of Y up to 1.0, the average temperature of the storage unit is on the order of the melting temperature. For values of Y equal to or greater than 2.0, the average temperature of the storage unit is significantly higher than the average temperature of the range used for melting temperature. For example, at melting temperature equal to 30 °C, latent heat equal to the nominal value (209 kJ/kg), and storage mass equal to 20 kg/m^2, the average temperatures of the storage unit are found to be 30, 49, and 57°C for values of Y equal to 1.0, 2.0, and 2.5, respectively. At the same conditions, the fractions of time that the storage unit operates in the liquid phase mode are 0.45, 0.72, and 0.79, respectively. For values of Y equal to or greater than 2.0, the

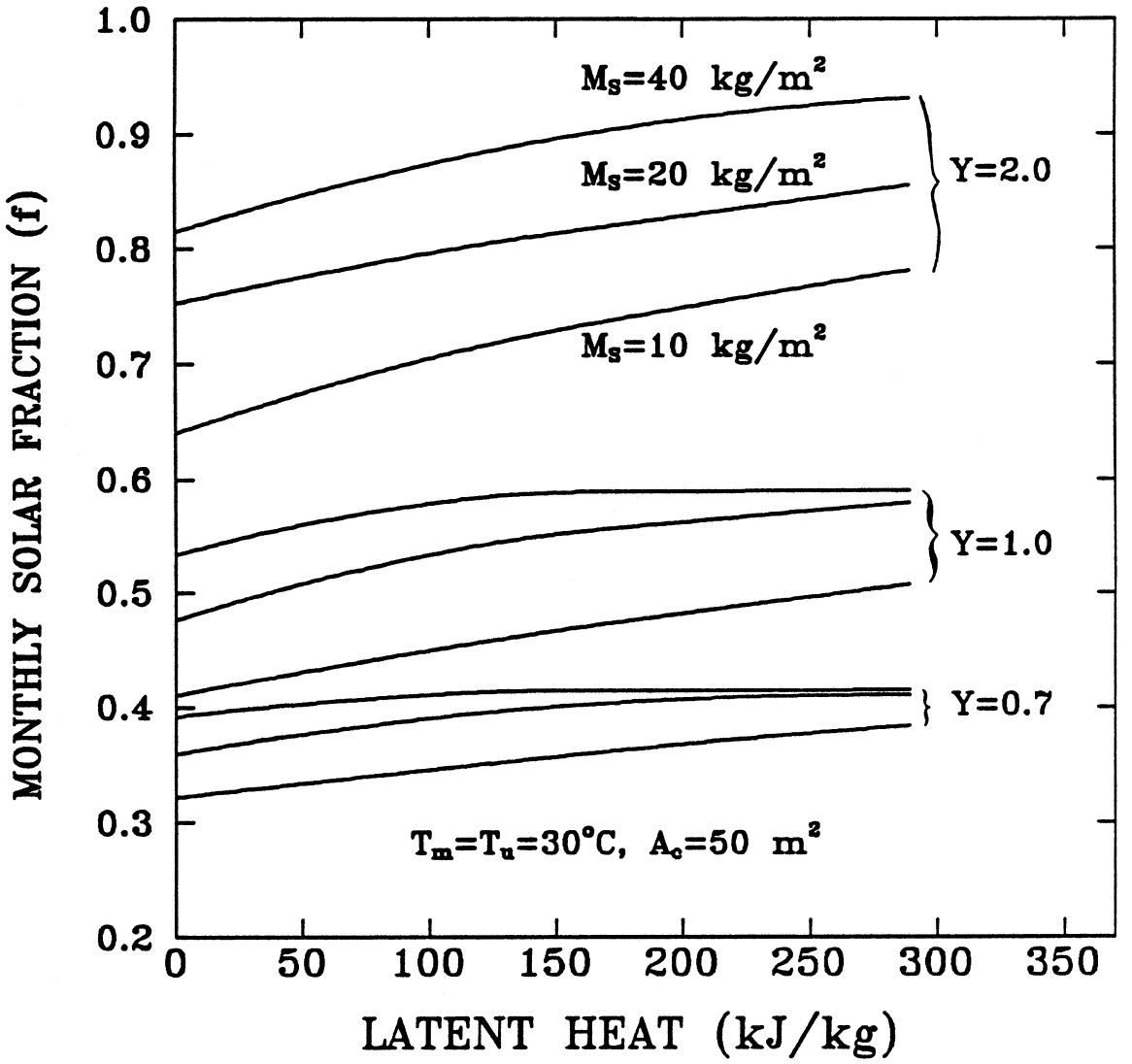

Figure 4.4 Variation of Monthly Solar Fraction with Latent Heat and Storage Mass.

temperature of the storage unit is significantly higher than the average temperature of the range used for melting temperatures, and the storage unit operates most of the time in the liquid phase mode. For these values of Y the melting temperature has no significant effect on the solar fraction.

To compare between the industrial grade and pure paraffins, the industrial grade paraffins were assumed to have a melting temperature bandwidth of 20 °C ($\Delta T=T_{m1}$ - T_{m2} =20 °C, where T_{m1}, and T_{m2} are the lower and upper limits of PCM melting temperature, respectively), i .e. ± 10 °C around the nominal melting temperature. Figures 4.5-4.7 show the variation of the solar fraction for industrial grade (h_{sl}=129 kJ/kg, ΔT =± 10 °C) and pure paraffins (h_{sl}=209 kJ/kg, ΔT = 0 °C), for two values of Y (1.0, and 2.0) at different storage masses (10, 20, and 40 kg/m^2). At storage mass equal to 10 kg/m^2, the use of industrial grade paraffins results in significantly lower solar fraction as seen in Figure 4.5. The difference between industrial grade and pure paraffins becomes smaller as storage mass is increased. At storage mass equal to 40 kg/m^2, similar thermal performance is obtained with both paraffins.

In conclusion, the present results indicate that for solar system design with small values of the ratio of incident solar energy to the heating load (values of Y less than about 1.0), and storage mass greater than 10 kg/m^2, the melting temperature has a greater effect on the thermal performance of the solar system than the latent heat. For these solar system designs, the candidate PCM should be chosen in the basis of its melting temperature only. On the other hand, for solar systems with a high value of the ratio of incident solar energy to the heating load (values of Y equal to or greater than about 2.0), the latent heat of the PCM has a greater effect on the thermal performance of the solar system than does the melting temperature, contrary to the conclusion reached by Jurinak et al.[28,29]. Also, the industrial grade paraffins (with h_{sl}=129 kJ/kg, and melting

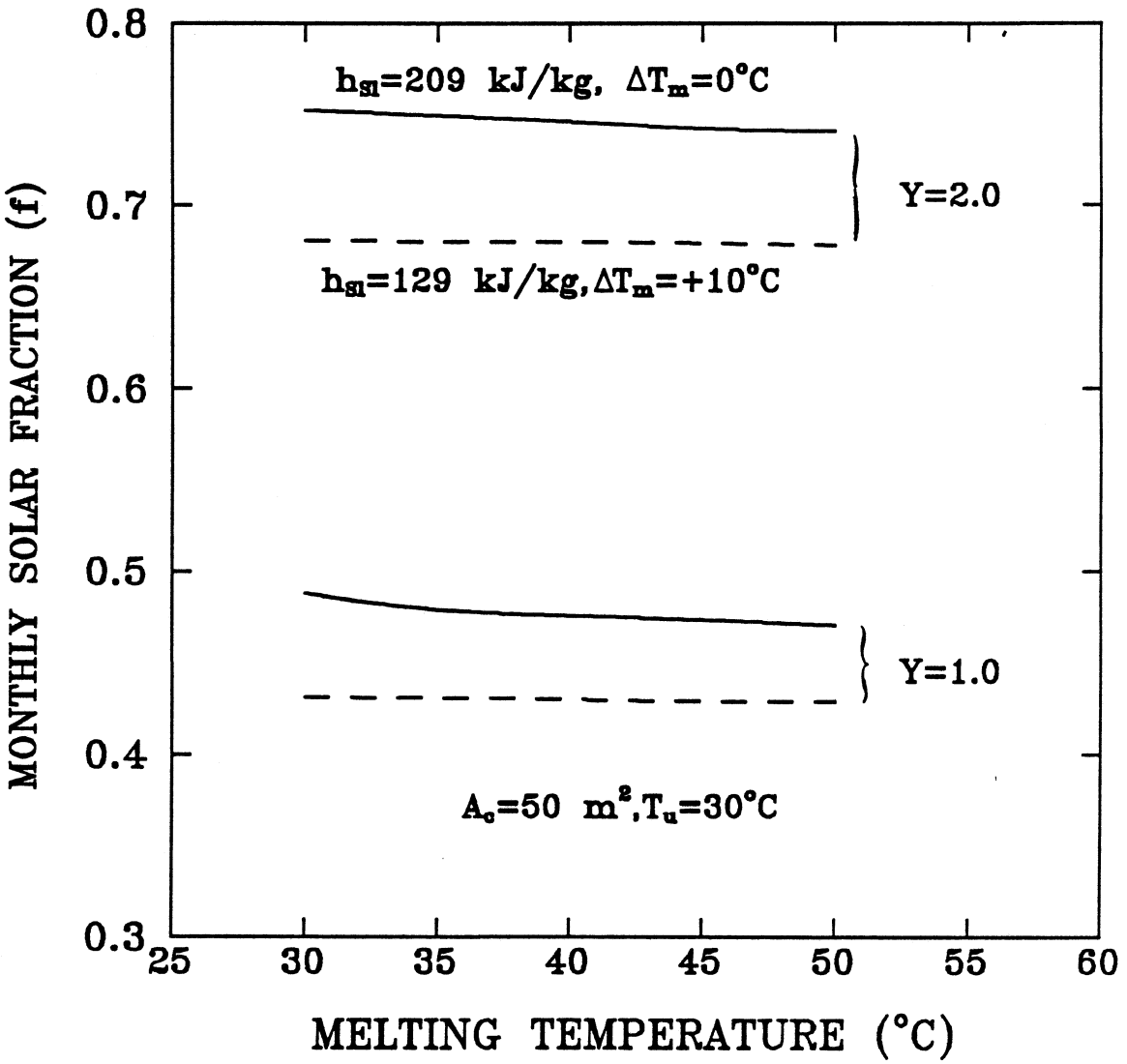

Figure 4.5 Comparison of the Monthly Solar Fraction of Solar Heating Systems Utilizing Industrial Grade and Pure Paraffins (M_S=10 kg/m^2).

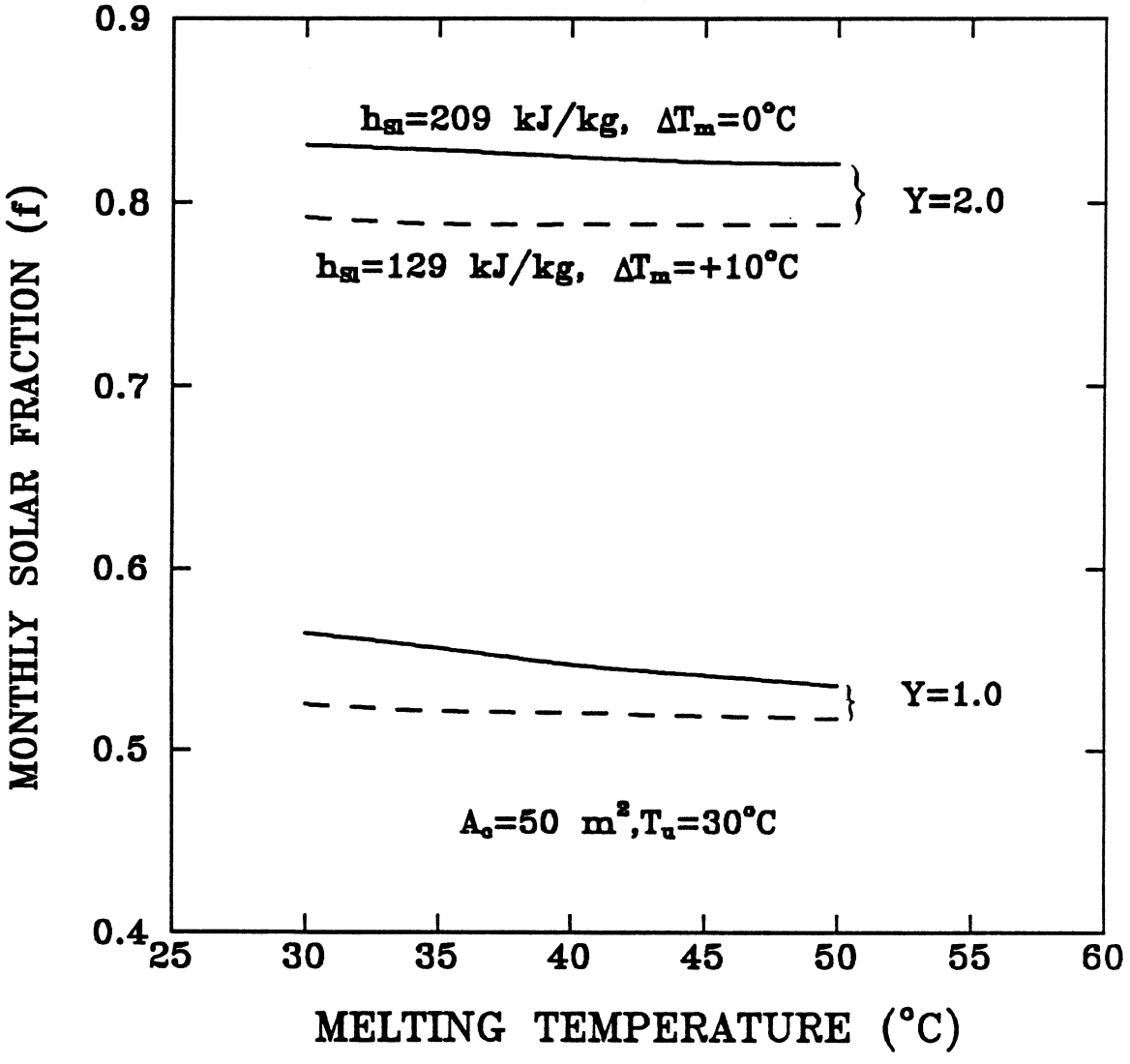

Figure 4.6 Comparison of the Monthly Solar Fraction of Solar Heating Systems Utilizing Industrial Grade and Pure Paraffins (M_S=20 kg/m^2).

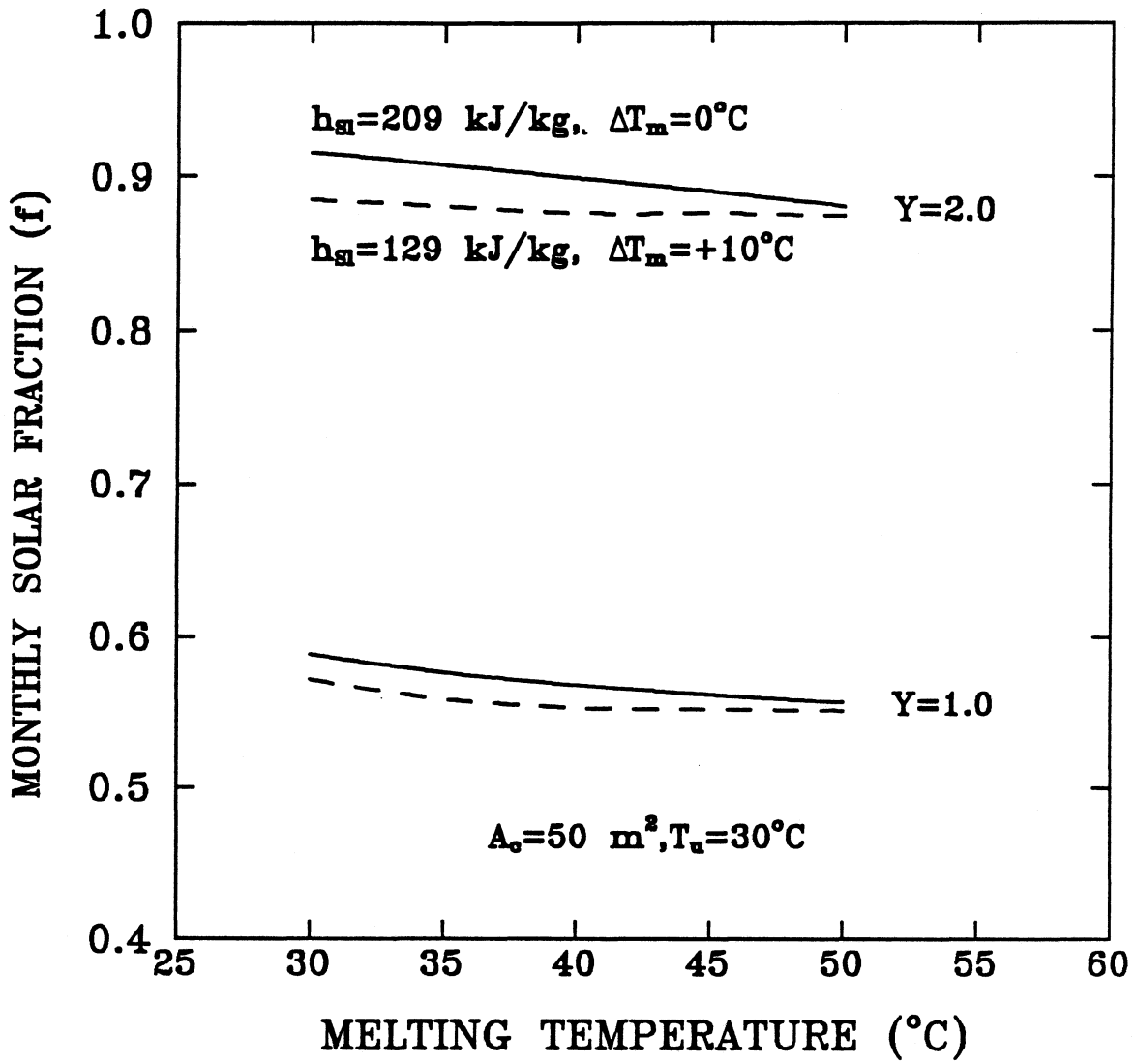

Figure 4.7 Comparison of the Monthly Solar Fraction of Solar Heating Systems Utilizing Industrial Grade and Pure Paraffins (M_S=40 kg/m^2).

temperature bandwidth of up to ± 10°C around the nominal melting temperature), for storage masses equal to or greater than 20 kg/m^2 can be used directly for PCES with little decrease in the solar fraction value taking advantage of their reduced cost. There is no need to seek candidate PCM for such conditions.

The same results and conclusions were obtained for seven different locations namely, Albuquerque (New Mexico), Charleston (South Carolina), Columbia (Missouri), Great Falls (Montana), Madison (Wisconsin), Alexandria (Egypt), Marsa-Matrouh (Egypt), and two different heating season months (January and March). The previous conclusions are location independent. An energy balance for the used TRNSYS deck for each simulation was performed. The simulations obtained in this study showed closure of 0.02-0.08%. The maximum standard deviation between the calculated and the plotted points (Figures 4.3-4.7) is about 0.03.

CHAPTER 5

COMPARISON OF THEORETICAL MODELS OF SENSIBLE HEAT STORAGE FOR AIR AND WATER-BASED SOLAR HEATING SYSTEMS

5.1 Introduction

Energy storage is usually in the form of sensible energy of a fluid or solid medium, or in the energy associated with the phase change of a material. In general, sensible energy storage is characterized by low cost and the availability of the storage medium. In this chapter, the performance of solar heating systems using a building material called 'Abu-Siebera clay' which is found in Abu-Siebera, Egypt is investigated. The grain-size distribution and the thermal properties of this material were determined experimentally in Faculty of Engineering, University of Alexandria. The present study uses the weather data of Alexandria, Egypt.

Section 2 of this chapter presents the result of grain-size distribution analysis. Section 3 of this chapter describes the experimental method used to determine the thermal properties of Abu-Siebera clay. Section 4 discusses the numerical method used to determine the performance of both air and water-based solar heating systems. Section 5 presents the results and conclusions of this investigation.

5.2 Grain-Size Distribution

To properly classify a soil, one must know the grain-size distribution in it. Sieve analysis was used to determine the grain-size distribution of Abu-Siebera clay. Sieve

analysis is conducted by taking a measured amount of dry sample and passing it through a stack of sieves with a pan at the bottom. The amount of sample retained on each sieve is measured, and the cumulative percentage of sample passing through each sieve is determined. The grain-size distribution of Abu-Siebera clay is presented in Table 5.1.

Table 5.1 Grain-Size Distribution of Abu-Siebera Clay

Sieve no.	Diameter (mm)	% retained	% passed
14	1.2	1.1	98.9
25	0.6	12.4	86.5
52	0.3	14.7	71.8
100	0.15	17.1	54.7
200	0.075	18.6	36.1

5.3 Thermal Properties Measurements

The experimental methods of determining the thermal properties of a medium are based on steady state or transient heat conduction conditions. Steady state methods are based on Fourier's equation of heat conduction. The medium which is initially in thermal equilibrium is perturbed by the introduction of a heat source or heat sink which creates a temperature gradient across the sample. In steady state conduction, this temperature gradient is independent of time. Reaching steady state condition is usually a slow process, so measurements will be time consuming.

An interesting alternative to the use of steady state methods is the transient heat conduction methods. The major advantage of transient heat conduction methods is that they are much faster than steady state methods. A widely used method for measuring the thermal conductivity and thermal diffusivity of soil is the transient probe method. The transient probe method was used to determine the thermal conductivity and thermal diffusivity of Abu-Siebera clay. In transient probe methods, a body of known dimensions and thermal properties (the probe) which contains a source of heat and a thermometer is immersed in the medium whose properties are to be determined. The thermal properties can be then determined from a record of probe temperature versus time. The main advantages of the transient probe method are quick measurements (about 15 minutes), and both the thermal conductivity and thermal diffusivity can be determined from a single measurement.

The thermal diffusivity (α) is given by the following relation :

$$\alpha = \frac{k}{\rho c} \tag{5.1}$$

where k, ρ, and c are the thermal conductivity, the density, and the specific heat of the material, respectively. Measuring k, and α using the probe method and then calculating the density of the specimen, the specific heat can now be calculated. Now, the thermal properties of the material (i.e. k, ρ, and c) which are necessary to determine its performance as a sensible storage medium are known. The theory of the transient probe method can be found in Blackwell [54].

5.3.1 Sample Preparation

The samples of Abu-Siebera clay were first dried in an oven for 24 hr at 120 °C before measuring the thermal properties to remove any moisture in the samples. The dried samples are then stored in a closed metal container of 98 mm diameter and 107 mm length. A hole was made in the center of the container's cover for immersing the thermal probe. The apparent density of the dried sample can be determined by calculating the difference between the weight of the full and empty container then dividing this difference by the container volume.

5.3.2 Apparatus

Figure 5.1 shows a schematic diagram of the experimental set-up used to determine the thermal properties of Abu-Siebera clay. The set-up consists of a laboratory thermal probe, thermal property analyzer (TPA), and a printer.

5.3.2.1 Thermal Probe

The probe is made of a stainless steel tube of a 3 mm diameter and 100 mm length. A thermocouple of copper-constantan is fixed at the middle of the tube. The probe is also provided with a heater to heat the specimen to the desired temperature. The length of the heater is 10 cm, and its resistance is 456 m Ω /cm.

5.3.2.2 Thermal Property Analyzer

The thermal property analyzer (TPA model 1000) consists of a current source and a six-input thermocouple reader under microprocessor control. It is manufactured by Geotherm, Canada. The probe current is determined on the basis of the resistance per unit length and the anticipated thermal resistivity to give one of the three probe powers

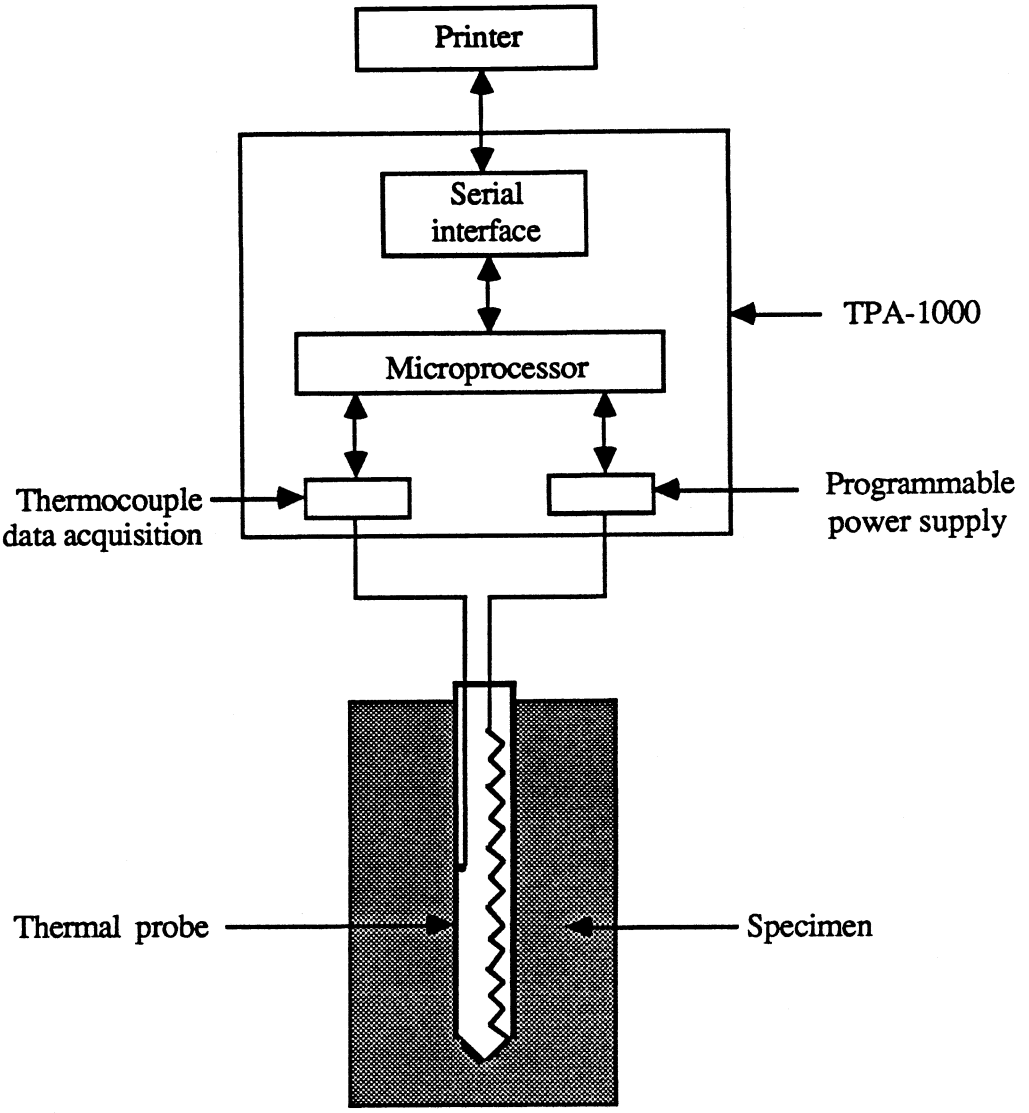

Figure 5.1 Schematic Representation of the Experimental Set-up

per unit length appropriate for high, medium, and low thermal resistivity (thermal resistivity =1/k). The microprocessor calculates the thermal resistivity and diffusivity from a least squares fit to time-temperature data collected between 300 and 1005 seconds. Thermal property analyzer (TPA) is provided by a special function key to make any desired variation, from the pre-set values stored in the microprocessor memory, in probe power, time, etc.

There are several features incorporated into the thermal property analyzer to reduce measurements errors. For example, probe power cannot be initiated until a thermal equilibrium between the probe and the specimen is reached. Also, a coefficient of determination is calculated for the least squares fit, and an error message is sent if this is less than a predetermined value (0.92) which means that probe power must be readjusted.

5.3.2.3 Printer

The printer is connected to the TPA, and it prints out the time and the temperatures for each active thermocouple.

The value of thermal diffusivity is given in cm^2/s, and the value of the thermal resistivity is given in cm °C/W. These values can be easily afterwards converted to any desired system of units.

5.3.3 Measurements Procedure

The measurements procedure steps are briefly described below.

1) Turn power switch ON and leave the apparatus to warm-up for at least ten minutes. The probe can be inserted at this time.
2) Set the probe current using the apparatus front panel switches. The value of the probe current must be appropriate to the thermal resistivity of the sample under test.

3) Connect printer and probe cables and observe the probe power.
4) Record the values of the thermal resistivity, thermal diffusivity, and coefficient of determination during and at the end of the experiment.

5.3.4 Probe Calibration

A calibration for the thermal probe was first done to check the accuracy of the measurements. The calibration was done using glycerin,whose thermal properties are well known. Since glycerin is a viscous liquid, there will be a good thermal contact between the probe and the measured medium. As a result, the contact resistance error can be neglected. In addition, if the test temperature rise is kept small the convective heat flow can be neglected due to glycerin viscosity.

The calibration was conducted by immersing the thermal probe in the center of a container filled with glycerin. The power of the heater (0.04 W/cm for this experiment) was adjusted to cause a maximum temperature rise of 5 °C. The relation between the temperature rise versus ln (time) is then plotted. This curve was found to be linear for large time (above 300 seconds). As explained in the discussion given by Blackwell [54], the thermal resistivity and the thermal diffusivity can be determined from the values of the slope of the straight line and the intercept with the vertical axis at ln time=0.0, respectively. The thermal resistivity and thermal diffusivity calculated for glycerin were 358.93 cm °C/W, and $9.87*10^{-4}$ cm^2/s, respectively. The published values of thermal resistivity and thermal diffusivity for glycerin (at 20 °C) are 349.65 cm °C/W, and $9.47*10^{-4}$ cm^2/s, respectively [55]. Thus, the errors in the measured values for thermal resistivity and thermal diffusivity are 2.65 and 4.2%, respectively.

It must be mentioned that the dry sample of Abu-Siebera clay can be considered as

mixtures of solid bodies and gases, i.e. porous material. The porosity greatly influences the density and the thermal conductivity of a porous material. Increasing porosity or gas content results in decreasing both the apparent density and the thermal conductivity of the material. In the present work, the measurements were repeated several times and each time the porosity of the dry sample is determined. The values of the thermal properties of Abu-Siebera clay used in this study are the values corresponding to porosity equal to 25%. These values are presented in Table 5.2.

Table 5.2 Thermal Properties of Sensible Storage Media

Properties	Rock	Abu-Siebera clay
c (kJ/kg K)	0.84	0.86
k (kJ/m h K)	0.45	0.72
ρ (kg/m^3)	2285	2150

5.4 Analysis

The infinite NTU model used by Huges et al. [50] to describe the performance of pebble bed unit is based on the following assumptions :

1) infinite thermal conductivity for the rock bed in the direction normal to the flow (radial direction); this assumption requires that Biot number is sufficiently sufficiently low such that the temperature gradients in the storage material normal to the flow direction can be ignored.

2) heat losses from the storage unit to the surroundings are negligible.

3) zero thermal conductivity for the storage material in the direction parallel to the flow (axial direction).

4) the number of transfer units of the storage unit, NTU, is sufficiently large so that the local film temperature difference between the fluid and the rock bed can be ignored.

The effect of taking these assumptions into consideration on the thermal performance of solar heating systems using Abu-Siebera clay as a storage medium has been investigated in the present study. For the present detailed model equations (3.1) and (3.2) can be used to describe the governing equations for both the storage medium and the circulating fluid. The storage unit configuration chosen for studying sensible energy storage is the same one used with phase-change energy storage (Figure 3.1). The same computer program discussed in Chapter 3 for phase-change energy storage was used for sensible energy storage by setting the melting temperature of the sensible material arbitrary high, so that all energy storage is in the form of sensible heat.

The standard air and water-based solar heating systems shown in Figures (3.3) and (3.4) were chosen for the present investigation. Control strategy, system description, and system parameters which were fixed during this study are the same as those given in Chapter 3. The only change in the system parameters is in the hot water load. The hot water profile chosen for this study is shown in Figure 5.2. This profile approximately represents the draw habits of the people in Alexandria, Egypt. This profile equal to a load of 600 kg/day of hot water, which can supply the hot water needs for a house of eight residents in Alexandria, Egypt. To check the reliability of the present results, an energy balance was done for each simulation study for both the sensible energy storage subroutine and the TRNSYS deck. The following results showed closure of 0.2-1.4%.

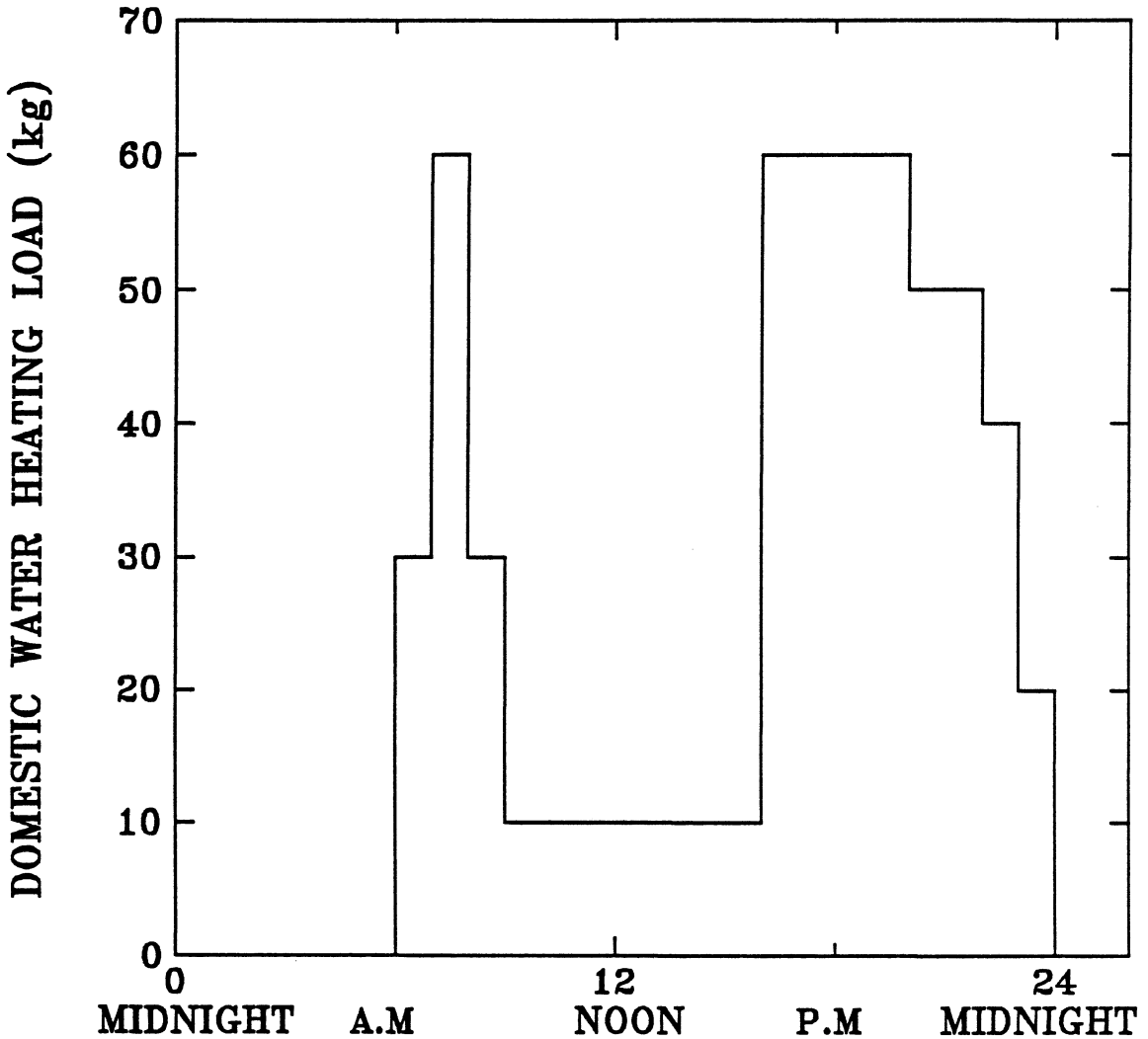

Figure 5.2 Usage Profile for Domestic Water Heating Load in Alexandria, Egypt.

5.5 Results and Discussion

In the following a discussion of the results obtained for both air and water-based solar heating systems.

5.5.1 Air-Based System

TRNSYS is used to determine the performance of the standard space and domestic water solar heating systems shown in Figures 3.3 and 3.4. In the present study, the weather data for Alexandria, Egypt (latitude 31.2°) was used. The data file of Alexandria [46] contains monthly average values of daily radiation on a horizontal surface, clearness index, ambient temperature, wind speed, and relative humidity. Since TRNSYS needs hourly values of the previous parameters, weather data generator developed by Knight [44] and Degelman [45] is used to generate hourly data from the monthly average data available for Alexandria. The weather data generator is a subroutine program compatible with TRNSYS. It generates hourly weather data given the monthly average values of solar radiation, temperature, humidity ratio, and wind speed. The data are generated approximately equal to the long-term statistics at the required location. So, the data generated represent a single year of typical data, similar to a Typical Meteorological Year (TMY) data.

The effect of storage capacity on system performance for the air-based system using both the present finite NTU model, and the infinite NTU model of Hughes et al. [50] is shown in Figure 5.3. These results are obtained from one week of simulation starting January 1 in Alexandria. There is a little difference between the finite and infinite NTU results (not more than 2% of the load at the smallest storage mass used 100 kg/m^2 (corresponding to NTU=1.5). As storage capacity increases (which increases the value of NTU for the finite NTU model), this difference becomes smaller and approximately

disappears completely at storage capacities above 500 kg/m^2 (corresponding to NTU=8). These results indicate that, for air-based systems, the infinite NTU can be used with a very small error taking advantage of its huge reduction in computational cost in comparison with the finite NTU model. Further results were obtained for the air-based system using the infinite NTU model.

The following results are generated using a four month heating season from December 1 to April 1 in Alexandria. Figure 5.4 shows the variation of solar fraction with storage mass capacity for both Abu-Siebera clay and pebble bed. The storage unit using Abu-Siebera clay gives slightly better performance than pebble bed. For example, a solar fraction value of 0.73 can be realized by using Abu-Siebera clay with a storage volume of 0.187 m^3/m^2 or a pebble bed with a storage volume of 0.195 m^3/m^2. The required storage volume of Abu-Siebera clay is roughly 96% of the storage volume required by pebble bed to achieve the same system performance. The storage volumes of the storage unit were calculated assuming a void fraction (i.e., the ratio between the fluid volume and the storage tank volume) of 0.3. The better performance of Abu-Siebera clay over rock may be attributed to its higher values of the specific heat and the thermal conductivity. From Figure 5.4 the value of the storage mass above which there is no significant increase in system performance for Abu-Siebera clay is 300 kg/m^2. The following results obtained using this recommended storage mass capacity.

Figure 5.5 shows the variation of solar fraction with collector tilt-latitude. Collector orientation affects performance in two ways. Most importantly, it directly affects the amount of solar radiation incident on the collector surface. In addition, collector orientation affects the transmittance of the transparent covers and the absorptance of the collector plate since both are functions of the angle at which radiation strikes the

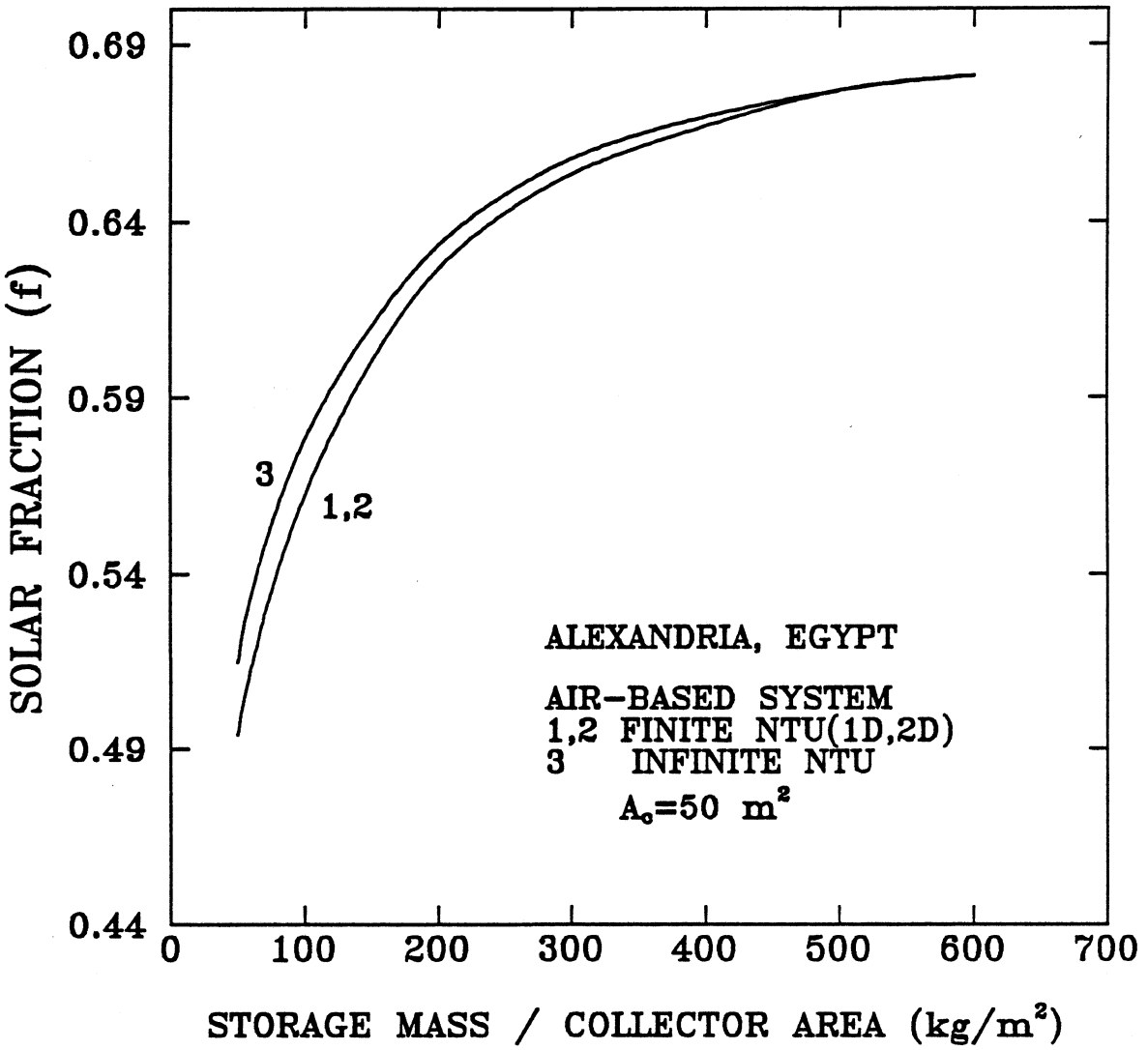

Figure 5.3 Variation of Solar Fraction with Storage Mass for Abu-Siebera Clay (One Week Simulation Starting January 1).

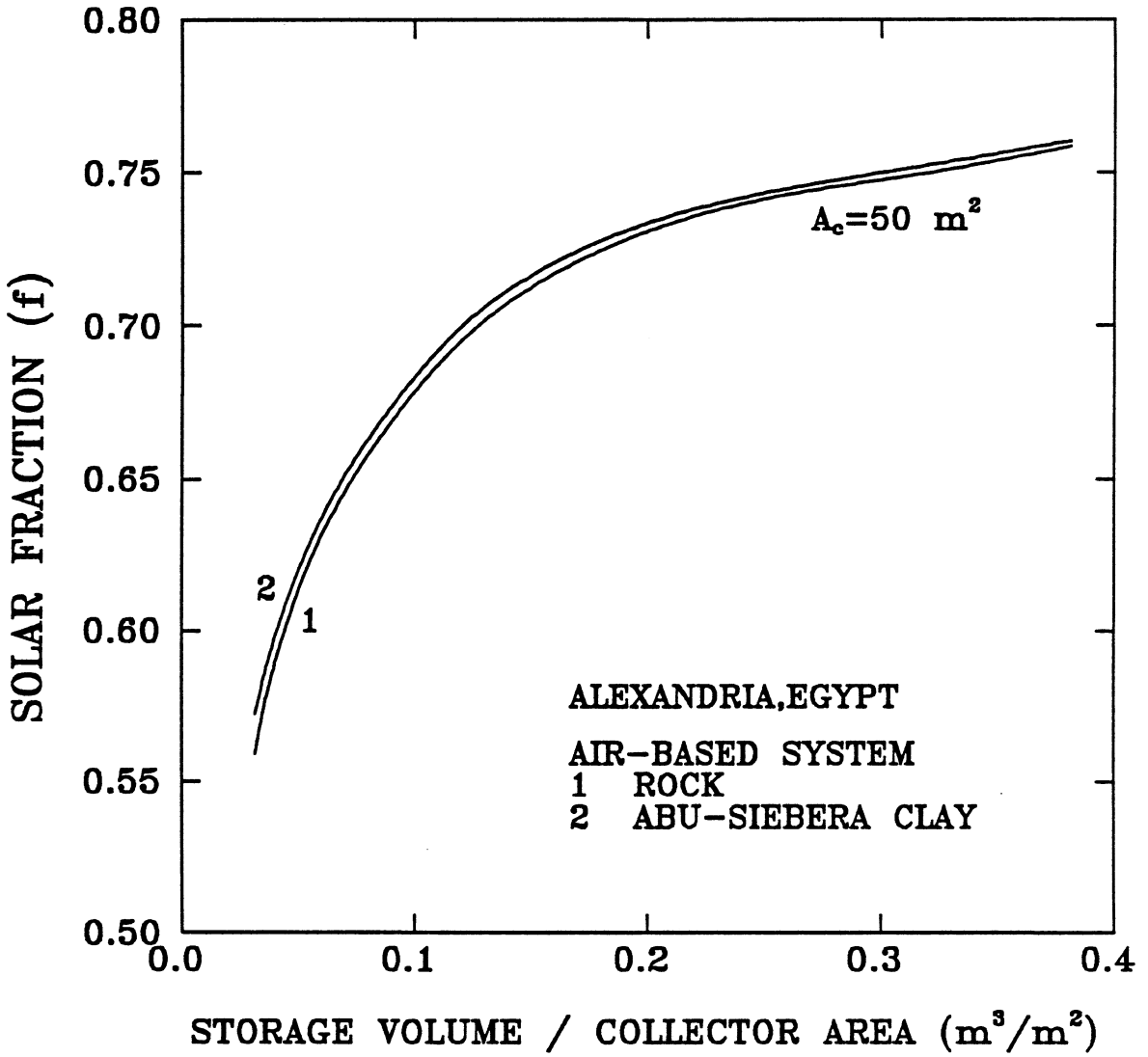

Figure 5.4 Variation of Solar Fraction with Storage Unit Volume for Rock and Abu-Siebera Clay in Alexandria, Egypt.

collector surface. The optimum collector orientation, that is, the orientation in which the solar heating system provides the largest fraction of the heating season load is due south at an angle equal to the latitude. However, the collector orientation is not critical. Deviations from the optimum by as much as 10° have little effect on the solar system performance.

Figure 5.6 shows the variation of the heating season solar fraction with collector area. At zero collector area, of course , the fraction supplied by solar energy is zero. As the collector area increases the solar fraction increases. This increase is not so pronounced for collector areas higher than 50 m^2. For example, increasing the collector area from 25-50 m^2, results in increasing the solar fraction by roughly 0.33 of the load (approximately 75% of the range). On the other side, increasing the collector area from 50 to 100 m^2, results in increasing the solar fraction by 0.19 of the load (approximately 25% of the range).

The recommended air-based solar heating system parameters for the heating season starting from December 1 to April 1 in Alexandria are : storage mass capacity equal to 300 kg/m^2, collector orientation equal to the latitude, and collector area of 50 m^2. These recommended parameters are based on the performance of solar heating system and calculated for the previously specified space and domestic water heating loads.

5.5.2 Water-Based Systems

For water-based systems, a parametric study for energy stored was conducted first because significant differences between the finite and infinite NTU models were expected due to the relatively large heat capacity of water. Figure 5.7 shows the variation of fluid outlet temperature with time for Abu-Siebera clay at different values of NTU. This figure has been generated for constant inlet fluid temperature (T_{fi}= 80 °C) during the heating

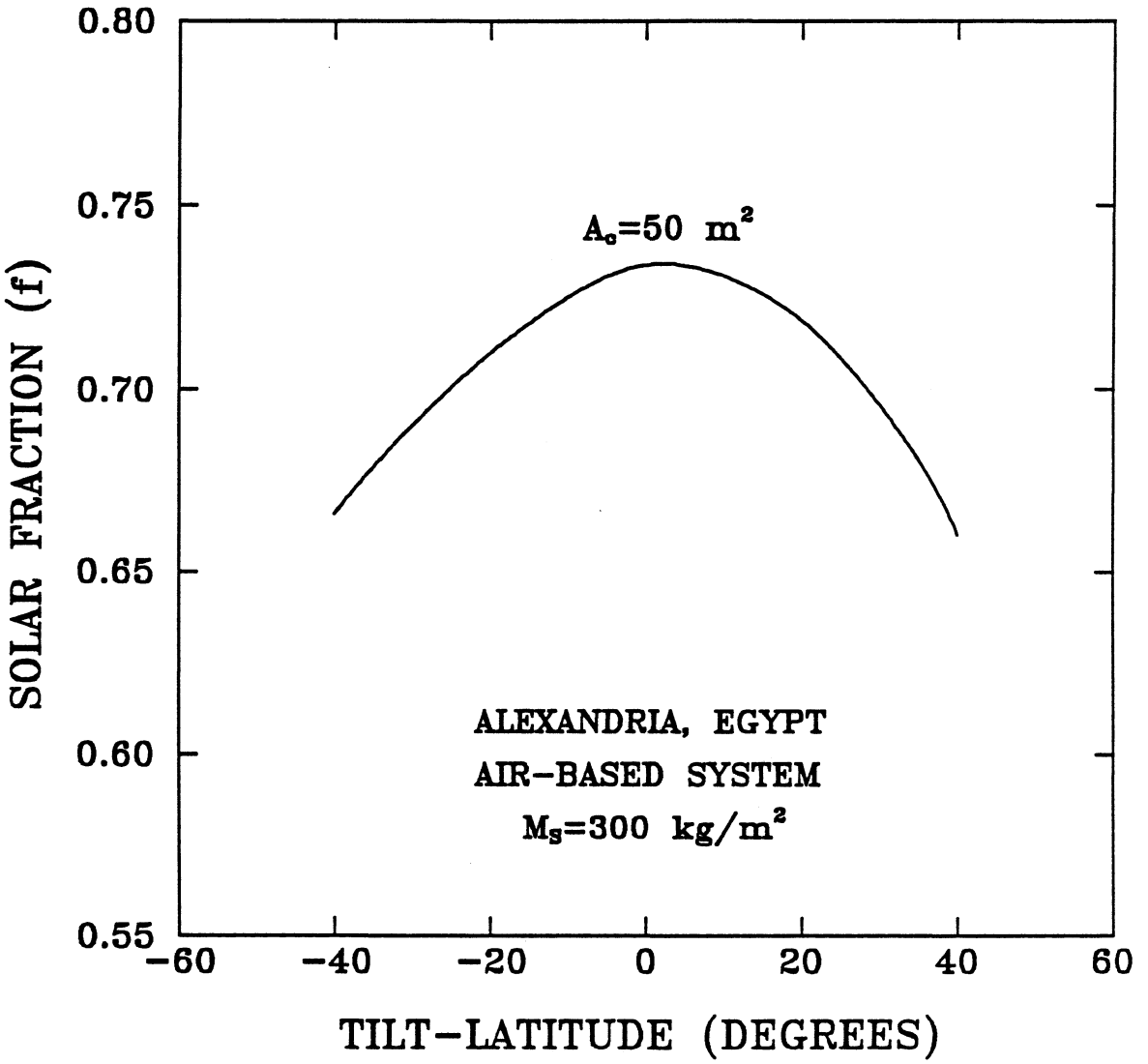

Figure 5.5 Variation of Solar Fraction with Collector Tilt-Latitude for Abu-Siebera Clay.

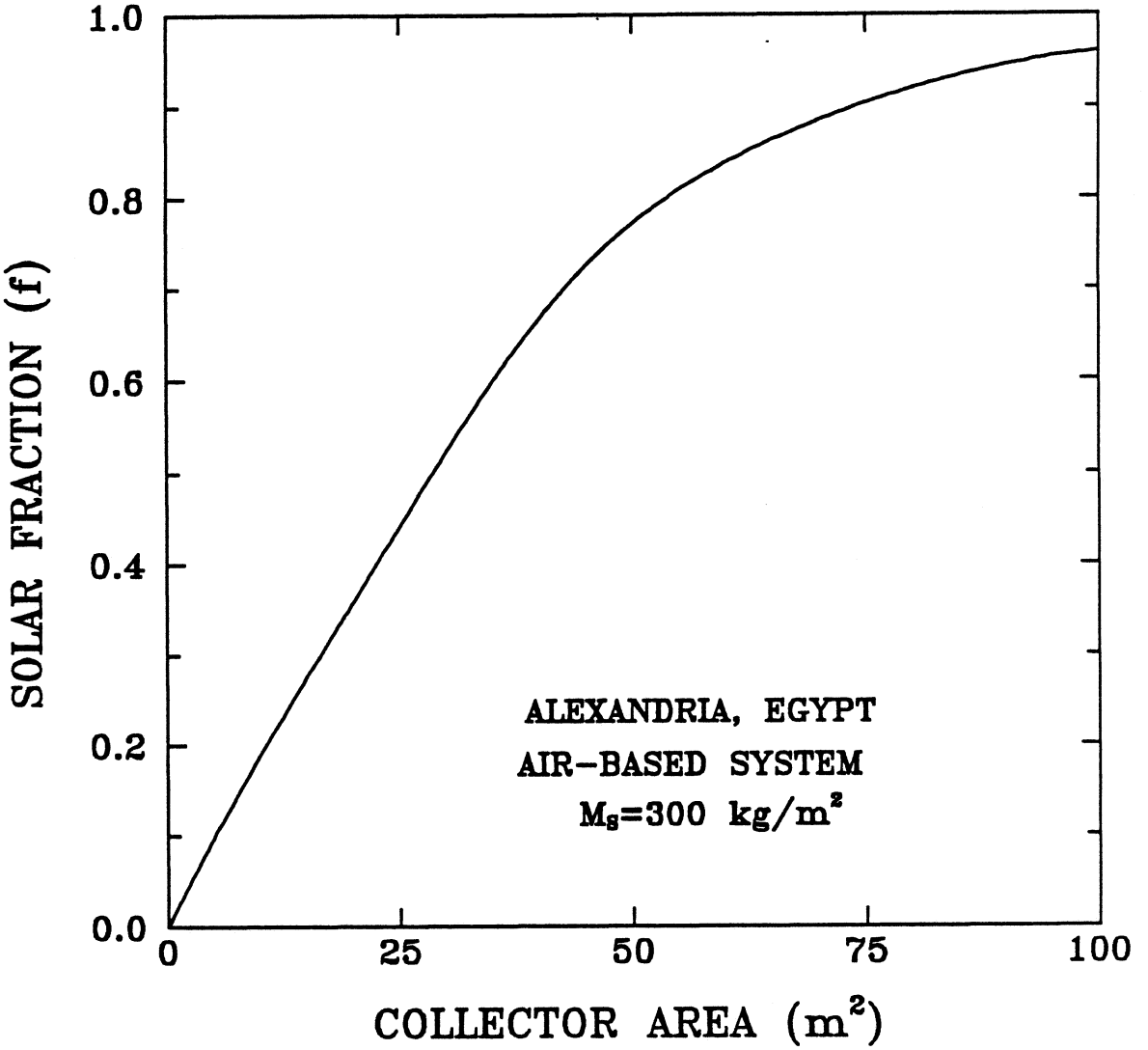

Figure 5.6 Variation of Solar Fraction with Collector Area for Abu-Siebera Clay.

mode only. As the NTU value increases at a given time, the outlet fluid temperature becomes smaller i.e. more heat is removed from the fluid and consequently more heat will be stored in the material. This Figure shows that there is a significant difference between the finite and infinite NTU model. Figure 5.8 shows the variation of stored energy with time for the different theoretical models used in this study. There is little difference between the finite NTU model 1D, and the finite NTU model, 2D but still there is a significant difference between the values of the stored energy obtained using the infinite NTU model and the finite NTU model about 25 % . The effect of both the number of radial points (M) and the number of axial points (N) on the stored energy for Abu-Siebera were studied. There is no significant variation in the stored energy with increasing the number of radial points above 5 (i.e. N=5) or with increasing the number of axial points above 10 (i.e. M=10).

A comparison was made between using the finite NTU, 1D, and the finite NTU, 2D at different values of NTU. As seen from Figure 5.9, the 2D model gives slightly better results and the difference between the two models becomes smaller as the NTU increases, and disappears for NTU values above 200. This behavior is due to many factors such as the amount of mass flow rate, system size, inlet fluid temperature, heat transfer coefficient between the fluid and material surface, fluid temperature distribution, and storage material temperature distribution. Since the stored energy in the material depends on the area under the temperature vs. distance curve, the result for the more accurate 2D case is due to the increase in this area when considering the temperature gradients in the storage material. Figure 5.10 shows the variation of the storage material temperature with the radial distance for Abu-Siebera clay for different times of heating the storage unit (T_{fi}= 80 °C, and $\dot{m}$=2500 kg/h). This figure shows that the area under the curves is larger for the 2D case.

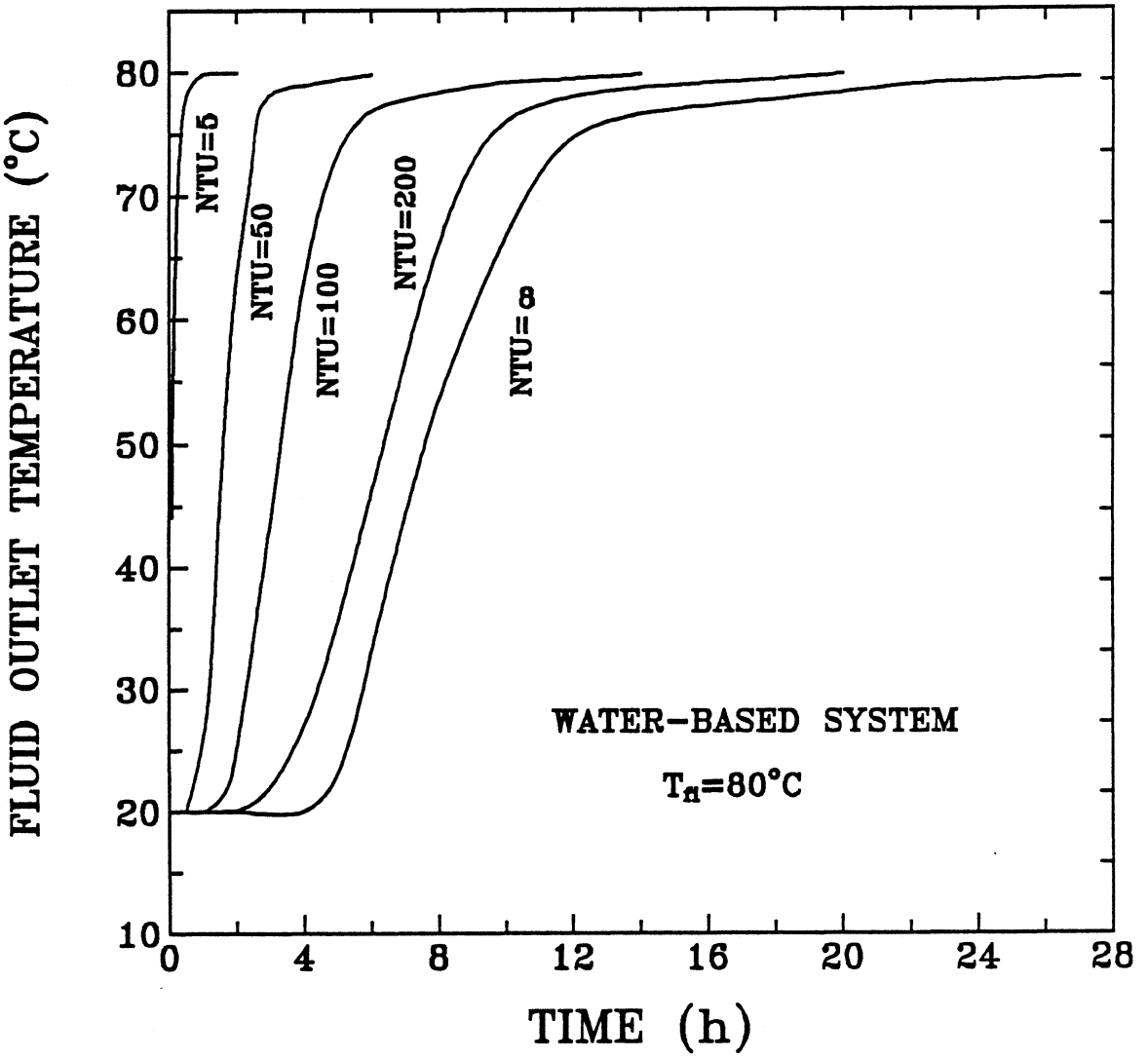

Figure 5.7 Variation of Outlet Fluid Temperature with Time for Different Values of NTU for Abu-Siebera Clay.

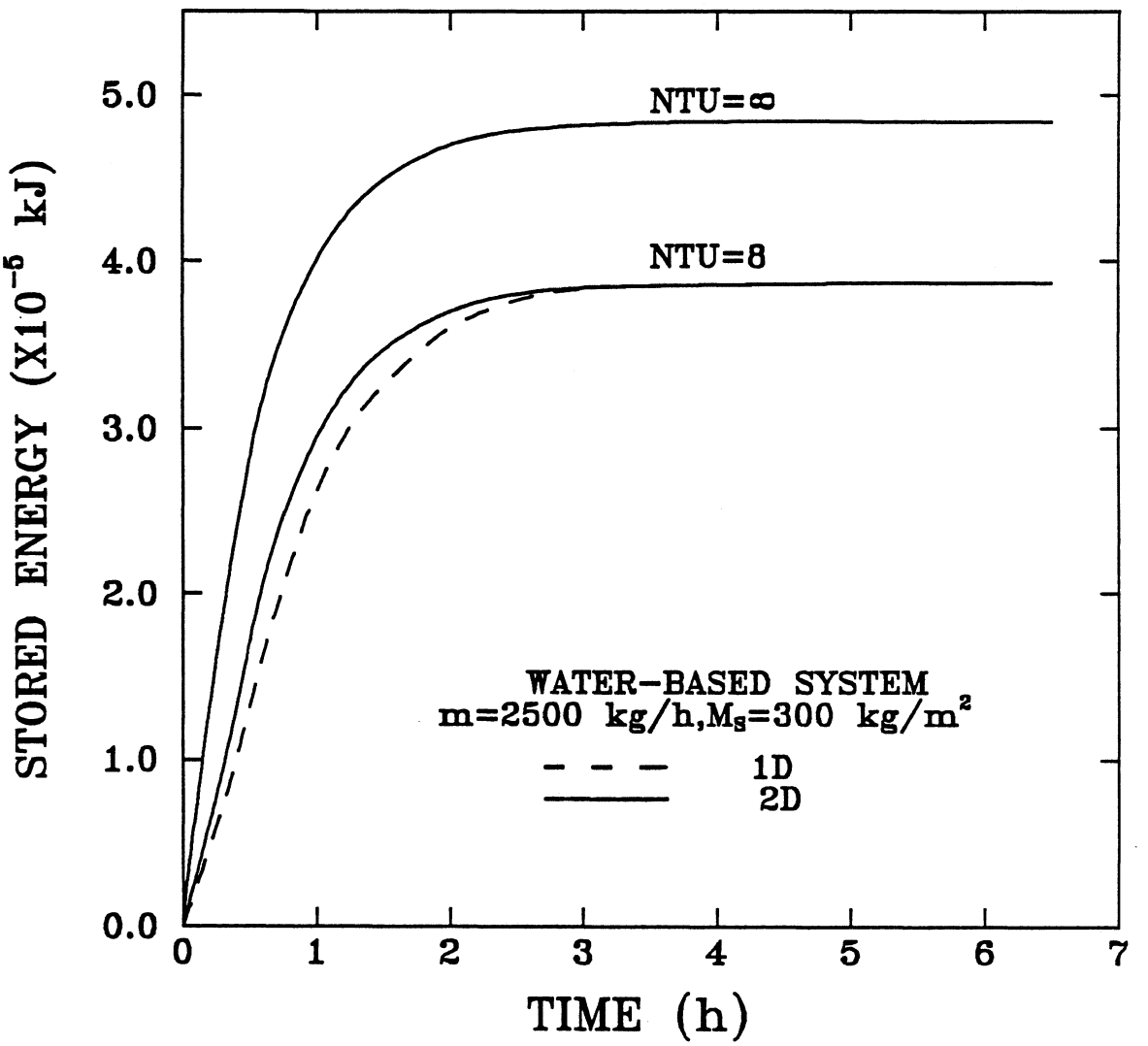

Figure 5.8 Variation of Stored Energy with Time for Abu-Siebera Clay Using Different Theoretical Models.

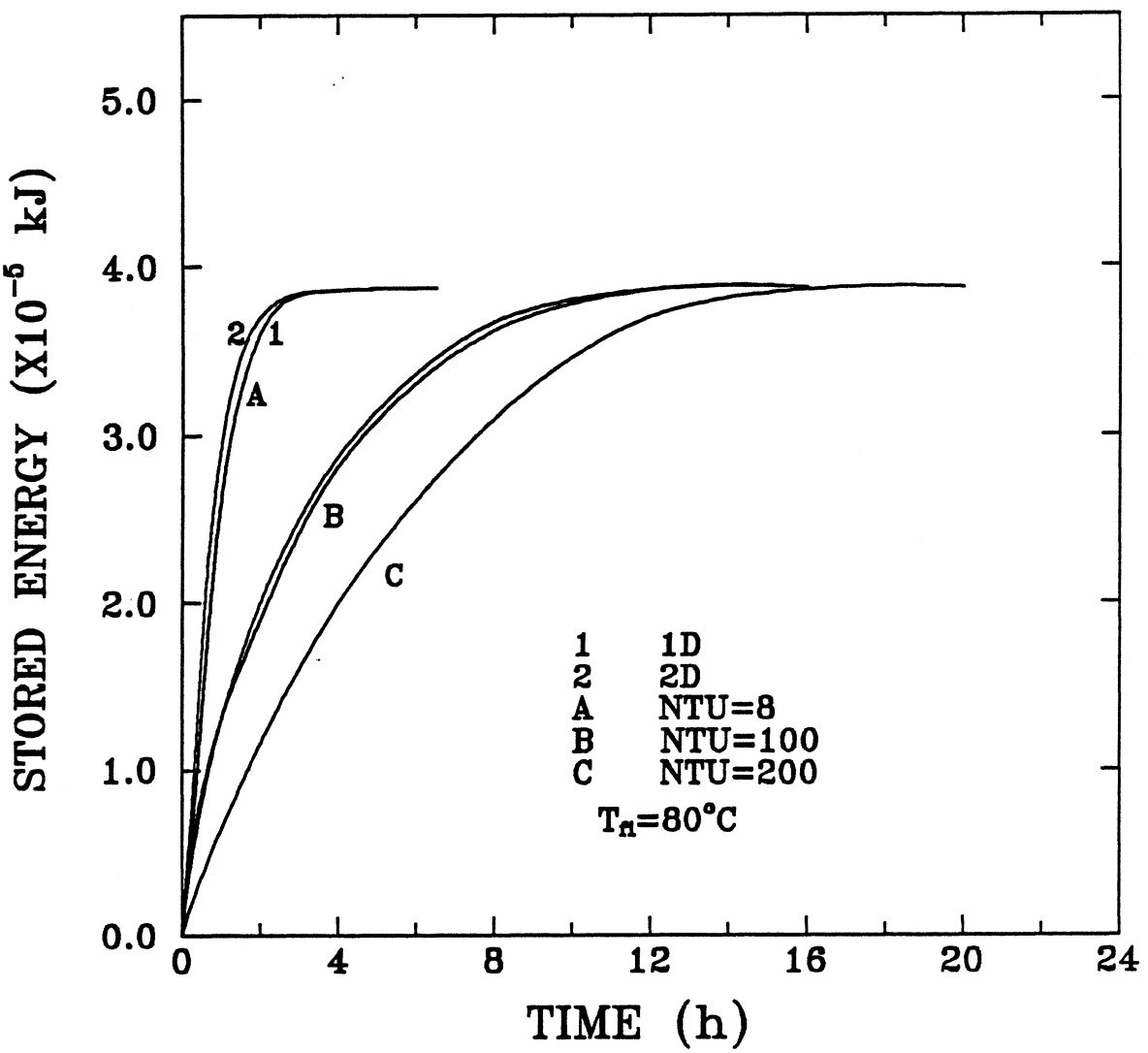

Figure 5.9 Comparison Between 1D, and 2D for Abu-Siebera Clay (Sensible Heat Storage) with Water-Based System.

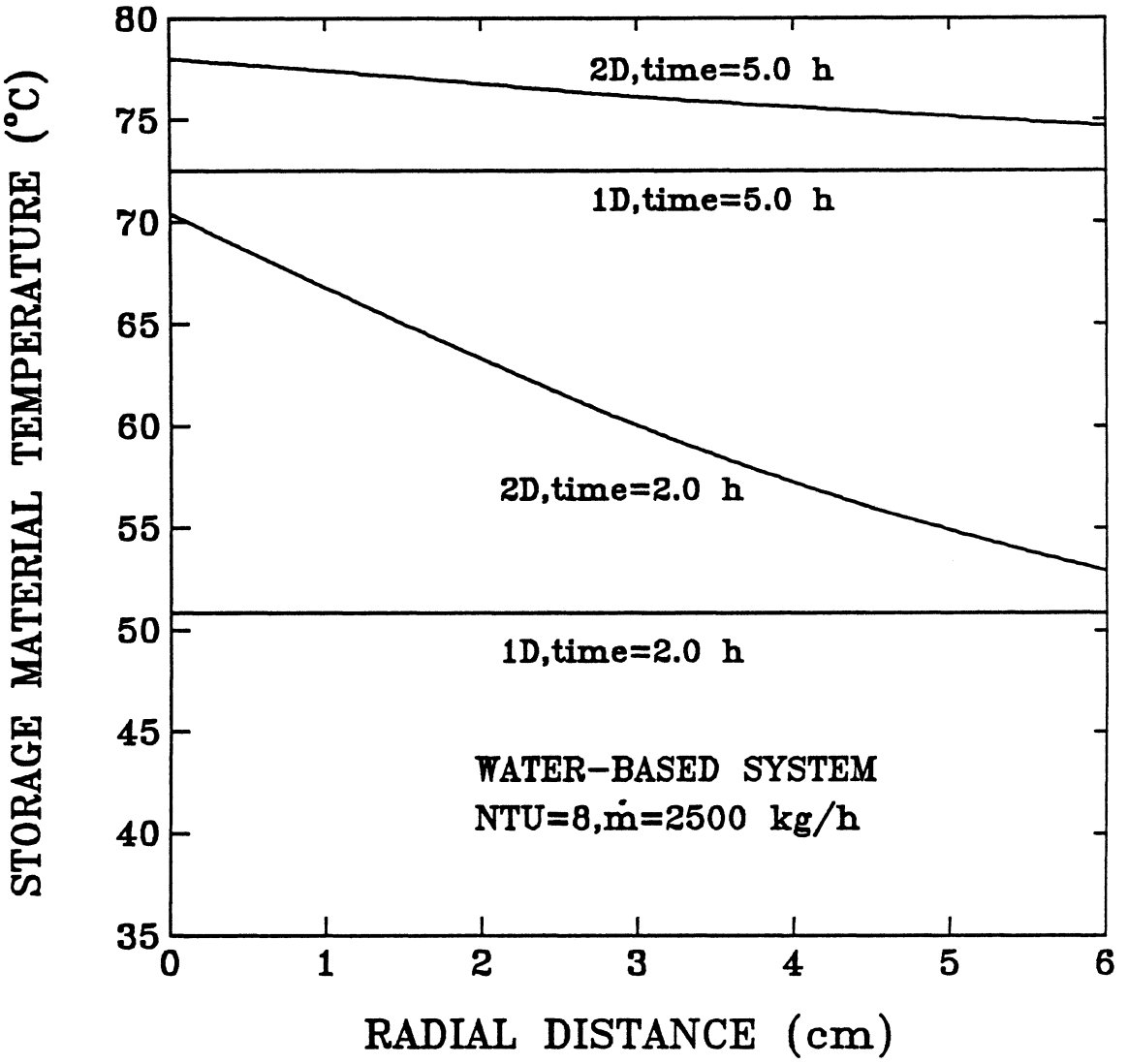

Figure 5.10 Variation of Storage Material Temperature with Radial Distance (Measured from Material Surface) for Abu-Siebera Clay.

Figures 5.11 and 5.12 show the variation of stored energy with both cylinder tube radius and void fraction. As seen from the figure, No significant improvement in the stored energy can be achieved with cylinder tube radius less than 6.0 cm or void fraction smaller than 0.3.

To study the effect of different models on the values of solar fraction, the standard water-based system shown in Figure 3.4 was simulated using Abu-Siebera clay. The simulations were run for one week starting January 1, in Alexandria. To examine this effect, consider a solar fraction of 0.65. From Figure 5.13, the recommended storage masses per unit collector area are 160 (0.106), 200 (0.133), and 210 kg/m^2 (0.140 m^3/m^2) for infinite NTU model, finite NTU (2D), and finite NTU model (1D) respectively. So, the use of infinite NTU model will give an error in the recommended storage volume value of about 20%, whereas the difference between finite 1D, 2D models values is roughly 5%. An accurate examination of the water-based system can be obtained only using the detailed solution, i.e. the finite NTU (2D) model. The approximation of infinite NTU model (unlike in the air-based system) gives a significant error in the determination of the system performance. The recommended storage mass per unit collector area for water-based system is the same as obtained for air-based system (300 kg/m^2). The recommended storage mass capacity does not depend on system configuration i.e. air or water-based solar heating system.

For water -based system the same results as air-based solar system are obtained for the variation of solar fraction with both collector tilt-latitude and collector area. Figure 5.14 shows the variation of solar fraction with collector mass flow rate per unit collector area for one week simulation starting January 1 in Alexandria. As the mass flow rate through the collector increases, the temperature rise through the collector decreases. This causes lower losses since the average collector temperature is lower which increases the collector hear removal factor (F_R). Lower flow rates result in lower values of F_R which

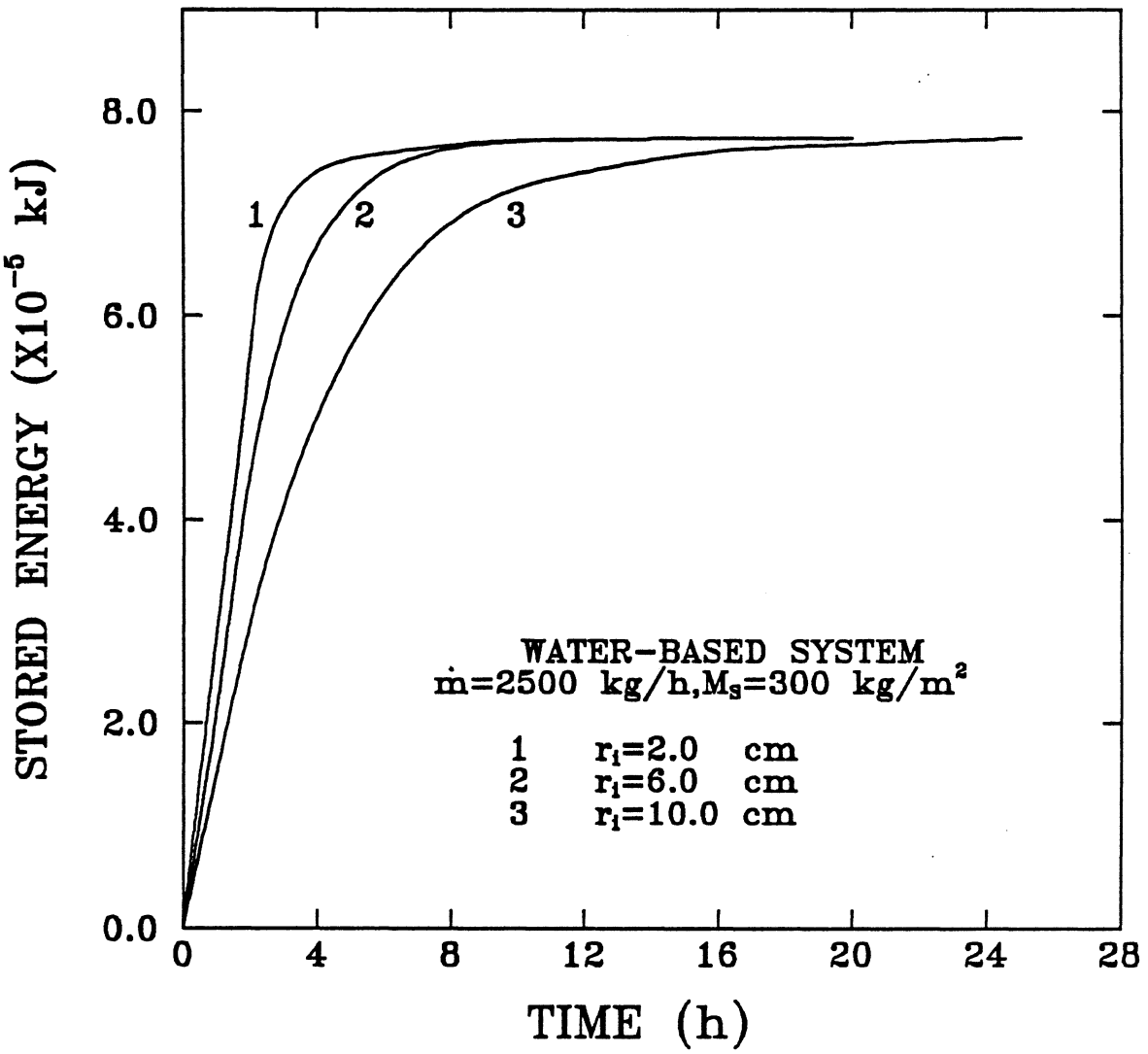

Figure 5.11 Variation of Stored Energy with Time at Different Radii for Abu-Siebera Clay.

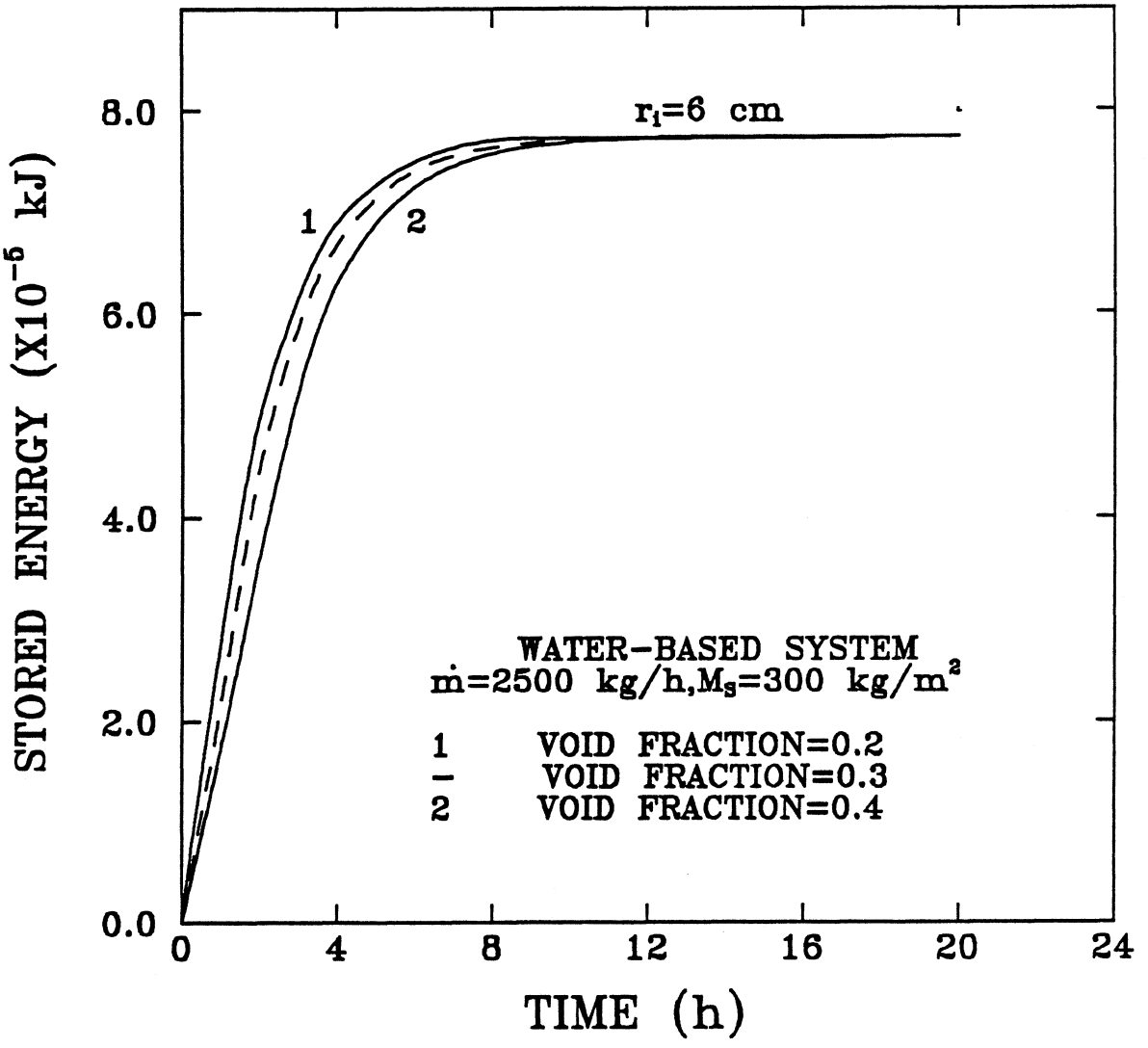

Figure 5.12 Variation of Stored Energy with Time at Different Values of Void Fraction for Abu-Siebera Clay.

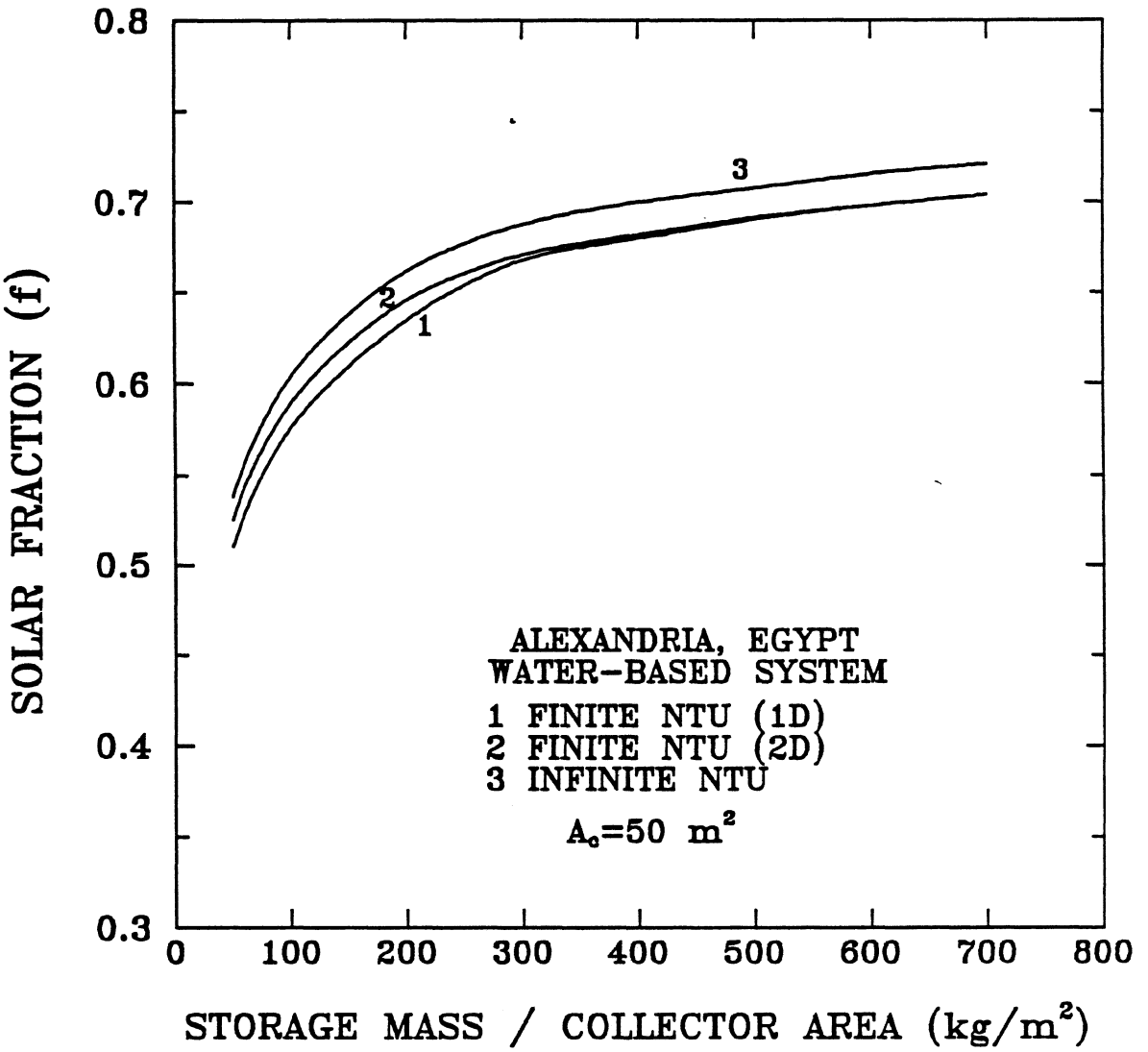

Figure 5.13 Variation of Solar Fraction with Storage Mass for Abu-Siebera Clay (One Week Simulation Starting January 1).

reduces collector efficiency factor (F'), but lower flow rates also result in a higher degree of thermal stratification. This increased stratification results in lower collector inlet temperatures and thus increased collector efficiency. The existence of optimum flow rate has been demonstrated by others [56,57,58].

The values of collector performance parameters $F_R U_L$ and $F_R (\tau\alpha)_n$, where U_L is the collector overall loss coefficient and $(\tau\alpha)_n$ is the transmittance-absorptance product at normal incidence, are affected by collector flow rate through the dependence of F_R on flow rate per unit collector area [52]. This dependence can be expressed as

$$F_R = \frac{\dot{m} c_f}{A_c U_L} [1 - \exp (- A_c F' U_L / \dot{m} c_f)] \tag{5.2}$$

The ratio, r, by which $F_R U_L$ and $F_R (\tau\alpha)_n$ are to be corrected to account for the changes in collector mass flow rate is given by

$$r = \frac{\frac{\dot{m} c_f}{A_c F' U_L} [1 - \exp (- A_c F' U_L / \dot{m} c_f)] \Big|_{use}}{\frac{\dot{m} c_f}{A_c F' U_L} [1 - \exp (- A_c F' U_L / \dot{m} c_f)] \Big|_{test}} \tag{5.3}$$

Using equation (5.1), with the value of $F' U_L$ at test conditions [53], the value of $F' U_L$ at test condition can be calculated. For water-based system, the value of $F' U_L$ can be used in both numerator and denominator of equation (5.2) to determine the value of the ratio r. As seen from Figure 5.14, no improvement in the system performance can be achieved with mass flow rates per unit collector area higher than 50 kg/h m^2.

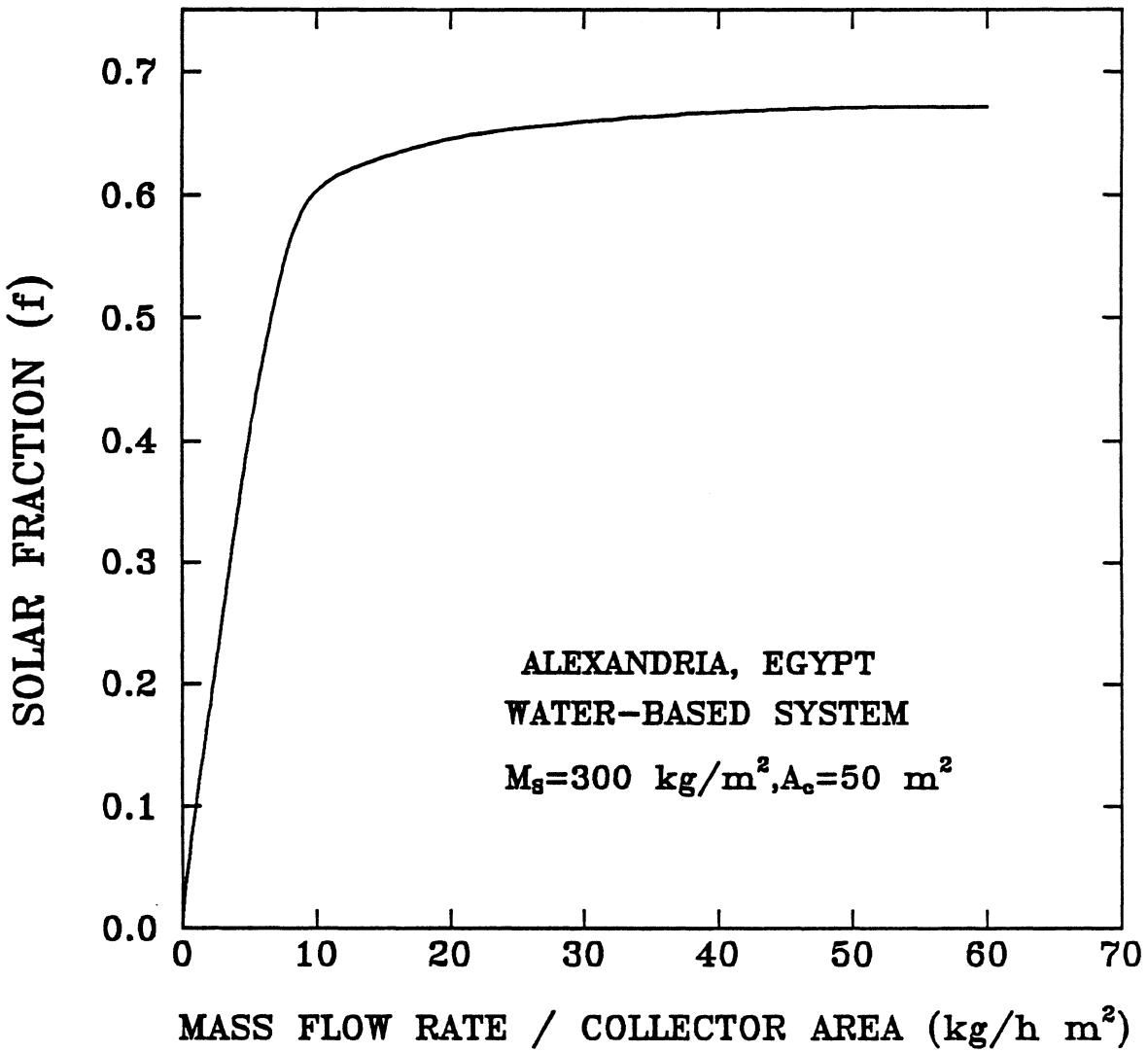

Figure 5.14 Variation of Solar Fraction with Mass Flow Rate per Unit Collector Area for Abu-Siebera Clay.

The recommended parameters based on the performance of water-based solar heating system using Abu-Siebera clay for the heating season starting from December 1 to April 1 in Alexandria, Egypt are : storage mass capacity equal to 300 kg/m^2, collector orientation equal to the latitude, collector area of 50 m^2, and mass flow rate of 50 kg/h m^2. These recommended parameters are calculated for the previously specified space and domestic water heating loads.

CHAPTER 6
INVESTIGATION OF SOLAR DOMESTIC HOT WATER SYSTEM PERFORMANCE IN ALEXANDRIA, EGYPT

6.1 Introduction

Solar domestic hot water (SDHW) systems are currently widely used that is because they are simple, easily maintained, and relatively inexpensive. In addition, in this type of thermal energy storage, heat added and removed from the storage unit by transport of the storage medium itself, thus eliminating the temperature drop between transport fluid and storage medium. Water-based systems usually use insulated water tanks for energy storage. Unlike conventional hot water systems, SDHW system performance is dependent on local climatic conditions, such as solar radiation and ambient temperature. Almost all SDHW systems have two major components in common, a collector and a storage tank, these components can be found in a wide variety of system configurations.

Detailed computer simulation programs, such as the transient simulation program (TRNSYS), can be used to estimate the long-term annual thermal performance of solar domestic hot water systems. The advantages of detailed simulations are flexibility and accuracy. Simulations, however, are not convenient. They require a high computer cost, hourly meteorological data, and a lot of experience. So, the detailed simulation programs are impractical as a long-term performance design tool. An interested alternative to the use of detailed simulation programs is the f-chart design method [19,20], which provides

estimates of monthly average system performance using monthly average weather data. One of the main objectives of the present chapter is to investigate the reliability of the f-chart design method in the Egyptian climate.

The main purposes of this chapter are :

1) to compare the thermal performance of solar domestic hot water (SDHW) system obtained using TRNSYS and the corresponding performance obtained using the f- chart method.
2) to study the effect of varying collector parameters, storage capacity, hot water load distribution, and thermal stratification on system performance.

6.2 System Description and Control Strategy

Figure 6.1 shows a schematic representation of the direct two-tank SDHW system chosen for the present study. This system was chosen because it is one of the standard system configurations used in the development of the f-chart design method. It consists of a preheat tank contains water which is circulated through the solar collectors when the incident solar radiation is sufficient to provide thermal energy. When solar radiation is not enough to satisfy the load, water is taken from the auxiliary tank. This water is replaced by solar heated water from the preheat tank.

The water in the auxiliary tank is maintained at a specified set temperature by internal heater. The system also contains a tempering valve which limits the temperature of the delivered water to the set temperature by mixing with mains water as needed. The circulation of water is controlled by a differential controller. When water temperature at collector outlet exceeds the water temperature in the bottom of the preheat tank (deadband upper limit) the circulation pump is activated. When this temperature difference falls below a certain value (deadband lower limit) circulation of the water is stopped.

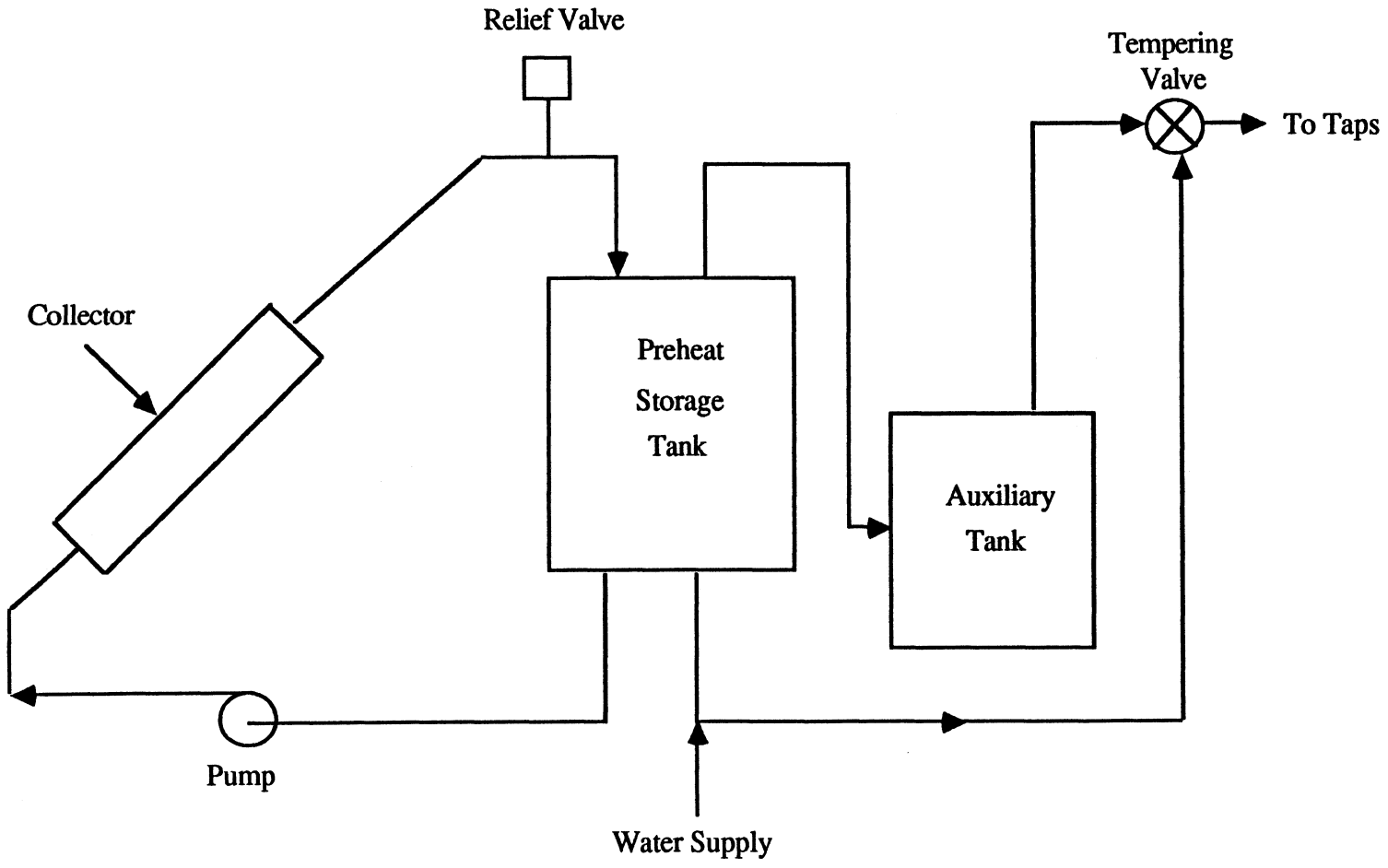

Figure 6.1 Configuration of Solar Domestic Hot Water System

Relief valve is used for dumping excess energy.

The profile of hot water usage is shown in Figure 6.2. This profile approximately represents the draw habits of the people in Alexandria, Egypt. This profile is equivalent to a water heating load of 2400 kg/day, which can supply the hot water needs for a house of eight families (approximately thirty two residents) in Alexandria, Egypt. The system parameters chosen for the comparison between system performance predicted by both TRNSYS and the f-chart design method are listed in Table 6.1.

Table 6.1 Solar Domestic Hot Water System Parameters

Location - Alexandria	
Latitude	31.2°
Collector	
Area	50 m^2
Tilt	Latitude
Number of collectors in series	1
Number of glass covers	2
Product of extinction coefficient and thickness of each glass cover	0.037
Refractive index	1.526
Absorptance (α)	0.9
Emittance (ε)	0.9
Intercept efficiency	$F_R (\tau\alpha)_n$ =0.7
Negative of the slope of the efficiency curve	$F_R U_L$=15 kJ/h m^2 K
Incident angle modifier	b_o =0.1

Table 6.1 (continued)

Piping

The collector circuit piping is divided into a cold side and a hot side, and the following data are the same for both sides.

Collector circuit pipe (each side)

Length	20 m
Diameter	0.05 m
Heat loss	18 kJ/h K
Fluid density	1000 kg/m^3
Fluid specific heat	4.197 kJ/kg K
Ambient temperature	20 °C

Preheat tank

Volume	3.5 m^3
Thermal loss	1.5 kJ/h m^2 K
Shape	H/D = 1
Cold water inlet temperature	18 °C
Ambient temperature	20 °C
Set point for hot water	60 °C

Controller

Collector	On when T_{coll} (out) > $T_{storage}$ + 5 °C
	Off when T_{coll} (out) > 95 °C
	Off when T_{coll} (out) ≤ T_{coll} (in)

Auxiliary Heater

Maximum rate at which inlet water can be heated	$1x10^7$ kJ/h

The auxiliary heater is required to heat the outlet water to 60° C if the inlet temperature to the load is less than 60 °C

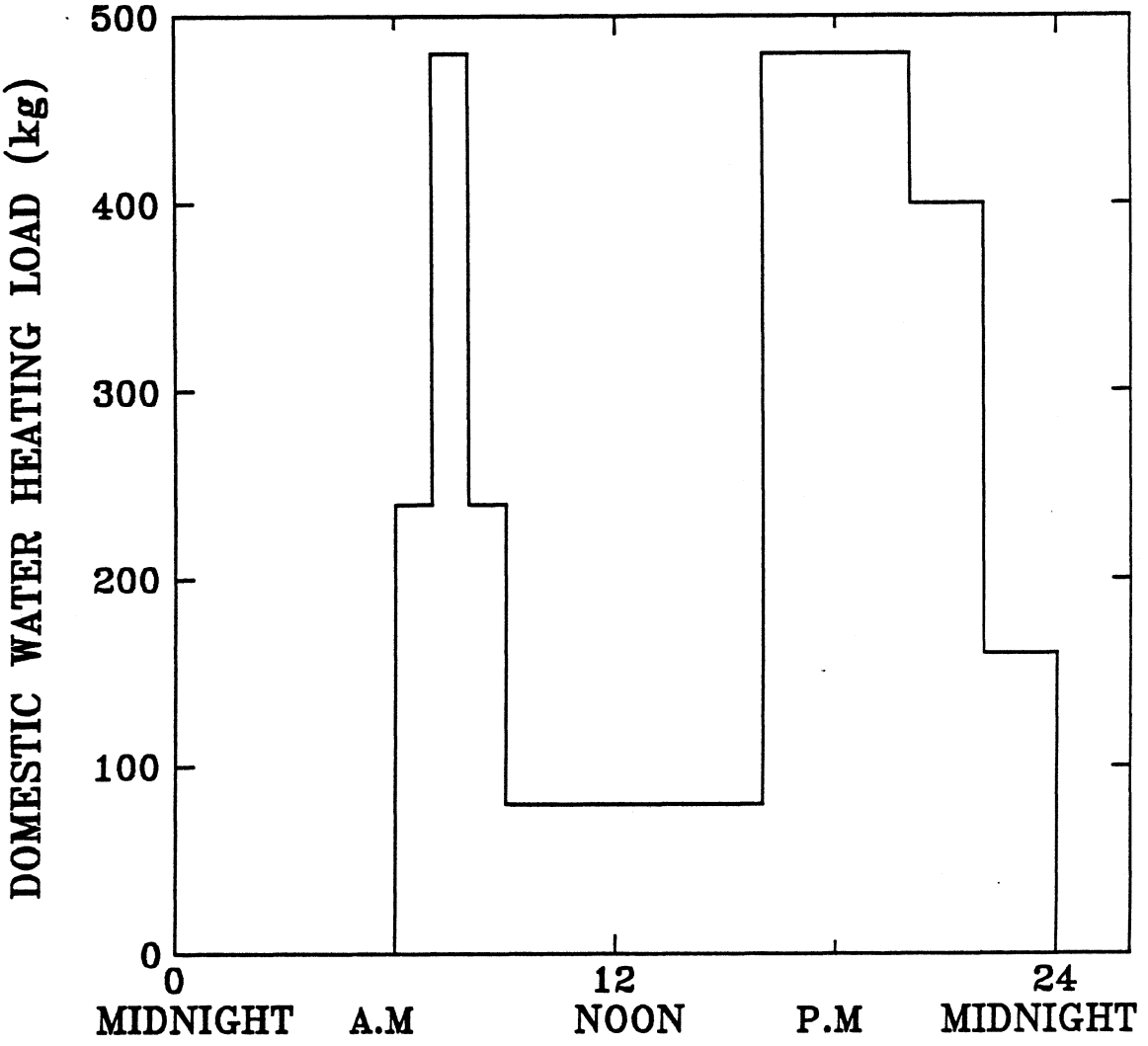

Figure 6.2 Usage Profile for Domestic Water Heating Load in Alexandria, Egypt.

6.3 Analysis

The system performance is predicted by calculating the annual solar fraction (F) which is defined as the fraction of the water heating load met by solar energy. TRNSYS is used to determine the performance of the standard SDHW system shown in Figure 6.1. In the present study, the weather data for Alexandria, Egypt (latitude 31.2°) was used. The data file of Alexandria contains monthly average values of daily radiation on a horizontal surface, clearness index, ambient temperature, wind speed, and relative humidity. Since TRNSYS needs hourly values of the previous parameters, the weather data generator developed by Knight [44] based on Degelman [45] was used.

The f-chart design method [19] provides a fast mean of estimating the fraction of the heating load that will be supplied by solar energy for a specified standard system configuration. The f-chart method has been developed for three standard system configuration, air and liquid-based systems for space and domestic water heating, and domestic hot water system only. It suggests that f (the fraction of the monthly heating load met by solar energy) is empirically related to the two dimensionless groups :

$$X = A_c F_R' U_L (T_{ref} - \overline{T}_a) \Delta t / L \qquad (6.1)$$

$$Y = A_c F_R' \overline{(\tau\alpha)} \overline{H}_T N / L \qquad (6.2)$$

where

A_c	is the area of the solar collector (m^2)
F_R'	is the collector-heat exchanger efficiency factor

U_L	is the collector overall energy loss coefficient (kJ/h m^2 K)
Δt	is the total number of seconds in the month
T_{ref}	is a reference temperature determined to be 100 °C
$\overline{T}_a$	is the monthly average ambient temperature (°C)
L	is the monthly total heating load (kJ)
$\overline{(\tau\alpha)}$	is the collector monthly average transmittance-absorptance product
$\overline{\overline{H}}_T$	is the monthly average daily radiation incident on the collector surface per unit area (kJ/m^2)
N	is the number of days in the month

These dimensionless groups have some physical meaning. Y is proportional to the ratio of the total energy absorbed on the collector plate surface to the total heating load during the month. X is proportional to the ratio of a reference collector energy loss to the total heating load during the month. The equations for X and Y can be rewritten in a more convenient form for calculations :

$$X=F_R\ U_L\ (F_R'/F_R)\ (T_{ref} - \overline{T}_a)\ A_c\ \Delta t / L \tag{6.3}$$

$$Y=F_R\ (\tau\alpha)_n\ (F_R'/F_R)\ [\ \overline{(\tau\alpha)} / (\tau\alpha)_n]\ A_c\ \overline{\overline{H}}_T\ N / L \tag{6.4}$$

where F_R is the collector heat removal factor, and $(\tau\alpha)_n$ is the collector monthly average transmittance-absorptance product at normal incidence. The detailed calculations of the

parameters on the right hand side of equations (6.3), and (6.4) can be found in [19]. For domestic water heating system, the mains water supply temperature (T_{main}) and the set point temperature of the hot water (T_{set}) affect the collector energy losses. So, the dimensionless group X, which is proportional to the collector energy losses must be corrected to account for this effect. The corrected dimensionless group X_c becomes

$$X_c=F_R\, U_L\, (F_R'/F_R)\, (11.6+1.18\, T_{set}+3.86\, T_{main} - 2.32\, \overline{T}_a)\, A_c\, \Delta t / L \qquad (6.5)$$

The correlation between X_c, Y, and f for domestic hot water is

$$f= 1.029\, Y - 0.065\, X_c - 0.245\, Y^2 + 0.0018\, X_c^2 + 0.0215\, Y^3 \qquad (6.6)$$

$$\text{for} \quad 0 < Y < 3 \quad \text{and} \quad 0 < X < 18$$

6.4 Results and Discussion

Table 6.2 shows a comparison between the monthly solar fraction values obtained by both TRNSYS and the f-chart design method in Alexandria, Egypt. As seen from the results, the annual solar fraction predicted by the f-chart design method is in a good agreement with the corresponding value obtained using TRNSYS. For this reason, the following results were generated using the f-chart design method to take advantage of its huge reduction in computer cost over the detailed simulation calculations using TRNSYS.

Figure 6.3 shows the variation of annual solar fraction with collector tilt-latitude. The optimum collector orientation, that is, the orientation in which the solar water heating system provides the largest fraction of the annual heating load is due south at an angle

Table 6.2 Comparison Between Monthly Solar Fraction Values Obtained by F-Chart Method and Those Obtained by TRNSYS

	Solar Fraction	
	F-Chart Method	TRNSYS
Jan	0.72	0.75
Feb	0.78	0.80
Mar	0.85	0.87
Apr	0.91	0.92
May	0.98	0.95
Jun	1.00	1.00
Jul	1.00	1.00
Aug	1.00	1.00
Sep	0.94	0.96
Oct	0.89	0.90
Nov	0.83	0.86
Dec	0.74	0.75
Year	0.89	0.90

equal to the latitude. However, the collector orientation is not critical. Deviations from the optimum by as much as 10° have little effect on the solar system performance.

Figure 6.4 shows the variation of the annual solar fraction with collector area. As the collector area increases the solar fraction increases. This increase is not so pronounced for collector areas higher than 50 m^2. For example, increasing the collector area from 25-50 m^2, results in increasing the solar fraction by roughly 30 % of the load. On the other side, increasing the collector area from 50-100 m^2, results in increasing the solar fraction by approximately 11 % of the load.

Figure 6.5 shows the variation of the annual solar fraction with the storage capacity of the preheat tank. As seen from the figure, the annual system performance is relatively insensitive to the storage capacity of the preheat tank, as long as the storage capacity is equal to or greater than 70 kg of water per unit collector area.

The effect of varying load distribution, on system performance can not be calculated with the f-chart method. The f-chart correlations are based on the Rand profile [59], and it assumes a fully mixed tank. TRNSYS is used to study the effect of these two parameters on the annual system performance. The actual load profile of the hot water usage is highly dependent upon the lifestyle of the house occupants. Zollner [60] concluded that a significant increase or decrease in performance can be obtained for an evening or morning weighted patterns, however the performance is insensitive to draw patterns which are not heavily weighted toward the morning or the evening. The difference between the performance of SDHW system obtained using the Rand profile and the corresponding performance obtained using the profile shown in Figure 6.2 is approximately 2% of the load.

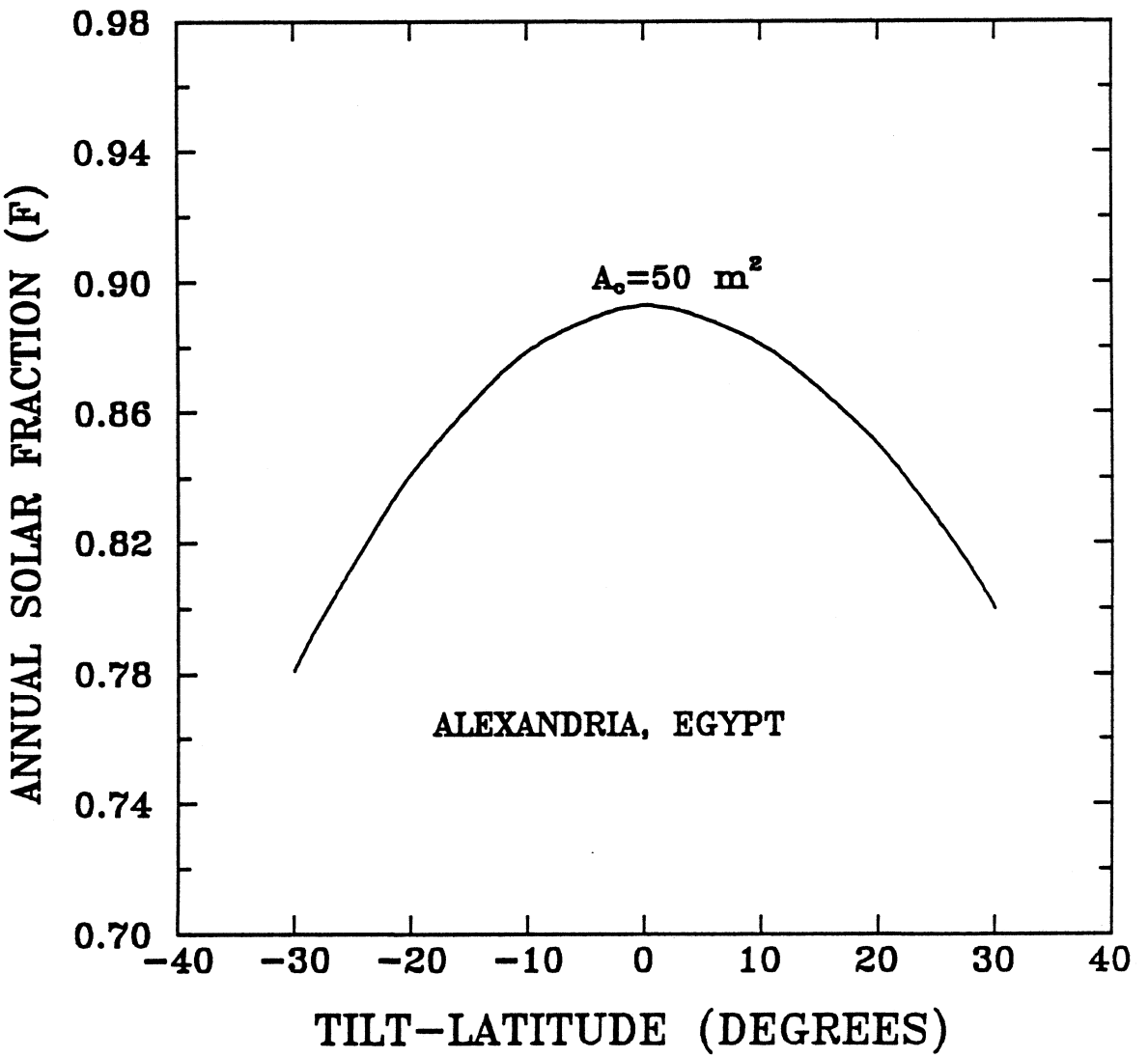

Figure 6.3 Variation of Annual Solar Fraction with Collector Orientation-Latitude for Solar Domestic Hot Water (SDHW) System.

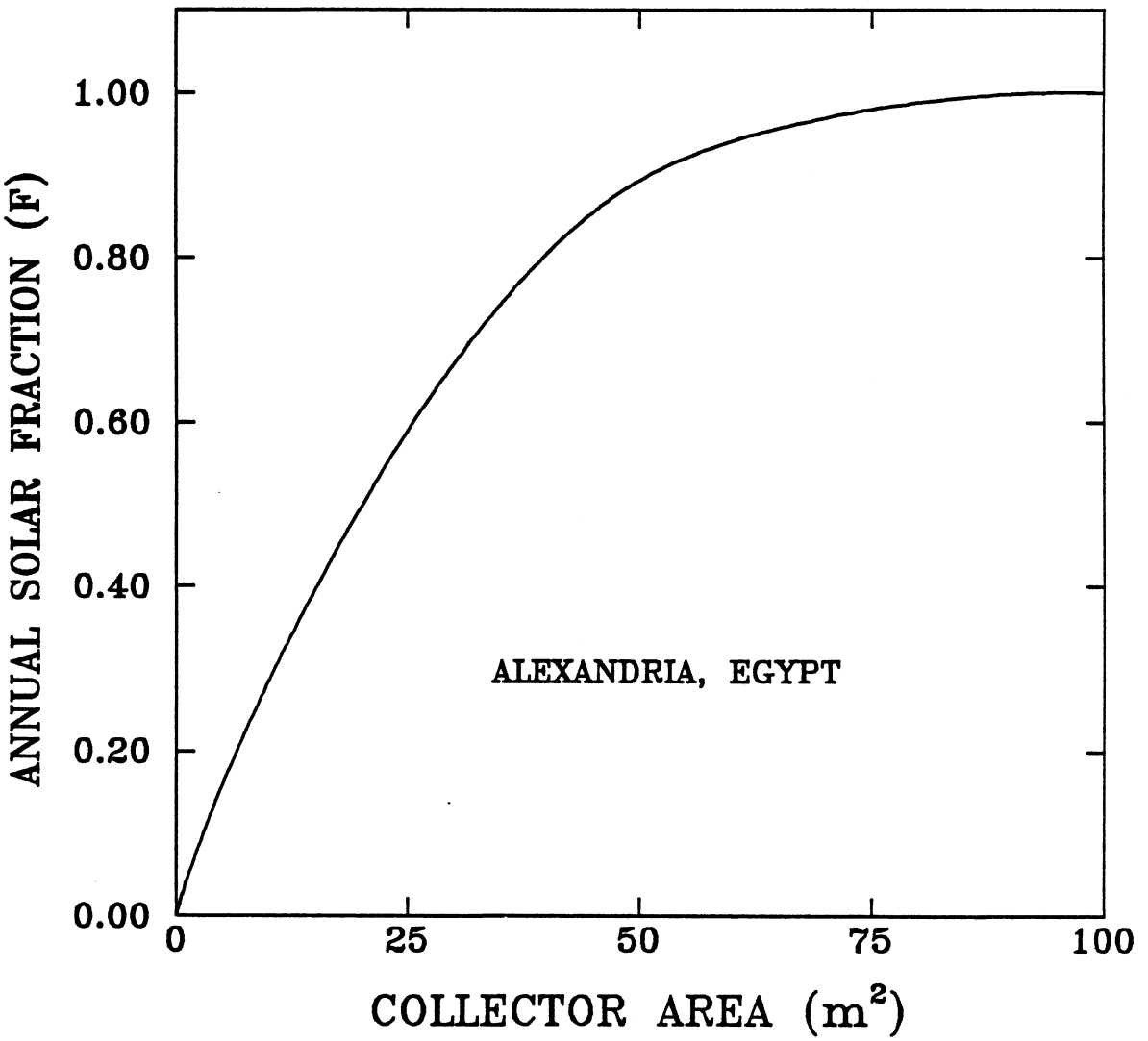

Figure 6.4 Variation of Annual Solar Fraction with Collector Area for Solar Domestic Hot Water (SDHW) System .

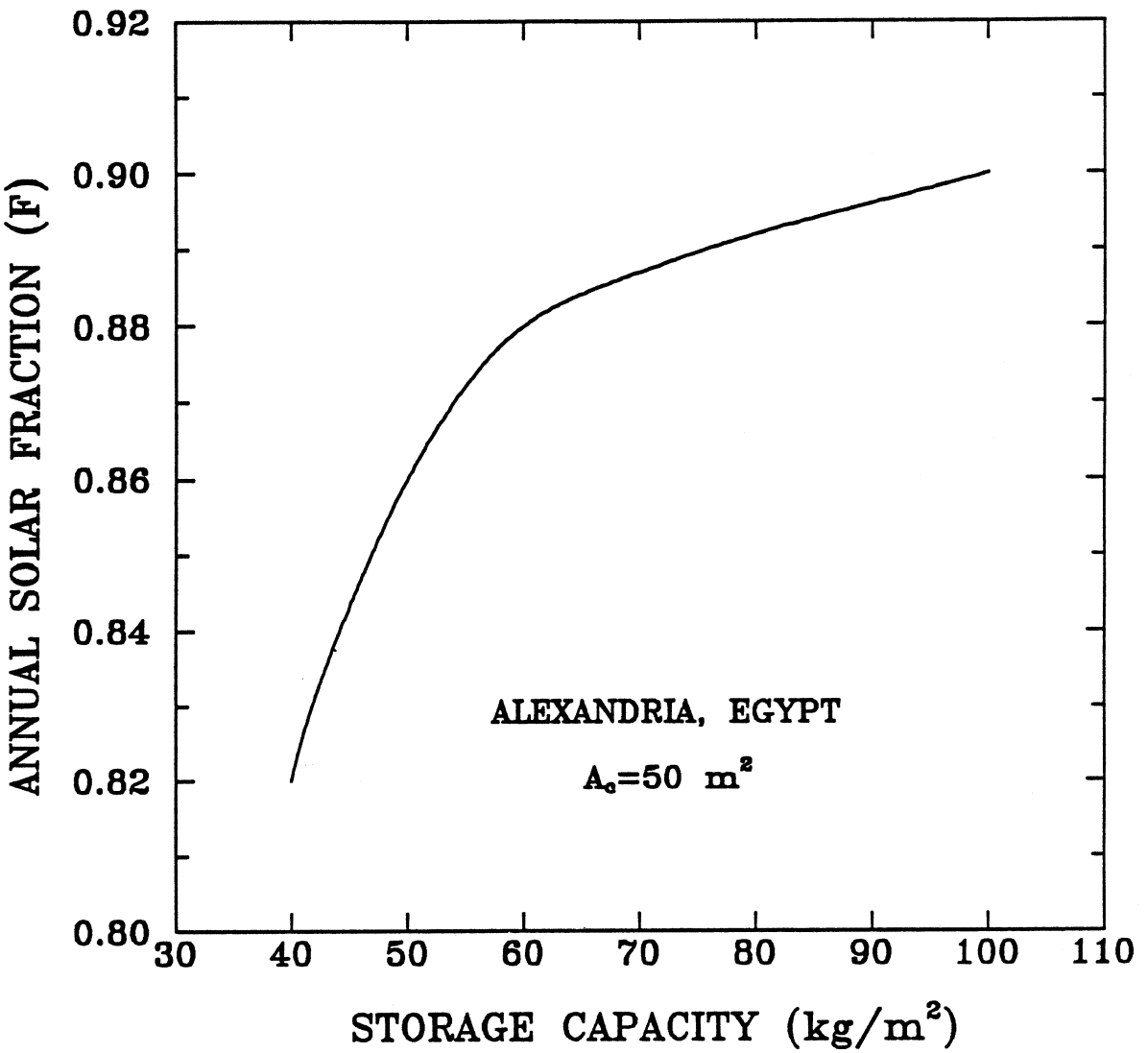

Figure 6.5 Variation of Annual Solar Fraction with Storage Capacity for Solar Domestic Hot Water (SDHW) System .

Also, the f-chart design method is based on the assumption that the storage tank is fully mixed and the solar fraction increases as the collector mass flow rate increases. This assumption is valid only for high collector flow rates, but for lower flow rates the f-chart method underpredicts the system performance. The values of collector performance parameters, $F_R U_L$ and $F_R (\tau \alpha)_n$, are affected by collector flow rate through the dependence of F_R on flow rate per unit collector area. This dependence was discussed in detail in Chapter 5.

A number of researcher have attempted to study the effect of thermal stratification. Phillips et al. [61] have studied the effect of thermal stratification for liquid-based solar heating systems. They used a stratification coefficient , defined as the ratio of the useful energy gain from a thermal stratification tank to the energy gain from an identical mixed-tank. Cole and Bellinger [62] have developed an analytical model to evaluate thermal stratification of liquid-based solar systems. They defined a stratification index ranges from zero for a fully mixed tank to one for a completely stratified (no recirculation) tank. The stratification index from their equation compares well with the experimental results. Copsey [63] presented a correction factor based on an equivalent collector area to account for thermal stratification in water-based systems. He defined the equivalent collector area as the collector area that a fully mixed system would require to obtain the same solar fraction as an otherwise identical stratified storage tank. However, the restrictions made in these studies limit their use. In this study, TRNSYS is used to investigate the effect of thermal stratification in the storage tank on the performance of SDHW system. The storage tank is modeled as being divided into a certain number of nodes. The effect of the number of the nodes on the performance of SDHW system was studied. No significant improvement in the system performance was found for a storage tank divided into more than three nodes.

Figure 6.6 shows the variation of the ratio between the solar fraction of a stratified tank (three nodes) and the solar fraction of a fully mixed tank (one node) with the mass flow rate per unit collector area. At high values of mass flow rates per unit collector area ($\geq$ 50 kg/h m^2), the benefits due to thermal stratification can be neglected and the storage tank can be considered fully mixed.

In conclusion, the f-chart method provides a good approximation of the annual performance of solar domestic hot water (SDHW) system in the Egyptian climate in comparison with the system performance predicted using TRNSYS. The recommended SDHW system parameters based on system performance in Alexandria are : collector orientation equal to the latitude, collector area of 50 m^2, storage mass capacity equal to 70 kg/m^2, and mass flow rate of 50 kg/h m^2. These recommended parameters were calculated for the previously specified domestic water heating load.

Comparisons with measured performance in many other places have shown that f-chart design method provides reliable estimates of long-term performance for SDHW systems. Fanny and Klein [64] have measured the performance of six different types of domestic hot water systems at the National Bureau of Standards (NBS) in Gaithersburg, Maryland. Their measurements were conducted over a one year period and compared to the performance predicted by the f-chart method. The annual solar fraction estimated by the f-chart design method was within 5% of the measured value for five active heating systems (the sixth system was a thermosyphon system, to which the f-chart method does not apply). Duffie and Mitchell [65] stated that there is a general agreement between the measured performance and the performance predicted by the f-chart method for systems with configurations close to the standard configuration used in developing the f-chart correlations. The present results represent a theoretical basis for comparison with any available measurements in Alexandria, Egypt.

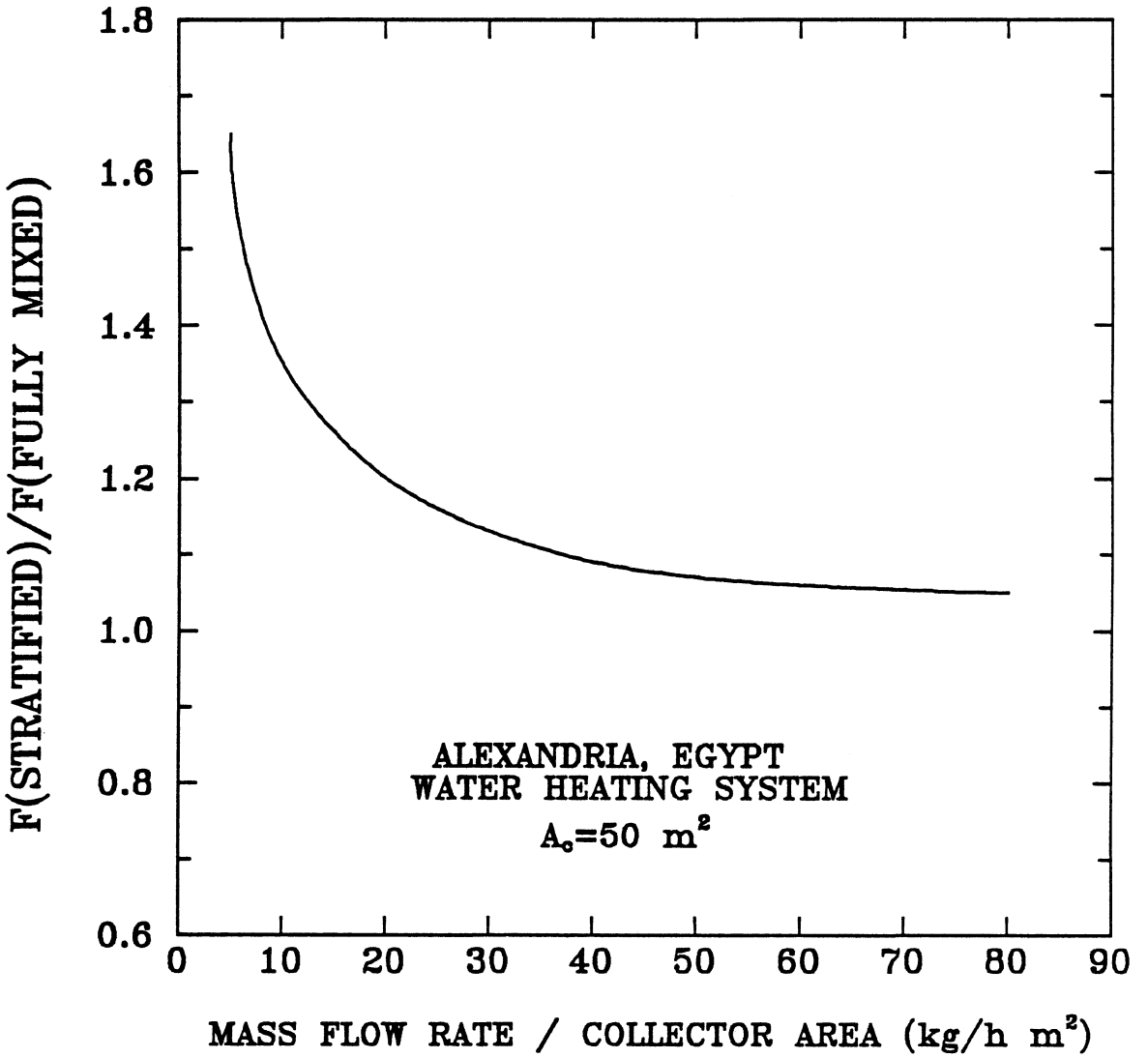

Figure 6.6 Variation of the Ratio Between the Performance of the Stratified Tank and Fully Mixed Tank with Mass Flow Rate per Unit Collector Area.

To check the reliability of the present results, an energy balance was performed on the used TRNSYS deck for each simulation. The simulation results obtained in the present study showed closure of 0.01-0.07 %.

CHAPTER 7
ANALYSIS OF COLLECTOR-STORAGE BUILDING WALLS USING PHASE-CHANGE MATERIALS

7.1 Introduction

The use of thermal storage walls that serve both as solar collector and thermal storage is well known. The wall is usually composed of masonry or containers filled with water to provide sensible heat storage, i.e, storage resulting from the specific heat capacity of a material as it increases in temperature. An interesting alternative to the standard materials are phase-change materials (PCMs) which employ latent heat storage. There are several transformations that a material may undergo, accompanied either by the absorption or the release of heat. Such as solid-liquid phase change, liquid-gas phase change, solid-gas phase change, and solid-solid transition. Liquid-gas, and solid-gas transformations are characterized by high heats of transition. However, the large changes in volume accompanying these transitions make their use complex and impractical. In solid-solid transition, heat is stored as the material is transformed from one solid phase to another. Solid-solid transition has the lowest storage capability, but could be used in special applications requiring a particular transition temperature. The solid-liquid phase change is preferred for many applications because of the much smaller volume change resulting in this transition for a given amount of energy storage.

The advantages of using PCMs as a collector-storage walls over the conventional methods (i.e. sensible storage) are : (1) significantly reduced storage mass, (2) high

collector efficiency as the collector works at low temperatures, and (3) reduced air temperature fluctuations that is because the energy exchanged in phase-change materials takes place at approximately constant temperature.

This chapter discusses the development of a numerical model compatible with TRNSYS to allow the use of phase-change materials as a collector-storage walls. The thermal performance of Sunoco's P116 paraffin wax, medicinal paraffin, and sodium sulphate decahydrate ($Na_2SO_4 \cdot 10H_2O$) as a collector-storage walls were investigated. A comparison between the thermal performance of these phase-change materials and the performance of concrete wall is presented. The effects of the thermal properties of PCMs on the thermal performance of collector-storage walls were also studied.

7.2 Analysis

The one-dimensional thermal circuit network used to predict the performance of the collector storage wall is presented in Figure 7.1 [66]. The network uses a control function, γ, which allows ventilation of the air gap either to the building or to the environment. Absorbed solar radiation on the outside surface of the wall transferred to the building by two different mechanisms. The first mechanism is conduction through the wall, then the energy conducted is convected and radiated from the inside surface of the wall to the building. The second mechanism is energy convection from the outside surface of the wall to the air in the gap between the wall and first cover, then transfer of this energy to the building air passing through the gap. The movement of air in the gap can be caused either by forced convection (for example by a fan) or by natural convection (buoyancy). In natural convection, heated air rises in the gap and enters the building through vents at the top of the wall. Heavier (cool) building air enters the gap through vents at the bottom of the wall.

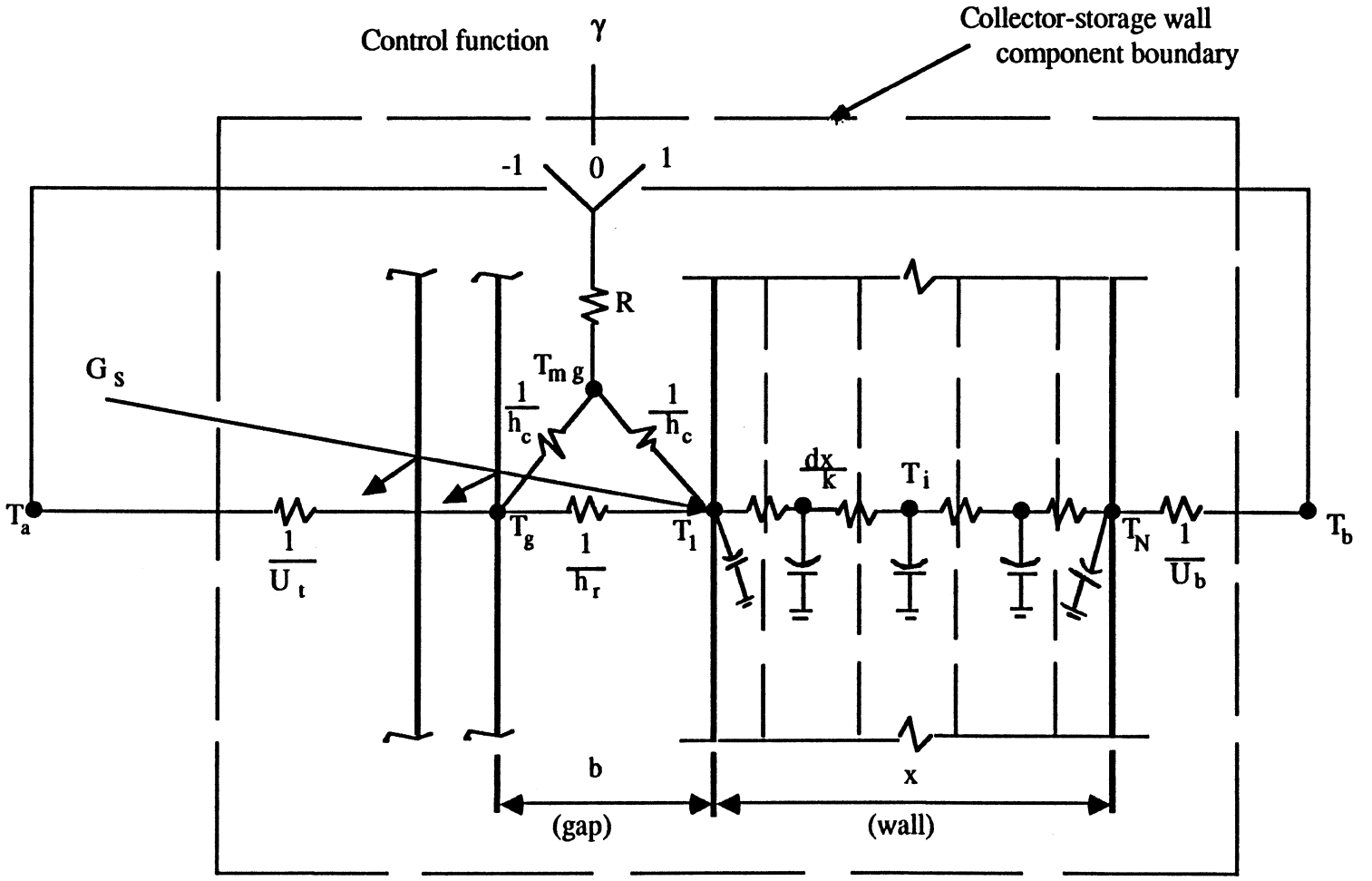

Figure 7.1 Thermal Circuit Network Used to Model Collector-Storage Wall

Figure 7.2 indicates the energy flows in and out of the collector-storage wall. An energy balance on the collector-storage wall yields

$$\dot{q}_{st} = \dot{q}_s - \dot{q}_l - \dot{q}_b - \dot{q}_v \tag{7.1}$$

where

$\dot{q}_s$ = is the rate at which energy is absorbed on the wall surface per unit collector area

$\dot{q}_l$ = is the rate of energy loss through glazing to the environment per unit collector area

$\dot{q}_b$ = is the rate at which energy is convected and radiated from the inside surface of the wall into the room per unit collector area

$\dot{q}_v$ = is the rate at which energy is carried away from the wall via airflow in the gap per unit collector area

$\dot{q}_{st}$ = is the rate of change of internal energy stored in the wall per unit collector area

Integrating equation (7.1) over the simulation period and multiplying by the collector-storage wall area gives

$$\Delta U = Q_s - Q_l - Q_b - Q_v \tag{7.2}$$

where ΔU is the change in the internal energy of the collector-storage wall.

The terms of equation (7.1) are calculated as follow :

$$\dot{q}_s = (\overline{\tau\alpha})\, G_s \tag{7.3a}$$

or

$$= G_b\, R_b\, f_i\, (\tau\alpha)_b + (\, G_d\, F_{c\text{-}s} + \rho\, G\, F_{c\text{-}g}\,)\, (\tau\alpha)_{dr} \tag{7.3b}$$

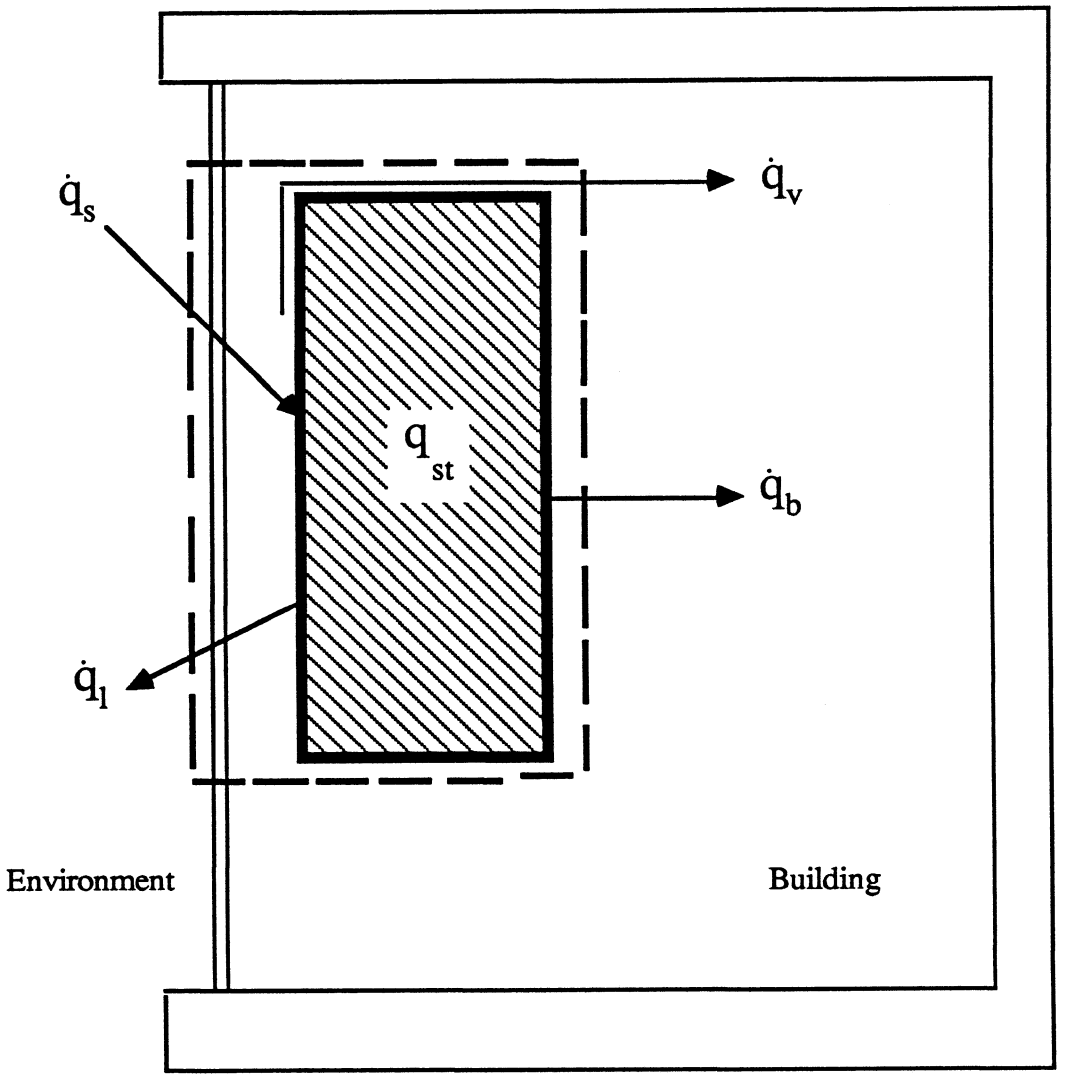

Figure 7.2 Energy Balance on Collector-Storage Wall

$$\dot{q}_l = U_t (T_g - T_a) \tag{7.4}$$

$$\dot{q}_b = U_b (T_N - T_b) \tag{7.5}$$

$$\dot{q}_v = \frac{\dot{m} c_f}{A_c} (T_o - T_{in}) \tag{7.6}$$

$$\dot{q}_{st} = \sum_{i=1}^{N} m_i \frac{d h_i}{d t} \tag{7.7}$$

The terms on the right sides of equations (7.3)-(7.7) are described below.

The parameters needed to calculate the rate of absorbed solar radiation per unit collector area, $\dot{q}_s$, from equation (7.3) are : fraction of the collector irradiated by direct beam (f_i), collector radiation view factor of the ground (F_{c-g}), collector radiation view factor of the sky (F_{c-s}), instantaneous total solar radiation on a horizontal surface (G), instantaneous beam solar radiation on a horizontal surface per unit area (G_b), instantaneous diffuse solar radiation on a horizontal surface per unit area (G_d), mean solar radiation incident on a shaded collector per unit area (G_s), the ratio of incident beam radiation on the collector surface to incident beam radiation on the horizontal surface (R_b), ground reflectance (ρ), the monthly average transmittance-absorptance product ($\overline{\tau\alpha}$), transmittance-absorptance product for beam radiation $(\tau\alpha)_b$, and transmittance-absorptance product for diffuse and ground reflected radiation $(\tau\alpha)_{dr}$. The detailed calculation of each of these terms can be found in [67].

The rate of energy loss through the glazing per unit collector area, $\dot{q}_l$, depends on the value of the top loss heat transfer coefficient (U_t). For one cover, U_t is given by

$$U_t = h_{ce} + h_{re} \tag{7.8}$$

where h_{ce} is the convection heat transfer coefficient between outer cover and environment calculated from the equation given by McAdams [68] :

$$h_{ce} = 5.7 + 3.8\, V_w \qquad (w/m^2\, K) \tag{7.9}$$

V_w is the wind speed in meters per second. h_{re} is the effective radiation heat transfer coefficient between the cover and the environment and can be represented by the following equation :

$$h_{re} = \varepsilon_g\, \sigma\, (T_g^2 + T_a^2)\, (T_g + T_a) \tag{7.10}$$

σ is the Stefan-Boltzman constant, and ε_g is the thermal emittance of the cover. T_g and T_a are the absolute temperatures of the cover glazing and the ambient air. For more than one cover, U_t can be calculated from a correlation developed by Klein [69].

The rate of energy transfer from the inside surface of the wall to the building per unit collector area, $\dot{q}_b$, can be calculated by assuming a constant value (30 kJ/h m^2 K) for the combined radiation and convection heat transfer coefficient (U_b). T_b is the room temperature, and T_N is the temperature of the inside surface of the collector-storage wall.

The rate of energy flow through the gap to the building or to the environment per unit collector area, $\dot{q}_v$, can be calculated using equation (7.6). A_c is the collector-storage wall area, c_f is the specific heat of the air, and $\dot{m}$ is the mass flow rate of air in the gap. T_{in} is the inlet air temperature. If γ equals 1, T_{in} equals T_b (room temperature), if γ equals -1, T_{in} equals T_a (ambient temperature). T_o is the gap outlet air temperature and it can be determined from an energy balance on a differential volume of air in the gap perpendicular to the flow (Figure 7.3 indicates this energy balance). The energy balance

on this differential volume yields

$$\dot{m}\, c_f \frac{dT}{dz} = h_c\, w\, (T_1 - T) + h_c\, w\, (T_g - T) \qquad (7.11)$$

where T is the temperature of the air in the gap at any position z, and w is the wall width.

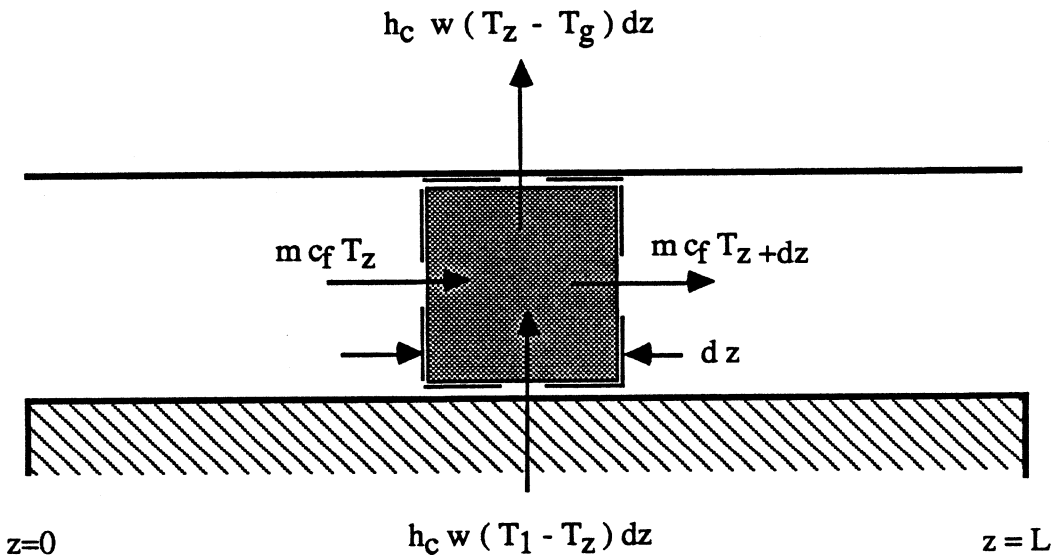

Figure 7.3 Energy Balance on a Differential Element of Air in the Gap

Integrating equation (7.11) over the air flow length, L, and solving the result for $(T_o - T_{in})$ gives

$$T_o - T_{in} = \frac{2\, T_{in} - T_1 - T_g}{2}\left[\exp - \left\{\frac{2\, h_c\, A_c}{\dot{m}\, c_f}\right\} - 1\right] \qquad (7.12)$$

At any position z, equation (7.12) takes the form,

$$T - T_{in} = \frac{2\,T_{in} - T_1 - T_g}{2}\left[\exp - \left\{\frac{2\,h_c\,w\,z}{\dot{m}\,c_f}\right\} - 1\right] \tag{7.13}$$

The mean air temperature in the gap, T_{mg}, is defined by

$$T_{mg} - T_{in} = \frac{1}{L}\int_0^L (T - T_{in})\,dz \tag{7.14}$$

Substituting from equation (7.13) into equation (7.14) and performing the integration gives

$$T_{mg} - T_{in} = \frac{2\,T_{in} - T_1 - T_g}{2}\left[-\frac{\dot{m}\,c_f}{2\,h_c\,A_c}\left\{\exp - \left\{\frac{2\,h_c\,A_c}{\dot{m}\,c_f}\right\} - 1\right\} - 1\right] \tag{7.15}$$

Defining the resistance to energy transfer through the air stream per unit area, R, as

$$R = \frac{\Delta T}{\dot{q}_v} = \frac{A_c\,(T_{mg} - T_{in})}{\dot{m}\,c_f\,(T_o - T_{in})} \tag{7.16}$$

Substituting the values of $(T_o - T_{in})$, and $(T_{mg} - T_{in})$ from equations (7.12), and (7.15) into equation (7.16) yields

$$R = \frac{A_c\left[\frac{-\dot{m}\,c_f}{2\,h_c\,A_c}\left\{\exp - \left(\frac{2\,h_c\,A_c}{\dot{m}\,c_f}\right) - 1\right\} - 1\right]}{\dot{m}\,c_f\left[\exp - \left(\frac{2\,h_c\,A_c}{\dot{m}\,c_f}\right) - 1\right]} \tag{7.17}$$

$\dot{q}_v$ can now be expressed in terms of T_{mg}, and R as

$$\dot{q}_v = \frac{(T_{mg} - T_{in})}{R} = \frac{(T_{mg} - T_{in})\,\dot{m}\,c_f \left\{ \exp - \left(\frac{2\,h_c\,A_c}{\dot{m}\,c_f} \right) - 1 \right\}}{A_c \left[\frac{-\dot{m}\,c_f}{2\,h_c\,A_c} \left\{ \exp - \left(\frac{2\,h_c\,A_c}{\dot{m}\,c_f} \right) - 1 \right\} - 1 \right]} \tag{7.18}$$

In this study, air circulation through the gap is assumed to be driven by density differences between the air in the gap and air in the building, i.e., thermocirculation. For thermocirculation case, the mass flow rate of air in the gap ($\dot{m}$) can be determined by applying Bernoulli's equation to the entire air flow system assuming that the density and temperature of the air in the gap varies linearly with collector-storage wall height (L). Solution of Bernoulli's equation for the mean air velocity in the gap yields

$$\overline{V} = \sqrt{\frac{2\,g\,L}{\left[C_1 \left(\frac{A_g}{A_v} \right)^2 + C_2 \right]} \cdot \left(\frac{T_{mg} - T_{in}}{T_{mg}} \right)} \tag{7.19}$$

A_g, and A_v are the total cross sectional area of the gap, and the total outlet area of the vent, respectively. The term $\left[C_1 \left(\frac{A_g}{A_v} \right)^2 + C_2 \right]$ represents the pressure drop in the gap and vents. The ratio $(A_g/A_v)^2$ accounts for the difference between the air velocity in the vents and the air velocity in the gap. C_1 and C_2 are dimensionless empirical constants. From data in Trombe et al. [70], values of C_1 and C_2 have been determined as 8.0, and 2.0, respectively by Utzinger [67].

The effective radiation heat transfer coefficient, h_r, between the outside wall surface and the first cover assuming infinite parallel plates is given by

$$h_r = \frac{\sigma (T_1^2 + T_g^2) (T_1 + T_g)}{1/\varepsilon_w + 1/\varepsilon_g - 1} \tag{7.20}$$

ε_w and ε_g are the wall and cover thermal emittances.

The value of the convection heat transfer coefficient, h_c, depends on whether there is a flow in the gap or not. When there is no air flow in the gap, h_c, is calculated from the following correlation given by Randall, et al. [71] for convection heat transfer between vertical parallel plates

$$h_c = \left[0.0965 \ (Gr \cdot Pr)^{0.29} \right] \frac{k_f}{b} \tag{7.21}$$

k_f is the thermal conductivity of the air. b is the plate spacing. Pr is the Prandtl number. Gr is the Grashof number. When air is flowing in the gap, the correlation for h_c will depend on the type of the flow (i.e. laminar or turbulent flow). For laminar flow ($Re \leq 2000$), the correlation given by Mercer et al. [72] is used

$$h_c = \left[4.9 + \frac{0.0606 \ (x)^{-1.2}}{1.0 + 0.0856 \ (x)^{-0.7}} \right] \frac{k_f}{b} \tag{7.22}$$

where

$$x = \frac{L}{Re \cdot Pr \cdot D_H} \tag{7.23}$$

Re is the Renolds number. D_H is the hydraulic diameter of the flow channel, which is

equal to four times the flow cross sectional area divided by the flow perimeter. L is the length of the flow channel. For turbulent flow (Re > 2000), h_c is given by Duffie, and Beckman [52] correlation for fully developed flow

$$h_c = \left[0.0158 \ Re^{0.8} \right] \frac{k_f}{b} \tag{7.24}$$

The present numerical model incorporates iterative scheme to solve for the wall temperatures and energy flows since the quantities h_c, h_r, $\dot{m}$, and U_t are functions of temperature. The iterative scheme uses temperatures from previous time step to calculate h_c, h_r, $\dot{m}$, and U_t, then using these values to calculate T_{mg}, and T_g. The iteration process is continued until the difference between the old and new values of T_{mg}, and T_g is equal to or less than 0.1 °C. The values of T_g, and T_{mg} are calculated from energy balances on their nodes (Figure 7.1).

$$0 = U_t (T_a - T_g) + h_r (T_1 - T_g) + h_c (T_{mg} - T_g) \tag{7.25}$$

$$0 = h_c (T_g - T_{mg}) + h_c (T_1 - T_{mg}) + \frac{1}{R} (T_{in} - T_{mg}) \tag{7.26}$$

Solving the above two equations for both T_g and T_{mg} gives

$$T_g = \frac{T_a U_t + T_{in} \dfrac{h_c / R}{2 h_c + \dfrac{1}{R}} + T_1 \left[h_r + \dfrac{h_c^2}{2 h_c + \dfrac{1}{R}} \right]}{h_r + U_t + h_c + \left[\dfrac{h_c^2}{2 h_c + \dfrac{1}{R}} \right]} \tag{7.27}$$

and

$$T_{mg} = \frac{(T_{in}/R) + (T_g + T_1)\, h_c}{2\, h_c + (1/R)} \tag{7.28}$$

The change in energy stored in the wall per unit collector area, $\dot{q}_{st}$, can be approximated as the sum of the energy stored in each element of the wall. The wall is divided into N finite elements in the direction perpendicular to the wall (x-direction). The effect of considering the energy conducted in the wall parallel to the air flow (i.e., the two-dimensional case) was studied. The energy flows parallel to the air flow was found to be approximately 0.001 of the energy conducted through the wall. For this reason, the one-dimensional model has been used in the present study. m_i is the mass of node i per unit collector area. For the interior wall nodes, m_i is given by

$$m_i = \rho\, \Delta x \qquad\qquad 1 < i < N \tag{7.29}$$

ρ is the phase-change material density, and Δx is the node thickness which is equal to the wall thickness divided by the quantity (N-1). The masses of the surface nodes (i.e. nodes 1 and N) per unit collector area are given by

$$m_1 = m_N = \frac{\rho\, \Delta x}{2} \tag{7.30}$$

Making an energy balance on each wall node, and using a finite difference approximation over a finite increment of time (Δt) for the rate of change of the specific enthalpy, $\frac{d\, h_i}{d\, t}$, one can obtain the following equations for wall nodes :

$$\frac{h_1^{p+1} - h_1^p}{\Delta t} = \frac{2}{\rho \Delta x}\left[\dot{q}_s + h_r (T_g - T_1^p) + h_c (T_{mg} - T_1^p) + k \frac{T_2^p - T_1^p}{\Delta x}\right] \qquad (7.31)$$

$$\frac{h_i^{p+1} - h_i^p}{\Delta t} = \frac{k}{\rho \Delta x^2}\left[T_{i-1}^p + T_{i+1}^p - 2 T_i^p\right] \qquad 1 < i < N \qquad (7.32)$$

$$\frac{h_N^{p+1} - h_N^p}{\Delta t} = \frac{2}{\rho \Delta x}\left[U_b (T_b - T_N^p) + \frac{k}{\Delta x} (T_{N-1}^p - T_N^p)\right] \qquad (7.33)$$

p refers to the time level. k, the local value of the thermal conductivity of the phase-change material, is given by equation (3.3).

The critical time step, Δt, for the component model using phase-change materials as collector-storage walls is given by

$$\Delta t = \frac{\rho \, c_s \Delta x}{2}\left[\text{Min} \left\{ \frac{1}{h_r + h_c + \frac{k}{\Delta x}}, \frac{1}{U_b + \frac{k}{\Delta x}} \right\}\right] \qquad (7.34)$$

The temperature of the wall nodes can be calculated knowing the specific enthalpy h_i of each node. The relations between the specific enthalpy, h, and the temperature, T, for different transition ranges are given by equations (3.8). The incorporation of the collector-storage wall component model using PCMs into TRNSYS resulted in a major problem. The time step, Δt, required to achieve reasonable accuracy and stability in the collector-storage wall component model was several times smaller than the time step required for other TRNSYS subroutines (ΔT_{TR}). The same procedure explained in

section 3.2.4 was used to solve this problem.

Now, all the terms in equation (7.1) are determined. Integrating equation (7.1) over the simulation period and multiplying by the collector-storage wall area, the energy absorbed, the energy stored in the wall, the energy lost to the environment, and the energy transferred to the building can be calculated. This model was incorporated into TRNSYS [17] to calculate the thermal performance of the collector-storage walls using phase-change materials. To check the reliability of the present model, an energy balance on the collector-storage wall component was performed for each simulation. The energy balances showed a closure of 0.07-0.2%. Also, for each simulation an energy balance was performed for the used TRNSYS deck. The energy balance showed a closure of 0.1-0.4%. The FORTRAN subroutine developed for the collector-storage wall component using phase-change materials is listed in Appendix C, and the component flow diagram is shown in Figure 7.4. The description of the inputs, parameters, and outputs of the collector-storage wall component using phase -change materials is given in the following.

PARAMETERS NO.	DESCRIPTION
1	Mode : 2 (1 if $\dot{m}$ is an input to the component)
2	System unit (SI)
3	h - Wall height (m)
4	w - Wall width (m)
5	x - Wall thickness (m)
6	N - Number of nodes
7	ρ_s - Density of PCM in solid phase (kg/m^3)
8	ρ_l - Density of PCM in liquid phase (kg/m^3)

INPUTS - 8

OUTPUTS - 10

PARAMETERS - 24

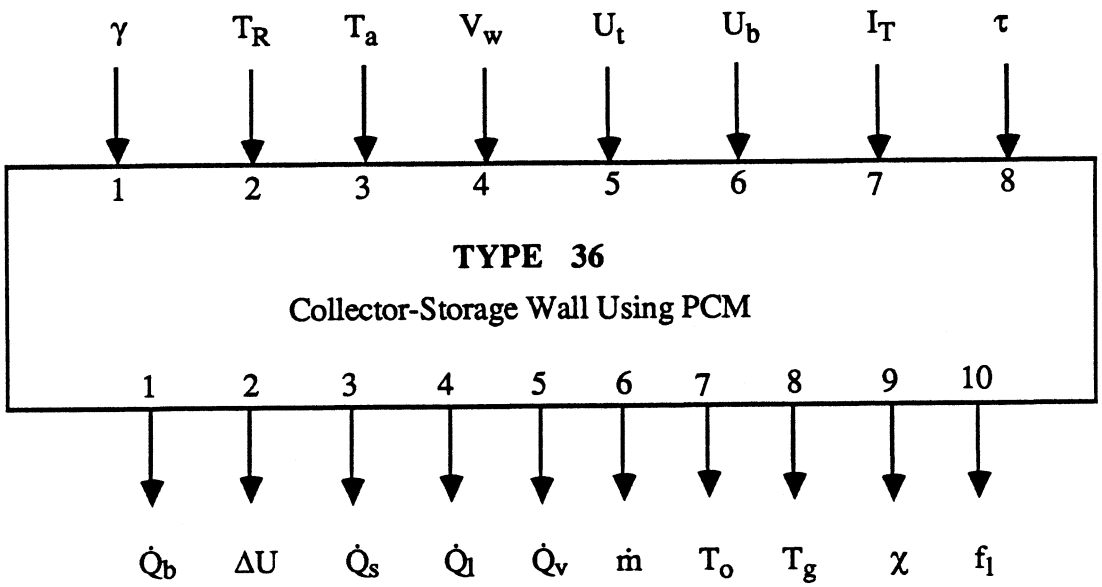

PARAMETERS

1. Mode
2. System Unit
3. h
4. w
5. x
6. N
7. ρ_s
8. ρ_l
9. α
10. ε_w
11. ε_g
12. N_g
13. b
14. c_s
15. c_l
16. k_s
17. k_l
18. T_{m1}
19. T_{m2}
20. h_{sl}
21. T_{int}
22. χ_{int}
23. A_v
24. h_v

Figure 7.4 Collector-Storage Wall Component Flow Diagram

9	α - Wall solar absorptance
10	ε_w - Wall thermal emittance
11	ε_g - Glazing thermal emittance
12	N_g - Number of glazing covers
13	b - Spacing between wall surface and first glazing (m)
14	c_s - Specific heat of PCM in solid phase (kJ/kg K)
15	c_l - Specific heat of PCM in liquid phase (kJ/kg K)
16	k_s - Thermal conductivity of PCM in solid phase (kJ/m h K)
17	k_l - Thermal conductivity of PCM in liquid phase (kJ/m h K)
18	T_{m1} -Lower boundary of the transition range (° C)
19	T_{m2} -Upper boundary of the transition range (° C)
20	h_{sl} - Solid-liquid transition latent heat (kJ/kg)
21	T_{int} - Initial temperature of PCM (° C)
22	χ_{int} - Initial liquid fraction
23	A_v - Vent outlet area (m^2)
24	h_v - Vertical distance between inlet and outlet vents (m)

INPUT NO.	DESCRIPTION
1	γ - Control function
2	T_R - Room temperature (°C)
3	T_a - Ambient temperature (°C)

4	V_w - Wind speed (m/s)
5	U_t - Heat transfer coefficient from first glazing to ambient (kJ/h m^2 °C)
6	U_b - Heat transfer coefficient between collector-storage wall inside surface and the building (kJ/h m^2 °C)
7	I_T - Total incident solar radiation (kJ/m^2)
8	τ – Transmittance of glazing

OUTPUT NO.	DESCRIPTION
1	$\dot{Q}_b$ - Rate of energy flow into the room (kJ/h)
2	ΔU - Change in the internal energy of the wall (kJ)
3	$\dot{Q}_s$ - Rate of energy absorbed by the wall (kJ/h)
4	$\dot{Q}_l$ - Rate of energy flow to the environment (kJ/h)
5	$\dot{Q}_v$ - Rate of energy flow through the vents either to the environment or to the building(kJ/h)
6	$\dot{m}$ - mass flow rate of air in the gap (kg/h)
7	T_o - Outlet air temperature at wall vent (°C)
8	T_g - Temperature of first glazing (°C)
9	χ - Liquid fraction
10	f_l - Fraction of run time that PCM operates in the liquid phase mode

7.3 Results and Discussion

A typical residential building with the characteristics listed in Table 7.1 was chosen for study.

Table 7.1 Building Characteristics [39,40]

Windows = double glazed
Ceiling =2.7 kJ/h m^2 K
Floor =2.2 kJ/h m^2 K
All exterior walls =2.0 kJ/h m^2 K
Infiltration = 0.5 ACH
Internal gains = 2000 kJ/h
Glazing (Storage Wall) = double
Vent area (Storage Wall) = 3% of total wall area

System performance is expressed in terms of the solar savings fraction (SSF), defined by

$$SSF = 1 - \frac{Q_{aux}}{L} \tag{7.35}$$

where L is the heating load (including infiltration) if the collector-storage wall were replaced by an adiabatic wall, and is given by

$$L = (UA)_{ns} (DD) \tag{7.36}$$

$(UA)_{ns}$ is the thermal conductance of the house with the collector storage wall is replaced

by an adiabatic wall. $(UA)_{ns}$ is also termed the building load coefficient [21,22], and DD is the heating degree days [73]. The auxiliary load required by a furnace (Q_{aux}) is the heating load required when using the collector-storage wall. Energy which is transferred from the wall to the room at times when heating is not required must be dumped and does not reduce Q_{aux}. (Note that solar savings fraction is not the same as the solar fraction that is commonly used in active solar heating, as the heating load L is not the total heating load in the building. The end result of interest using either solar savings fraction or solar fraction is Q_{aux}, the energy that must be purchased).

Solar savings fraction is presented in terms of the load collector ratio (LCR), which is given by

$$LCR = (UA)_{ns} / A_c \tag{7.37}$$

where A_c is the collector-storage wall area.

To check the reliability of the present results, the predicted performance of a concrete storage wall was compared to the performance predicted by the solar load ratio method (SLR) developed at Los Alamos [21,22]. SLR method is based on correlations for SSF as a function of load collector ratio and system type (i.e. direct gain, sunspace, collector-storage wall, etc.). These correlations are only valid for six generic systems, so the Passive Solar Design Handbook [21,22] has a series of graphical correction factors which account for changes from these reference systems. The correction factor curves are also presented for various specified locations. If one wants to use a different

location, he must interpolate these curves to obtain the correction factor corresponding to his desired location. The two predictions agreed reasonably well. Table 7.2 shows a comparison between the heating load required using a concrete storage wall with thickness equal to 0.30 m, by both the SLR method and the present model for the heating season (from Nov. 1 to Apr. 1) in Albuquerque.

Table 7.2 Comparison Between Heating Loads Required Using Both the SLR Method and the Present Model

	$Q_{aux} \times 10^{-6}$ (SLR method)	$Q_{aux} \times 10^{-6}$ (present model)
Nov.	0.26	.25
Dec.	1.02	1.11
Jan.	1.22	1.30
Feb.	0.90	0.94
Mar.	0.59	0.57
total	3.99	4.17

The solar savings fraction values for a 0.30 m thickness of concrete for the heating season in Albuquerque at LCR=20 kJ/h m^2 K were found to be 0.67 and 0.65 using both the SLR method and the present model, respectively.

Figures 7.5a and 7.5b show the variation of the solar savings fraction with thickness at different values of the load collector ratio (LCR), for the three different storage media investigated in this study. These results were generated using typical

meteorological year (TMY) data for Albuquerque for the heating season (from Nov. 1 to Apr. 1). All the materials show an optimum thickness which can be explained as follows. The SSF first increases with increasing wall thickness because the storage mass carries over enough solar energy to heat the building then decreases because of the increased thermal resistance of the wall. To further investigate this behavior, the effect of air vents was studied. As seen from Figure 7.6, the performance of the collector-storage wall without air vents sharply decreases as thickness increases because heat conduction is the only mechanism for energy transfer from the wall to the room and the thermal resistance increases with increasing thickness.

Figures 7.5a and 7.5b show sodium sulphate decahydrate to have the best computed thermal performance. A wall of sodium sulphate decahydrate can achieve the same performance of concrete storage wall with a thickness approximately five times larger (without consideration for the support materials for the PCM). For medicinal paraffin, a wall with approximately half thickness of concrete can give the same performance, i.e. approximately one sixth the storage mass. The excellent performance of sodium sulphate decahydrate can be attributed to its relatively low melting temperature and its relatively high thermal conductivity (see Table 3.3). The main problems involved in using sodium sulphate decahydrate (Glauber's salt) are the occurrence of supercooling and stratification which were not considered in the simulations. Telkes [11] indicated that a 3-5% concentration of a nucleating agent like borax (sodium tetraborate decahydrate) prevents supercooling in $Na_2SO_4 \cdot 10H_2O$, and reported that a marked improvement in the problem of stratification can be achieved by mixing in a thixotropic agent.

The performance of paraffins can be improved by increasing the thermal conductivity and by using paraffins with low melting temperature. Paraffins have a wide range of melting temperatures. A member of the paraffin family can be found which

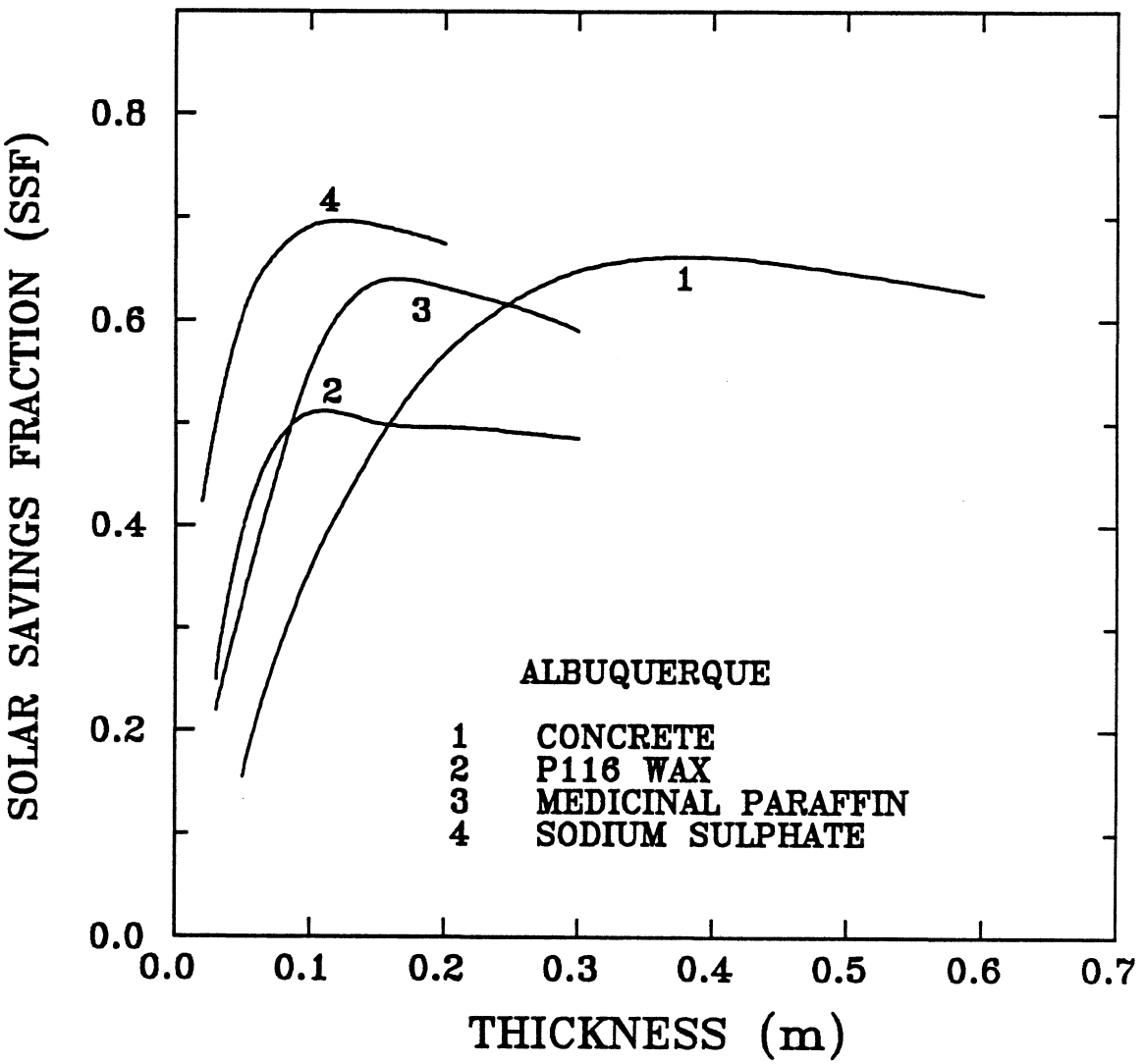

Figure 7.5a Variation of Solar Savings Fraction with Wall Thickness for Different Storage Media (LCR=20 kJ/h m^2 K).

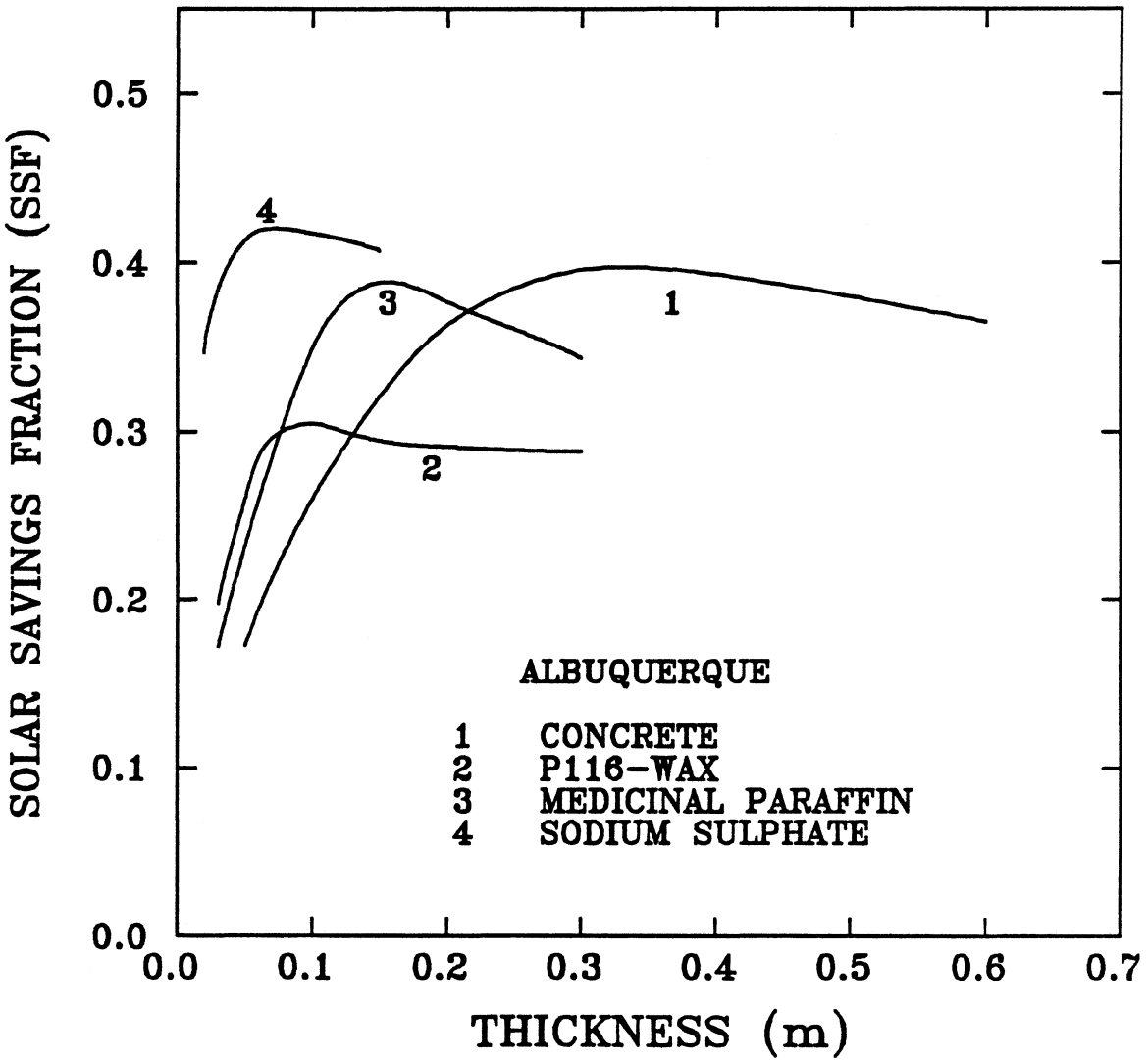

Figure 7.5b Variation of Solar Savings Fraction with Wall Thickness for Different Storage Media (LCR=40 kJ/h m^2 K).

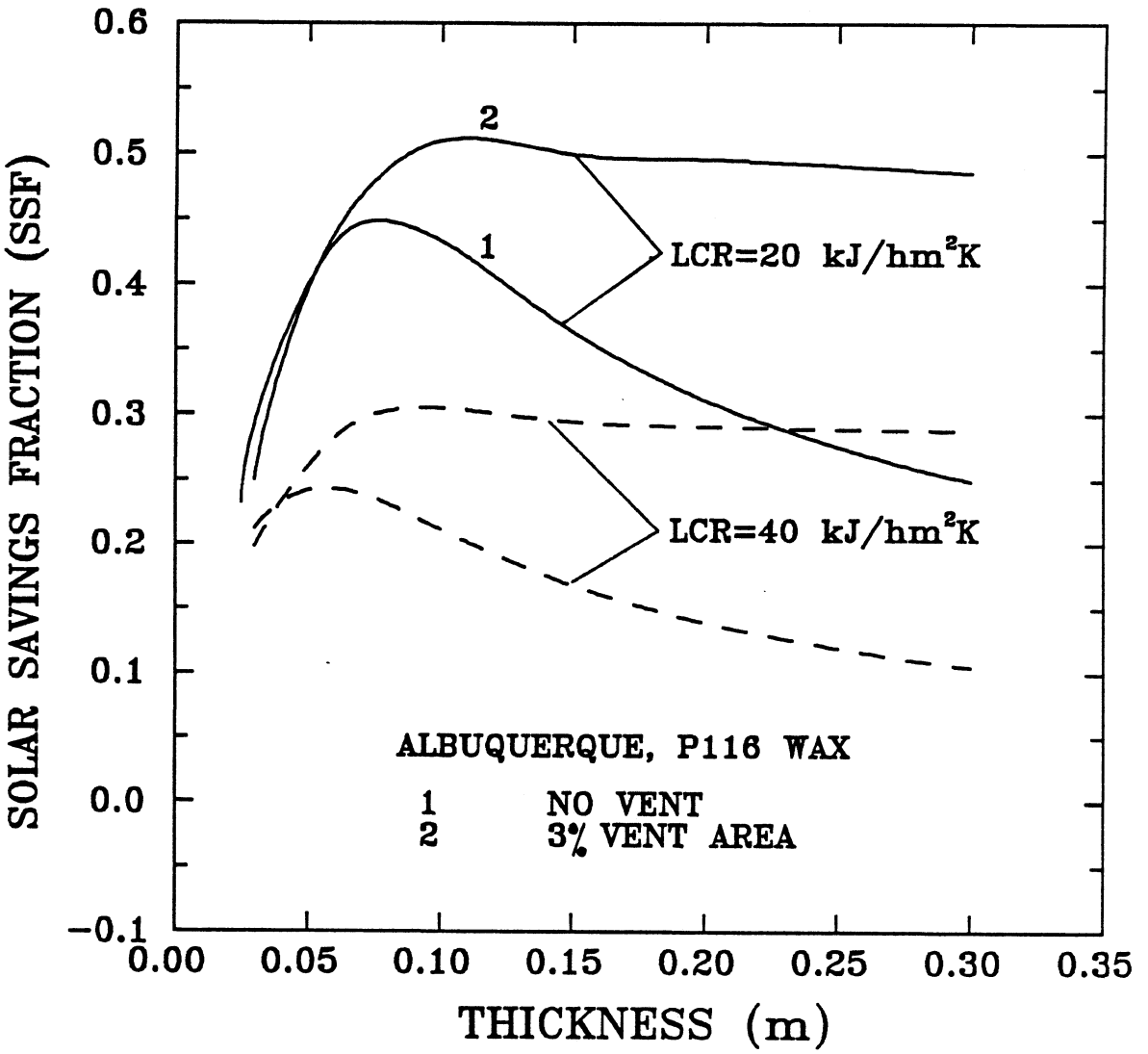

Figure 7.6 Variation of Solar Savings Fraction with Vent Area for P116 Wax.

melts at any desired temperature (20 to 50 °C). The thermal conductivity of paraffins can be increased by using a filler with a high thermal conductivity. Figure 7.7 shows the potential improvement in the performance due to increasing thermal conductivity at different values of LCR. Figures 8-10 are generated using the optimum thickness for P116 wax at LCR=20 kJ/h.m^2 K, i.e., 0.12 m (from Figure 7.5a).

Figure 7.8 shows the variation of SSF with melting temperature at two different thermal conductivities. At a low transition temperature (25° C), and a large thermal conductivity (2.5 kJ/h m K), the solar savings fraction (SSF) has the highest value because the rate of heat conduction to the interior surface of the wall and into the room in this case causes most of the wall to reach its transition temperature. Once charged, the wall discharges and loses heat at a lower rate. The average liquid fraction over the heating season period for this case was found to be approximately equal to 0.85, and the PCM operates in the liquid phase mode most of the time. For a high phase transition temperature (46.7 °C), and a large thermal conductivity, the system performance is low because during charging, heat is conducted to the interior surface of the wall and into the room at a such rate that the wall is at its melting temperature only a small fraction of the time. Once charged, the wall discharges and loses heat to the environment. The average liquid fraction over the heating season period in this case was found to be approximately equal to 0.12, and the PCM behaves approximately as a sensible store. At a high melting temperature and low thermal conductivity, the performance is slightly improved. In this case there is a compromise between the heat conduction rate through the wall during charging and the heat loss rate during discharging.

Figure 7.9 shows the variation of SSF with latent heat at different melting temperatures and with LCR. The latent heat of paraffins varies between 129-289 kJ/kg [7]. As the latent heat increases, the amount of energy stored in the material increases

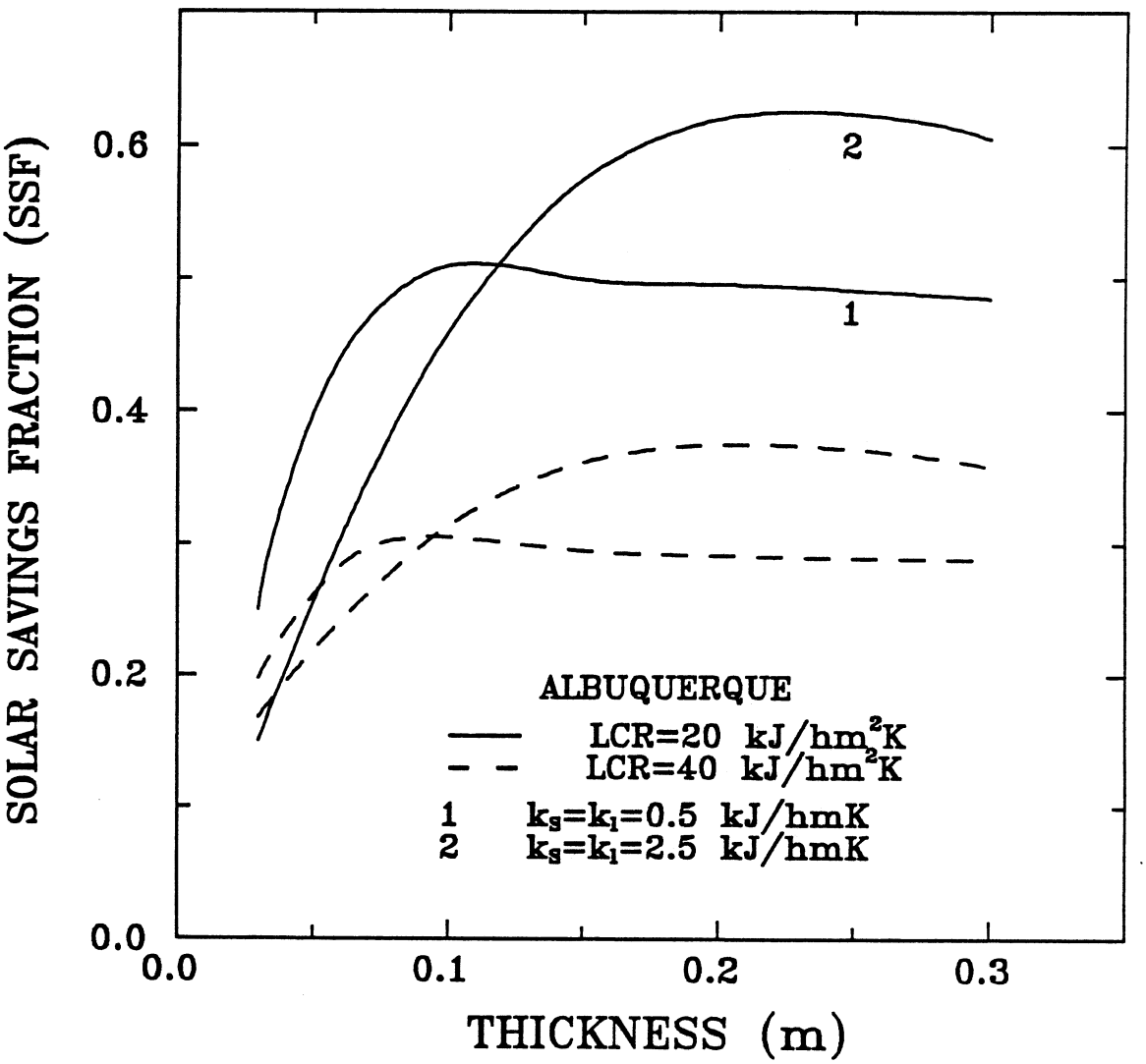

Figure 7.7 Variation of Solar Savings Fraction with Wall Thickness and Thermal Conductivity for Paraffins.

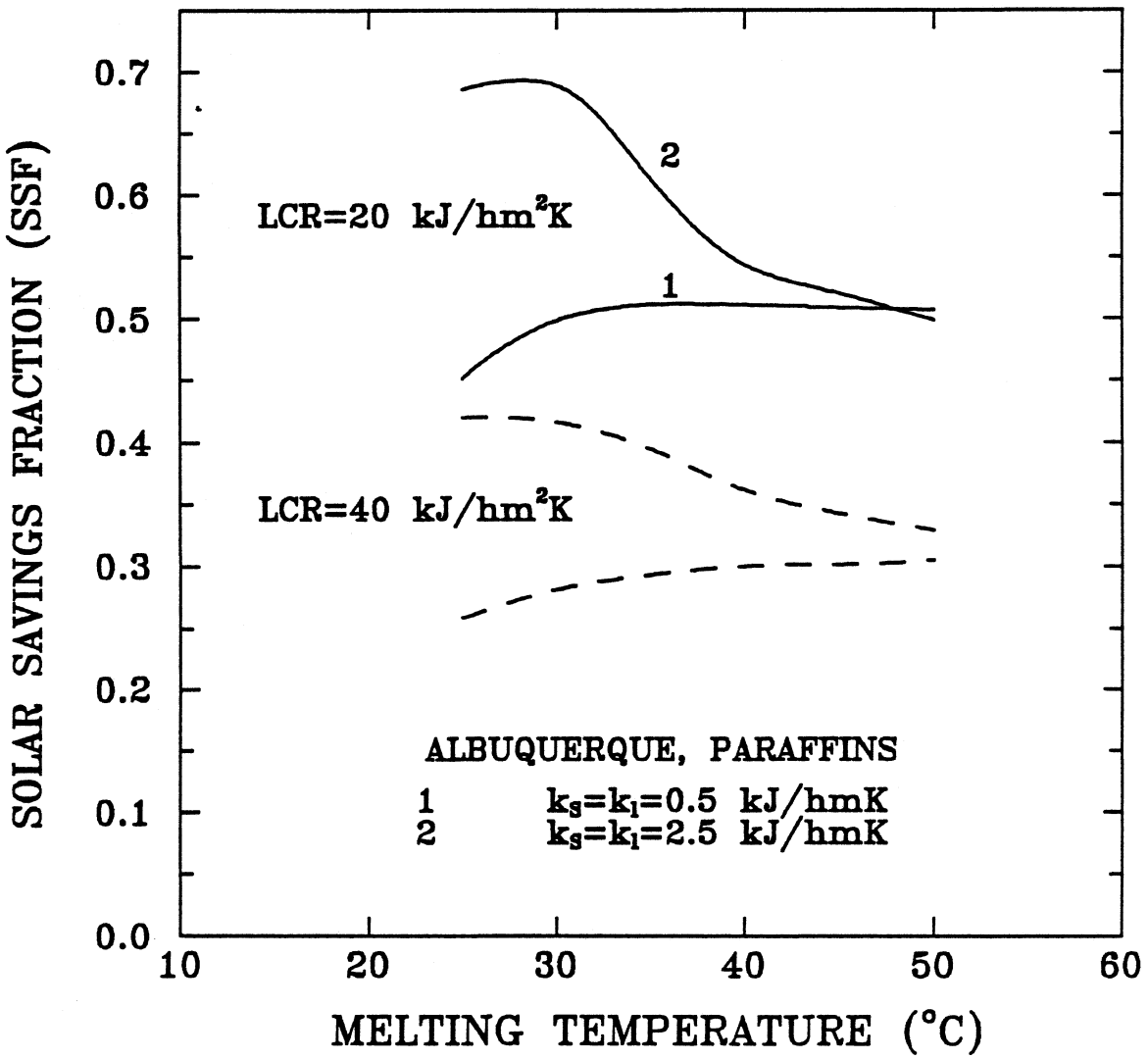

Figure 7.8 Variation of Solar Savings Fraction with Melting Temperature at Different Thermal Conductivities (h_{sl}=209 kJ/kg).

and this subsequently increases the solar savings fraction. But, as seen from the figure, the latent heat has a little effect on the SSF value. For high melting temperature (46.7 °C), the behavior of the PCM is approximately equal to that for the concrete wall, and no significant improvement in the system performance can be realized with PCM with such higher temperatures. To confirm this behavior, the liquid fraction was calculated. The average liquid fraction over the heating season period was found to be approximately 0.14, i.e., the PCM operates most of the time in the solid phase (i.e. sensible store).

Figure 7.10 shows the effect of melting temperature bandwidth for industrial grade paraffins. The industrial grade paraffins were assumed to have a melting temperature bandwidth up to 20 °C, i.e. ± 10 °C around the nominal melting temperature. As seen from the figure, the melting temperature bandwidth has little effect on the system performance. Figure 7.11 compares between the industrial grade paraffins (h_{sl}=129 kJ/kg, ΔT_m=±10 °C), and pure paraffins (h_{sl}=209 kJ/kg, ΔT_m=0 °C) at different thicknesses. Up to the optimum thickness, there is a little difference between the system performance predicted for both industrial grade paraffins and pure paraffins. The industrial grade paraffins can be used directly as a collector-storage wall materials, taking advantage of their reduced cost.

Figure 7.12 was generated using wax with the best thermal properties in the range investigated, i.e. T_m=25 °C, and k_s=k_l=2.5 kJ/h m K. As seen from the figure, there is a significant increase in the system performance in comparison with the performance of both concrete and P116 wax (T_m=46.7 °C, and k_s=k_l=0.5 kJ/h m K).

In conclusion, PCMs seem to be candidate materials for use in solar passive systems, and they may be preferable alternatives to the use of sensible store (masonry, and water) as a collector-storage walls on the basis of volume, mass, and thickness.

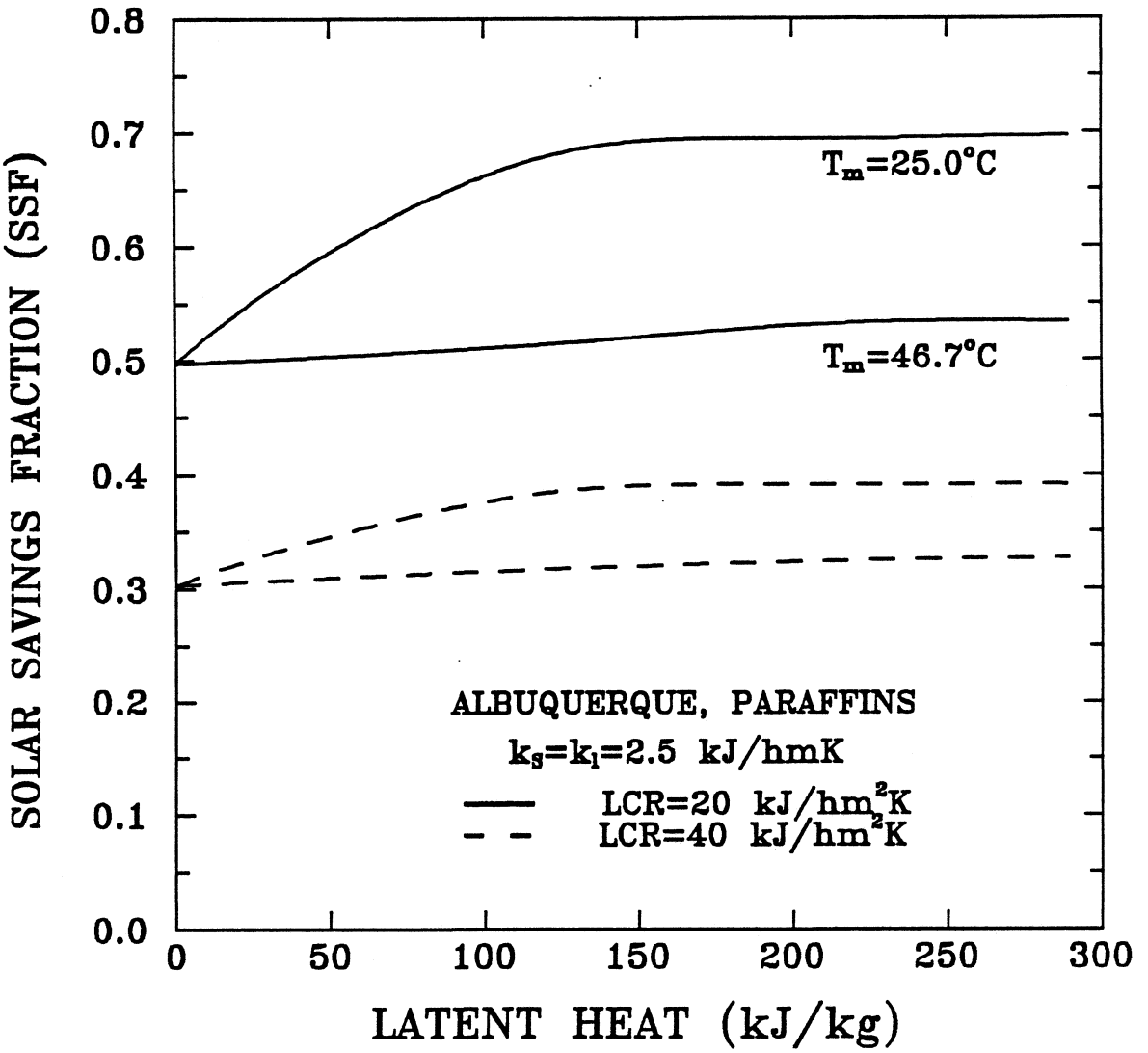

Figure 7.9 Variation of Solar Savings Fraction with Latent Heat at Different Melting Temperatures and LCR.

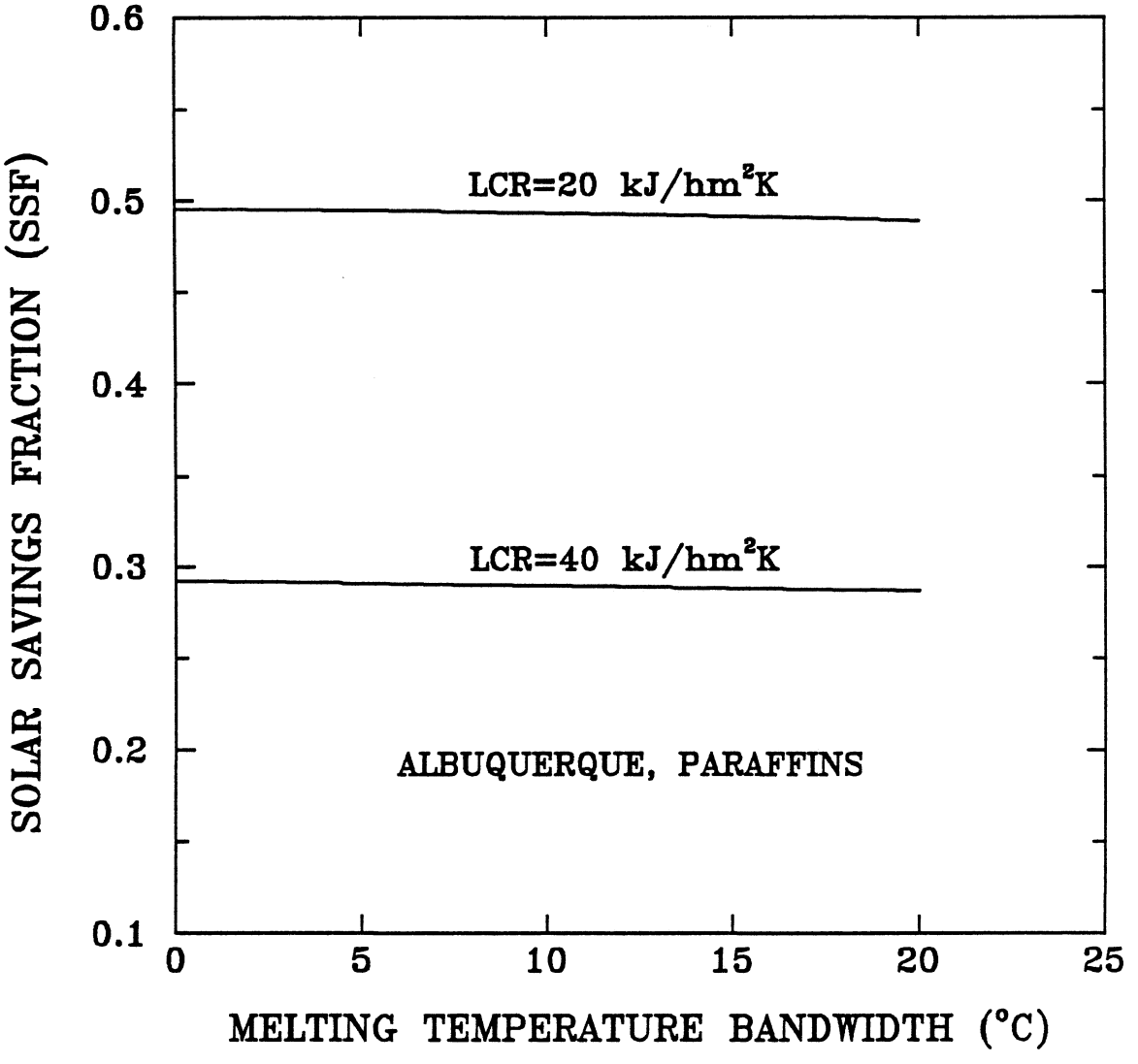

Figure 7.10 Variation of Solar Savings Fraction with Melting Temperature Bandwidth for Industrial Grade Paraffins (T_m=46.7 °C).

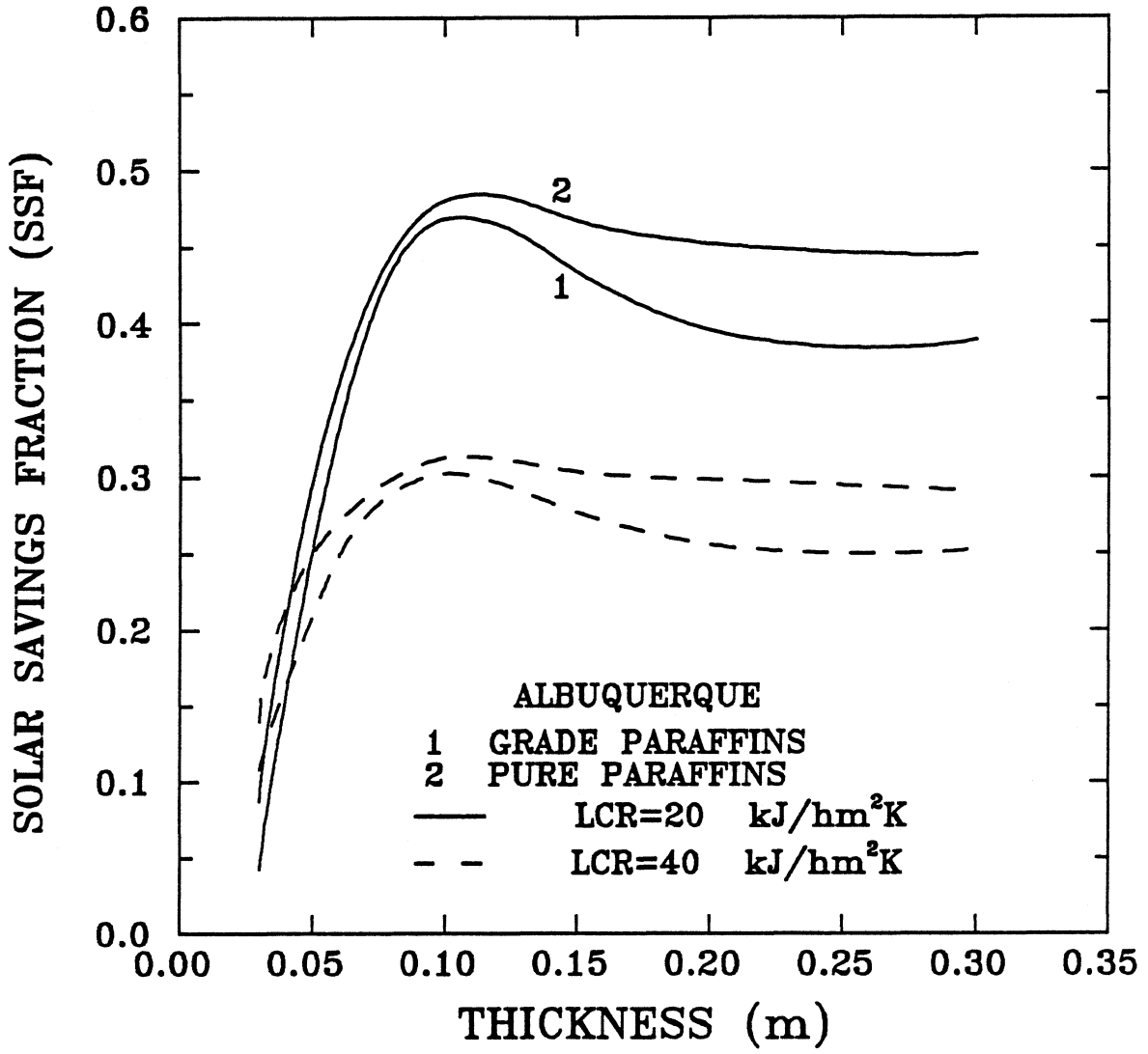

Figure 7.11 Variation of Solar Savings Fraction with Thickness for Industrial Grade and Pure Paraffins.

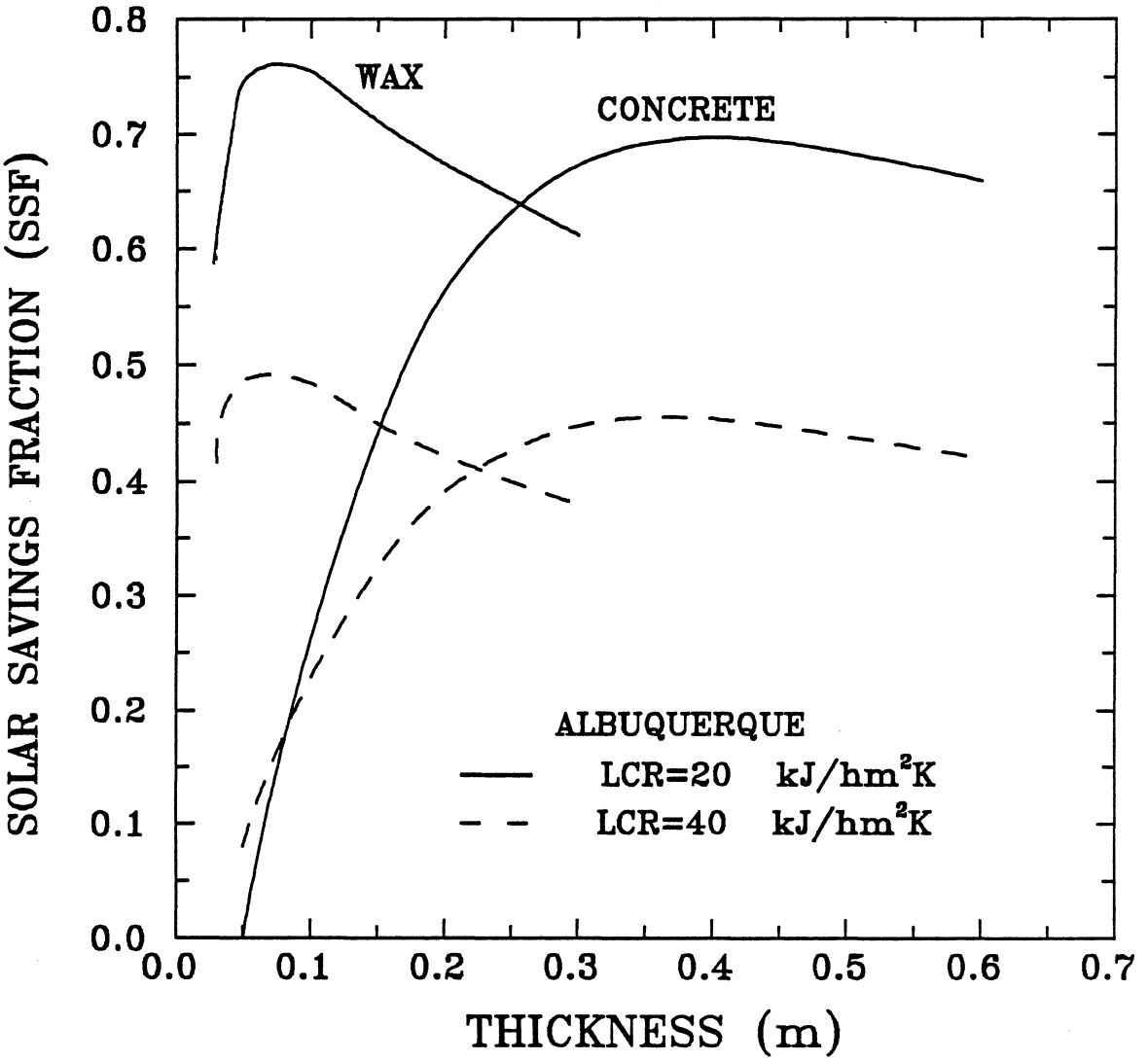

Figure 7.12 Variation of Solar Savings Fraction with Thickness for Concrete and Wax (k_s=k_l=2.5 kJ/h m K, and T_m=25 °C).

and its packaging should be chemically compatible to insure long term durability of the containers. The container must also provide an efficient heat transfer surface for energy exchange between the storage material and the building.

CHAPTER 8
CONCLUSIONS AND RECOMMENDATIONS FOR FUTURE WORK

8.1 Conclusions

The following conclusions were obtained from the results of the present work.

8.1.1 Active Solar Heating Systems

Based on the results of this study for both sensible and latent heat energy storage, the following conclusions can be drawn.

8.1.1.1 Sensible Heat Storage

1) The use of the infinite NTU model of Hughes et al [50], after taking the energy losses from the storage unit into the surroundings into account, for air-based solar heating systems results in a very small error taking advantage of its huge reduction in computational cost in comparison with the present finite NTU model.

2) The required storage volume of Abu-Siebera clay is roughly 96% of the storage volume required by pebble bed to achieve the same system performance. The better performance of Abu-Siebera clay over rock can be attributed to its relatively higher values of the specific heat and the thermal conductivity.

3) The recommended air-based solar heating system parameters using Abu-Siebera clay as a sensible energy storage medium, for the heating season starting from December 1 to April 1 in Alexandria, Egypt are : storage mass capacity equal to 300 kg/m^2, collector

orientation equal to the latitude, and collector area of 50 m^2. These values are based on solar system performance. No significant increase in the solar fraction value can be obtained with increasing the value of these parameters. Also,these values were calculated for the space and domestic water heating loads specified in Chapter 5.

4) For water-based solar heating systems, there is a significant difference between the system performance obtained using the present detailed model (i.e. finite NTU model) and the corresponding values obtained using the infinite NTU model. An accurate estimate of the performance of the water-based system can be obtained only using the detailed solution, i.e. the finite NTU (2D) model. The approximation of infinite NTU model (unlike in the air-based system) gives a significant error in the determination of the system performance.

5) The recommended water-based solar heating system parameters, based on solar system performance, using Abu-Siebera clay as a sensible energy storage medium for the heating season starting from December 1 to April 1 in Alexandria, Egypt are : storage mass capacity equal to 300 kg/m^2, collector orientation equal to the latitude, collector area of 50 m^2, and mass flow rate per unit collector area of 50 kg/h m^2. These parameters were calculated for the space and domestic water heating loads specified in Chapter 5.

6) The recommended storage mass of Abu-Siebera clay per unit collector area for both air and water-based system is equal to 300 kg/m^2. The recommended storage mass capacity does not depend on system configuration.

7) The f-chart method provides a good approximation of annual performance of solar domestic hot water (SDHW) system in the Egyptian climate in comparison with the system performance predicted using TRNSYS.

8) The recommended SDHW system parameters, based on solar system performance, in Alexandria, Egypt are : collector orientation equal to the latitude,

collector area of 50 m^2, storage mass capacity equal to 70 kg/m^2, and mass flow rate per unit collector area of 50 $kg/h\ m^2$. These recommended parameters were calculated for the domestic water heating load specified in Chapter 6.

8.1.1.2 Latent Heat Storage

1) For air-based systems, the infinite NTU model of Morrison et al. [26], after taking energy losses from the storage unit into consideration, can be used with a very small error taking advantage of its huge decrease in computational cost in comparison with the present finite NTU model.

2) A significant reduction in the storage unit volume can be achieved using PCMs as energy storage media in comparison with the storage volume needed with the sensible heat unit using pebbles in order to achieve the same system performance.

3) The present recommended storage capacities of sodium sulphate and wax are higher than those indicated by Morrison et al. due to the effect of energy losses from the storage unit which had been taken into consideration in the present model. The recommended storage capacities are based on the performance of solar heating system.

4) The storage volume required for medicinal paraffin is larger than the storage volumes required for sodium sulphate and paraffin wax because it has the lowest latent heat (146 kJ/kg) and a relatively high melting temperature (40 - 44 °C).

5) For water-based solar heating systems, the use of the infinite NTU model of Morrison et al. will give a significant error in the solar fraction value. An accurate examination of water-based systems can be obtained only using the detailed solution, i.e. the finite NTU (2D) model. The approximation of the infinite NTU model (unlike in air-based systems) gives a significant error in the determination of the system performance.

6) The recommended storage volume does not depend on system configuration,

i. e. air-based or water-based solar heating system, for any of the materials studied.

7) For air-based solar heating systems design with small values of the ratio of incident solar energy to the heating load (values of Y less than about 1.0), and storage mass greater than 10 kg/m^2, the melting temperature has a greater effect on the thermal performance of the solar system than the latent heat. For these solar system designs, the candidate PCM should be chosen in the basis of its melting temperature only.

8) For air-based solar heating systems having a high value of the ratio of incident solar energy to the heating load (values of Y equal to or greater than about 2.0), the latent heat of the PCM has a greater effect on the thermal performance of the solar system than does the melting temperature, contrary to the conclusion reached by Jurinak et al. [28,29]. The candidate PCM should be chosen in this case on the basis of its latent heat.

9) The industrial grade paraffins (with h_{sl}=129 kJ/kg, and melting temperature bandwidth of up to ±10 °C around the nominal melting temperature), for storage masses equal to or greater than 20 kg/m^2 can be used directly for PCES with little decrease in the solar fraction value taking advantage of their reduced cost.

10) Conclusions 7-9 are location independent.

8.1.2 Passive Solar Heating System

1) Phase-change materials seem to be candidate materials for use in solar passive systems, and they may be preferable alternatives to the use of sensible store (masonry, and water) as a storage wall on the basis of volume, mass, and thickness.

2) The industrial grade paraffins (with h_{sl}=129 kJ/kg, and melting temperature bandwidth of up to ±10°C around the nominal melting temperature), can be used directly as a storage wall materials without a significant reduction in the solar savings fraction, taking advantage of their reduced cost.

8.2 Recommendations for Future Work

There are certain other areas of investigation which are not studied in this thesis. Research should be continued in the following areas :

1) Abu-Siebera clay should be installed in real solar systems to compare between the solar system performance obtained from the present theoretical analysis and the corresponding values obtained from measurements.

2) Economic study which take pressure drop into consideration must follow to compare between pebble bed system and the channel system using Abu-Siebera clay.

3) Comparisons with measured performance in many other places have shown that f-chart method provides reliable estimate of long-term performance for SDHW systems. The present results represent a theoretical basis for comparison with any available measurements in Alexandria, Egypt.

4) This study examined two-tank direct SDHW system. Both single tank and indirect systems should also be investigated.

5) The recommended air and water-based solar heating system parameters calculated in this study for sensible energy store are based on system performance only. Economic analysis should be followed to determine the optimum system parameters.

6) The PCES models explained in this work do not take into account such phenomena as supercooling, crystallization, and property degradation with repeated cycling. So, the capability of the PCES models should be extended to study the effects of taking these factors into consideration on the performance of solar heating systems.

7) Economic analysis should be followed to compare between the PCES units and the conventional storage media.

8) The effect of PCM container and heat exchanger design must be studied and advanced fabrication techniques for reducing their costs must be studied.

9) The combination of collector-storage wall using PCMs and direct gain systems should be studied. By combining these two types, one can have both a warm radiant heat source (the collector-storage wall), and visual connection through the south wall of the house.

10) The investigation of collector-storage walls using PCMs was made for one location (Albuquerque). The effects of using a variety of climate types on the conclusions obtained in this study should be investigated.

11) This study examined the calculations of heating loads only. An analysis which parallels the work in this thesis should be performed for cooling loads calculations.

12) Chemical energy storage is another possibility for energy storage which could allow storage volume reductions. Attention must be paid to this type of energy storage to test its reliability as energy storage unit.

APPENDIX A
TRNSYS COMPONENT DESCRIPTION

This appendix describes the TRNSYS component (TYPE 38) which is developed for the finite NTU model of phase-change energy storage (PCES) units. The discussion of the finite NTU model was presented in Chapter 3.

PARAMETERS NO.		DESCRIPTION
1	c_s	Specific heat of PCM in solid phase (kJ/kg K)
2	cl	Specific heat of PCM in liquid phase (kJ/kg K)
3	k_s	Thermal conductivity of PCM in solid phase (kJ/m h K)
4	k_l	Thermal conductivity of PCM in liquid phase (kJ/m h K)
5	ρ_s	Density of PCM in solid phase (kg/m3)
6	ρ_l	Density of PCM in liquid phase (kg/m3)
7	h_{sl}	Solid-liquid transition latent heat (kJ/kg)
8	T_{m1}	Lower boundary of the transition range (°C)
9	T_{m2}	Upper boundary of the transition range (°C)
10	T_{int}	Initial temperature of PCM (°C)
11	χ_{int}	Initial liquid fraction
12	ρ_f	Density of the heat transfer fluid (kg/m3)
13	c_f	Specific heat of heat transfer fluid (kJ/kg K)

14	k_f	Thermal conductivity of the heat transfer fluid (kJ/m h K)
15	η_f	Dynamic viscosity of the heat transfer fluid (kg/m h)
16	U'	Total loss heat transfer coefficient (kJ/h m^2 K)
17	N_c	Number of cylinders
18	L	Storage tank height (m)
19	r_i	Radius of PCM tube (m)
20	V_t	Storage tank volume (m^3)
21	M	Number of radial nodes
22	N	Number of axial nodes

INPUT NO.		DESCRIPTION
1	T_t	Temperature of the heat transfer fluid entering the PCES unit from the top (°C)
2	$\dot{m}_t$	Mass flow rate of the heat transfer fluid entering the PCES unit from the top (kg/h)
3	T_b	Temperature of the heat transfer fluid entering the PCES unit from the bottom (°C)
4	$\dot{m}_b$	Mass flow rate of the heat transfer fluid entering the PCES unit from the bottom (kg/h)
5	T_{env}	Temperature of the environment (°C)

OUTPUT NO.		DESCRIPTION
1	T_N	Bottom PCM node temperature (°C)
2	$\dot{m}_t$	Mass flow rate of the heat transfer fluid from the top (kg/h)

3	T_1	Top PCM node temperature (°C)
4	$\dot{m}_L$	Mass flow rate of the heat transfer fluid entering the PCES from the bottom (kg/h)
5	T_{fm}	Mean temperature of the heat transfer fluid (°C)
6	ΔU	Change in the internal energy of the PCES unit from its initial value (kJ)
7	$\dot{Q}_L$	Rate of energy transfer from the storage unit to the load (kJ/h)
8	$\dot{Q}_s$	Rate of energy transfer from the heat source to the storage unit (kJ/h)
9	$\dot{Q}_{env}$	Rate of energy loss to the surroundings (kJ/h)
10	χ	Nodal average Liquid fraction
11	f_l	Fraction of run time that PCM operates in the liquid phase mode
12	N_s	Number of subroutine time steps per TRNSYS time step

APPENDIX B
TRNSYS CONTROL DECKS

The TRNSYS control deck listed in B.1 is for detailed air-based solar heating system. The location is Albuquerque, New Mexico. The storage material is Sunoco's P116 paraffin wax, and PCES unit is TYPE38. The nominal air-based system parameters discussed in Chapter 3 are used. The simulation period is one year.

The TRNSYS control deck used for the simulations of detailed water-based solar heating system in Alexandria, Egypt is listed in B.2. The storage material is Abu-Siebera clay. TYPE38 which is developed for PCES units is used for sensible store by setting the material melting temperature arbitrary high, so that all energy storage is in the form of sensible heat. The simulation period is one week starting January 1. The nominal water-based system parameters discussed in Chapter 3 are used. The simulations require as input hourly data of solar radiation on horizontal surface (kJ/m^2), wind speed (m/s), ambient dry bulb temperature (°C), and humidity ratio. The weather data file available for Alexandria, Egypt contains the monthly average values of these data. Weather data generator (TYPE 54) contained in TRNSYS library is used to generate hourly data from these monthly data.

B.1

DETAILED AIR-BASED SYSTEM TRNSYS DECK

```
**********************************************************************
*    TRNSYS CONTROL DECK FOR SIMULATION OF DETAILED AIR-BASED
*    SOLAR HEATING SYSTEM (DOMESTIC WATER AND SPACE HEATING
*    THE STORAGE UNIT IS A FINITE NTU PCES.  THE PCM IS SUNOCO'S
*    P116 PARAFFIN WAX (20 KG/M2).  THE LOCATION IS ALBUQUERQUE,
*    NEW MEXICO (LATITUDE 35°).  SIMULATION PERIOD IS ONE YEAR
*    STARTING JANUARY 1.
**********************************************************************
*    OUTPUT NOMENCLATURE :
*    QCIN/M2 = INCIDENT RADIATION ON COLLECTOR PER UNIT AREA
*    QCOUT   = USEFUL ENERGY GAIN BY THE COLLECTOR
*    QINW    = RATE AT WHICH ENERGY IS SUPPLIED TO THE PREHEAT
*              TANK
*    QLOADW= TOTAL DOMESTIC HOT WATER LOAD
*    QAUXW = RATE AT WHICH AUXILIARY ENERGY IS SUPPLIED TO
*              MEET DOMESTIC HOT WATER LOAD
*    QLOADS = TOTAL SPACE HEATING LOAD
*    QAUXS  = RATE AT WHICH AUXILIARY ENERGY IS SUPPLIED TO
*              MEET SPACE HEATING LOAD
*    DELSPH = CHANGE IN THE INTERNAL ENERGY OF SPACE HEATING
*              LOAD
*    QENV    = RATE AT WHICH ENERGY IS LOST FROM THE STORAGE
*              TANK TO ITS ENVIRONMENT
*    EFFC    = COLLECTOR EFFICIENCY
*    FSOLW   = FRACTION OF HOT WATER LOAD MET BY SOLAR
*    FSOLS   = FRACTION OF SPACE HEATING LOAD MET BY SOLAR
*    FSOLT   = FRACTION OF TOTAL LOAD MET BY SOLAR
*    FLPH    = FRACTION OF TOTAL RUN TIME THAT PCES UNIT
*              OPERATES IN THE LIQUID PHASE MODE
*    BTAV    = THE AVERAGE TEMPERATURE OF PCES BOTTOM NODE
*    TTAV    = THE AVERAGE TEMPERATURE OF PCES TOP NODE
*    PHXAV   = TIME AVERAGE PCES AVERAGE LIQUID FRACTION
**********************************************************************
```

```
*C
SIMULATION  1 8760 .25
*C
LIMITS  50 50
*C
TOLERANCES  -.01 -.01
*C
UNIT 9 TYPE 9  DATA READER
PARAMETERS 16
5 1 -1 1 0 -2 1 0 3 .1 0 4 0.0001 0 20 1
(9X,F4.0,1X,F4.0,1X,F4.0,1X,F6.0,1X,F2.0)
*C
UNIT 16 TYPE 16  RADIATION DATA PROCESSOR
PARAMETERS 6
2 1 1 35 4871 -7
INPUTS 6
9,2 9,19 9,20 0,0 0,0 0,0
0 0 0 0.2 45 0
*C
UNIT 14 TYPE 14  DOMESTIC HOT WATER LOAD
PARAMETERS 56
0 0 5.5 0 5.5 20.833 6.5 20.833 6.5 41.666 7.5 41.666
7.5 20.8333 8.5 20.833 8.5 7.426 11.5 7.426 11.5 20.833
12.5 20.833 12.5 7.426 16.5 7.426 16.5 20.833 17.5 20.833
17.5 41.666 19.5 41.666 19.5 33.333 20.5 33.333 20.5 24.999
21.5 24.999 21.5 16.666 22.5 16.666 22.5 7.426 23.5 7.426 23.5 0 24 0
*C
UNIT 1 TYPE 1  SOLAR COLLECTOR - MODE 3
PARAMETERS 12
3 1 1 50 1.012 0.7 0.75 0.9 0.95 2 1.526 .037
INPUTS 10
30,1 30,2 9,3 16,6 9,5 16,4 16,5 0,0 16,9 0,0
25 0 0 0 0 0 0 0 .2 0 45
```

```
*C
UNIT 22  TYPE 2   COLLECTOR CONTROLLER
PARAMETERS  3
3  5  0
INPUTS  3
1,1  10,1  22,1
25  0  0
*C
UNIT 31  TYPE 31   COLLECTOR HOT DUCTS
PARAMETERS  6
.4  20  8  1.204  1.012  20
INPUTS  3
1,1  1,2  0,0
20  0  20
*C
UNIT 23  TYPE 23   DOMESTIC HOT WATER SUBSYSTEM
PARAMETERS  14
-1  .35  1000  4.197  1.5  1  60  1.012  530  .55  5 0  30  90
INPUTS  5
3,1  31,2  0,0  0,0  14,1
25  0  15  20  0
*C
UNIT 34  TYPE 3   COLLECTOR FAN
PARAMETERS  1
2200
INPUTS  3
23,1  23,2  22,1
25  0  0
*C
UNIT 11  TYPE 11   MODE 2 COLLECTOR OUTLET FLOW DIVERTER
PARAMETERS  1
2
```

```
INPUTS  3
34,1  34,2  8,1
25  0  0
*C
UNIT 10  TYPE 38   PCES UNIT
PARAMETERS  22
2.89  2.89  .5  .5  786  786  209  46.7  46.7
20  0  1.204  1.012  0.095  0.071  1.5  506
 2  .02  1.818  5  10
INPUTS  5
11,1  11,2  21,1  21,2  12,4
25  0  25  0  20
*C
UNIT 19  TYPE 11   COLLECTOR INLET TEE-PIECE
PARAMETERS  1
1
INPUTS  4
10,1  10,2  21,3  21,4
25  0  25  0
*C
UNIT 30  TYPE 31   COLLECTOR COLD DUCTS
PARAMETERS  6
.4  20  18  1.204  1.012  20
INPUTS  3
19,1  19,2 0,0
20  0  20
*C
UNIT 20  TYPE 15   ADDER FOR QLOSS
PARAMETERS  1 2
0 0 0 3 3 3 3 3 -4
INPUTS  6
10,9  23,8  30,3  31,3  40,3  41,3
0 0 0 0 0 0
```

```
*C
UNIT 7  TYPE 11   LOAD INLET T-PIECE
PARAMETERS  1
1
INPUTS  4
10,3  10,4  11,3  11,4
25  0  25  0
*C
UNIT 8  TYPE 8   2-STAGE THERMOSTAT
PARAMETERS  7
4  1  0  40  20  18.5  1.5
INPUTS  2
12,4   10,1
20  25
*C
UNIT 41  TYPE 31   HOUSE SUPPLY DUCTS
PARAMETERS  6
.4  15  10.8  1.204  1.012  20
INPUTS  3
7,1  7,2  0,0
20 0 20
*C
UNIT 17  TYPE 3   LOAD FAN
PARAMETERS  1
2200
INPUTS  3
41,1  41,2  8,1
25  0  0
*C
UNIT 6  TYPE 15   SPACE HEATING AUXILIARY
PARAMETERS  5
0.  -1  60000  1  -4
```

```
INPUTS  1
8,2
0
*C
UNIT 12  TYPE 12  ONE NODE UA LOAD  (MODE 4)
PARAMETERS  6
4  1200  20000  20  1.012  2226
INPUTS  6
17,1  17,2  9,3  0,0  6,1  0,0
25  0  0  0  0  0
*C
UNIT 40  TYPE 31   HOUSE COLD DUCTS
PARAMETERS  6
.4 15  10.8  1.204  1.012  20
INPUTS  3
12,1  12,2 0,0
20  0  20  0
*C
UNIT 21  TYPE 11 LOAD OUTLET FLOW DIVERTER  (MODE 2)
PARAMETERS  1
2
INPUTS 3
40,1 40,2 22,1
25  0  0
*C
UNIT 35 TYPE 15   DOMESTIC HOT WATER LOAD
PARAMETERS  4
0  0  3  -4
INPUTS  2
23,6  23,7
0  0
*C
```

```
UNIT 47  TYPE 15  CHANGE IN INTERNAL ENERGY OF THE HOUSE
PARAMETERS 6
0 0 3 0 4 -4
INPUTS 3
12,5  6,1  12,3
0 0 0
*C
UNIT 48  TYPE 28  SIMULATION SUMMARY 1
PARAMETERS 24
8760  1  10000  0  1  0  -1  50  1  -4  0  -4
0  -4  0  -4  0  -4  0  -4  0  -4  0  -4
INPUTS 8
16,6  1,3  23,5  6,1  23,7  47,1  12,3  35,1
LABELS 8
QCIN  QCOUT  QINW  QAUXS  QAUXW  DELSPH
QLOADS  QLOADW
*C
UNIT 49  TYPE 28  SIMULATION SUMMARY 2
PARAMETERS 40
8760  1  10000  0  1  0  0 -1  50  1  2  -4  0  0  3  0  0  3  2  7  -1  1  3  -4
-13  -16  2  7  -1  1  3  -4  -14  -15  2  7  -1  1  3  -4
INPUTS 6
1,3  16,6  23,7  6,1  12,3  35,1
LABELS 4
EFFC  FSOLT  FSOLW  FSOLS
*C
UNIT 50  TYPE 28  STORAGE ENERGY BALANCES
PARAMETERS 24
8760  1  10000  0  1  2  -17  -18  3  -19  3  -4
-11  -12  3  -13  3  -14  3  -15  3  -16  3  -4
INPUTS 9
10,6  23,9  20,1  35,1  12,3  47,1  1,3  6,1  23,7
LABELS 2
```

```
QINT  QOUTT
CHECK  .02  1,-2
*C
UNIT 24  TYPE 24  INTEGRATOR
INPUTS  9
16,6  1,3  23,5  6,1  23,7  47,1  12,3  35,1  10,9
0 0 0 0 0 0 0 0 0
*C
UNIT 25 TYPE 25   PRINTER
PARAMETERS  1
2920
INPUTS  10
24,1  24,2  24,3  24,4  24,5  24,6  24,7  24,8  24,9  10,11
QCIN/M2  QCOUT  QINW  QAUXS  QAUXW  DELSPH
QLOADS  QLOADW  QENV  FLPH
*C
UNIT 5  TYPE 28   SIMULATION SUMMARY 3
PARAMETERS  21
8760  1  10000  0  1  0  -2  2  -4  0  -2  2  -4  0  -2  2  -4  0  -2  2  -4
INPUTS  3
10,1  10,3  10,10
LABELS  3
BTAV  TTAV  PHXAV
*C
UNIT 46  TYP  28   SIMULATION SUMMARY 3
PARAMETERS  15
8760  1  100000  0  1  1  0  0  3  0  3  -4  0  7  -4
INPUTS  4
10,6  10,7  10,9  10,8
LABELS  2
EIN  EOUT
CHECK  .04  1, -2
*C
END
```

B.2

DETAILED WATER-BASED SYSTEM TRNSYS DECK

```
**********************************************************************
*    TRNSYS CONTROL DECK FOR SIMULATION OF DETAILED WATER-
*    BASED SOLAR HEATING SYSTEM (DOMESTIC WATER AND SPACE
*    HEATING). THE LOCATION IS ALEXANDRIA, EGYPT (LATITUDE 31.2°).
*    THE STORAGE MATERIAL IS ABU-SIEBERA CLAY (300 KG/M2). THE
*    SIMULATION PERIOD IS ONE WEEK STARTING JANUARY 1.
**********************************************************************
*    OUTPUT NOMENCLATURE :
*    QCIN    = INCIDENT RADIATION ON COLLECTOR
*    QCOUT   = USEFUL ENERGY GAIN BY THE COLLECTOR
*    DELUS   = CHANGE IN THE INTERNAL ENERGY OF THE STORAGE
*              UNIT
*    QTRANL  = RATE AT WHICH ENERGY IS SUPPLIED FROM THE
*              STORAGE UNIT TO THE LOAD
*    QINS    = RATE AT WHICH ENERGY IS SUPPLIED FROM THE HEAT
*              SOURCE TO THE STORAGE UNIT
*    QENV    = RATE AT WHICH ENERGY IS LOST FROM THE STORAGE
*              UNIT TO ITS ENVIRONMENT
*    QLOADW= TOTAL DOMESTIC HOT WATER LOAD
*    QAUXW   = RATE AT WHICH AUXILIARY ENERGY IS SUPPLIED TO
*              MEET DOMESTIC HOT WATER LOAD
*    QLOADS  = TOTAL SPACE HEATING LOAD
*    QAUXS   = RATE AT WHICH AUXILIARY ENERGY IS SUPPLIED TO
*              MEET SPACE HEATING LOAD
*    FSOLW   = FRACTION OF HOT WATER LOAD MET BY SOLAR
*    FSOLS   = FRACTION OF SPACE HEATING LOAD MET BY SOLAR
*    FSOLT   = FRACTION OF TOTAL LOAD MET BY SOLAR
*    BTAV    = THE AVERAGE TEMPERATURE OF THE STORAGE UNIT
*              BOTTOM NODE
*    TTAV    = THE AVERAGE TEMPERATURE OF THE STORAGE UNIT TOP
*              NODE
**********************************************************************
```

```
*C
SIMULATION  1  168  .25
*C
WIDTH  72
*C
LIMITS  50  50
*C
TOLERANCES  -.01  -.01
*C
UNIT 50  TYPE 54  WEATHER DATA GENERATOR
PARAMETERS  17
1  1  10  1  1  4.4  4.4  4.6  4.3  4.0  4.0  4.4  4.0  3.6  3.1  3.4  4.1
*C
UNIT 16  TYPE 16  RADIATION DATA PROCESSOR
PARAMETERS  6
2  1  1  31.2  4871  0
INPUTS  6
50,7  9,19  9,20  0,0  0,0  0,0
0  0  0  0.2  41.2  0.0
*C
UNIT 14  TYPE 14  DOMESTIC HOT WATER LOAD
PARAMETERS  38
0  0  6  0  6  30  7  30  7  60  8  60  8  30  9  30  9  10  16  10  16
60  20  60  20  50  22  50  22  40  23  40  23  20  24  20  24  0
*C
UNIT 1  TYPE 1  COLLECTOR MODE 1
PARAMETERS  12
1  1  50  4.19  1  50  .7  15  -1  4.197  1  .1
INPUTS  10
30,1  30,2  30,2  50,4  16,6  16,4  16,5  0,0  16,9  0,0
25  0  0  0  0  0  0  .2  0  31.2
*C
```

```
UNIT 31  TYPE 31   COLLECTOR HOT PIPES
PARAMETERS  6
.05  20  18  1000  4.197  20
INPUTS  3
1,1  1,2  0,0
40  0  20
*C
UNIT 13  TYPE 13   RELIEF VALVE
PARAMETERS  2
95  4.197
INPUTS  3
31,1  31,2  10,1
40  0  40
*C
UNIT 2  TYPE 2   CONTROLLER
PARAMETERS  3
3  5  0
INPUTS  3
1,1  4,1  2,1
25  0  0
*C
UNIT 10  TYPE 38   SENSIBLE STORAGE UNIT
PARAMETERS  22
.86  .86  .72  .72  2250  2250  209  1000  1000
20  0  1000  4.197  2.16  2.75  1.5  295  2
.06  9.52  5  10
INPUTS  5
13,1  13,2  11,1  11,2  12,4
25  0  25  0  20
*C
UNIT 3  TYPE 3   PUMP
PARAMETERS  1
3000
```

```
INPUTS  3
10,1  10,2  2,1
25  0  0
*C
UNIT 30  TYPE 31   COLLECTOR COLD PIPES
PARAMETERS  6
.05  20  18  1000  4.197  20
INPUTS  3
3,1  3,2  0,0
30  0  20
*C
UNIT 23  TYPE 23   SERVICE HOT WATER
PARAMETERS  14
-1  .6  1000  4.19  1.51  1  60  4.197  600  .6  5  1  30  90
INPUTS  5
10,1  0,0  0,0  0,0  14,1
40  600  15  20  0
*C
UNIT 33  TYPE 31   HOUSE HOT PIPES
PARAMETERS  6
.05  15  10.8  1000  4.197  20
INPUTS  3
10,3  10,4  0,0
30  0  20
*C
UNIT 12  TYPE 12   HOUSE LOAD
PARAMETERS  6
1  2500  20  750  4.197  1146
INPUTS  4
33,1  33,2   50,4  17,1
25  0  0  0
*C
```

```
UNIT 34  TYPE 31   HOUSE COLD PIPES
PARAMETERS  6
.05  15  10.8  1000.  4.197  20
INPUTS  3
12,1  12,2  0,0
20  0  20
*C
UNIT 11  TYPE 11   TEE PIECE
PARAMETERS  1
1
INPUTS  4
23,1  23,2  34,1  34,2
25  0  25  0
*C
UNIT  18  TYPE  15   QIN
PARAMETERS  9
0  0  4  0  1  -1  4.197  1  -4
INPUTS   3
13,1  3,1  3,2
0  0  0
*C
UNIT 19  TYPE 15   QCOUT
PARAMETERS  4
0  0  4  -4
INPUTS  2
1,3  13,3
0  0
*C
UNI 17  TYPE 15   LOSS SUM  ( TANKS,RLF VLV,PIPES )
PARAMETERS  14
0  0  0  0  0  0  0  3  3  3  3  3  3  -4
INPUTS  7
23,8  10,9  31,3  13,3  30,3  33,3  34,3
```

```
0 0 0 0 0 0 0
*C
UNIT 35 TYPE 15 DOMESTIC HOT WATER LOAD
PARAMETERS 4
0 0 3 -4
INPUTS 2
23,6 23,7
0 0
*C
UNIT 40 TYPE 28 SIMULATION SUMMARY 1
PARAMETERS 20
168 0 10000 0 1 0 -4 0 -1 50 1
-4 0 -4 0 -4 0 -4 0 -4
INPUTS 6
16,6 19,1 12,6 12,3 23,7 35,1
LABELS 6
QCIN QCOUT QAUXS QLOADS QAUXW QLOADW
*C
UNIT 41 TYPE 28 SIMULATION SUMMARY 2
PARAMETERS 21
168 0 10000 0 1 -11 -12 2 -4
-13 -14 2 -4 -11 -13 3 -12 -14 3 2 -4
INPUTS 4
12,5 12,3 23,6 35,1
LABELS 3
FSOLS FSOLW FSOLT
*C
UNIT 24 TYPE 24 INTEGRATOR
INPUTS 8
16,6 12,3 12,6 23,7 35,1 10,7 10,8 10,9
0 0 0 0 0 0 0 0
*C
```

```
UNIT 25  TYPE 25   PRINTER
PARAMETERS  1
24
INPUTS  9
24,1  24,2  24,3  24,4  24,5  24,6  24,7  24,8  10,6
QCIN  QLOADS  QAUXS  QAUXW  QLOADW  QTRANL
QINS  QENV  DELUS
*C
UNIT 49  TYPE 28   TOTAL ENERGY BALANCES
PARAMETERS  22
168  1  10000  0  1  2  -16  -17  3  -18  3  -4
-11  -12  3  -13  3  -14  3  -15  3  -4
INPUTS  8
10,6  23,9  17,1  35,1  12,3  1,3  12,6  23,7
LABELS  2
QINT  QOUTT
CHECK  .04  1,-2
*C
UNIT 46  TYP  28   STORAGE TANK ENERGY BALANCES
PARAMETERS  15
168  1  100000  0  1  1  0  0  3  0  3  -4  0  7  -4
INPUTS  4
10,6  10,7  10,9  10,8
LABELS  2
EIN  EOUT
CHECK  .04  1, -2
*C
END
```

APPENDIX C
FORTRAN CODE : COLLECTOR-STORAGE WALL USING PHASE-CHANGE MATERIALS

This appendix contains the list of a FORTRAN code for collector-storage wall using phase-change material. Absorbed solar radiation reaches the room by either of two paths. One path is the energy conduction through the wall. This energy is transferred from the inside wall surface to the room by convection and radiation. The second path is convection from the outer surface of the wall to air in the gap. This component offers four modes of operation. The total solar radiation, glazing transmittance, and mass flow rate of air in the gap are inputs to the component in mode 1. In mode 2, the mass flow rate is driven by air temperature differences (buoyant forces) and computed internally. In mode 3, the mass flow rate of air is input and the transmittance of beam and diffuse radiation are considered separately. The transmittance-absorptance product is determined by Function Subroutine TALF contained in TRNSYS library. Mode 4 is the same as mode 3 except that the mass flow rate of air in the gap is driven by temperature differences and computed internally.

```
C*****************************************************************
C  THIS SUBROUTINE DETERMINES ENERGY FLOWS IN A THERMALLY
C  MASSIVE SOLAR COLLECTOR WALL.  ENERGY IS EXCHANGED WITH
C  THE BUILDING EITHER BY CONDUCTION THROUGH THE COLLECTOR
C  OR BULK AIR FLOW IN THE GAP BETWEEN THE COLLECTOR AND THE
C  FIRST GLAZING.  TRANSPORT OF ENERGY VIA BULK AIR FLOW IS
C  DRIVEN BY A FAN (MODE 1) OR BY BUOYANT FORCES (MODE 2)
C*****************************************************************
      SUBROUTINE TYPE36(TIME,XIN,OUT,T,DTDT,PAR,INFO)
      REAL NUSLT
      DIMENSION XIN(10),OUT(20),U(20),TT(20),XX(20),XK(20)
     1,PAR(30),INFO(10) , USAV(20), XSAV(20), TSAV(20)
      DIMENSION SIGMA(2), VISC(2), CC1(2), CC2(2), CNVT(2)
      DIMENSION GRAV(2), RHOREF(2), CP(2), AB(2), TST(2)
      DIMENSION WCNVT(2)
      COMMON / SIM / TIMEO,TFINAL,DELT
      DATA WCNVT/1.,0.447/
      DATA IUNIT/0/,C/459.819212/
      DATA SIGMA/0.20411E-06,0.17141E-8/
      DATA GRAV/9.8067,32.1742126/,RHOREF/353.0774,39.67545/
      DATA CP/1.,0.23889/,CNVT/3.6,3.41214/
      DATA AB/273.2,459.76/,TST/1.,1.8/,IGAM2/0/
      DATA CC1/0.0827,0.0133/,CC2/0.000232,0.000021/
      DATA VISC/0.181E-04,0.1215E-04/,PRNTL/0.72/
      IF (INFO(7).GT.-1) GO TO 10
      IUNIT=INFO(1)
      INFO(6) = 18
C**  SET PARAMETERS
      MODE = INT(PAR(1)+0.1)
      NU = INT(PAR(2)+0.1)
      HTL = PAR(3)
      WT = PAR(4)
      A = WT * HTL
```

```
      X = PAR(5)
      N=PAR(6)
      NM1=N-1
      DX = X/FLOAT(N-1)
      RW = PAR(7)
      AS = PAR(8)
      EMW = PAR(9)
      EMG = PAR(10)
      HR = SIGMA(NU)/(1./EMW+1./EMG-1.)
      NC = INT(PAR(11)+0.1)
      SPC = PAR(12)
      CWS=PAR(13)
      CWL=PAR(14)
      XWS=PAR(15)
      XWL=PAR(16)
      TM1=PAR(17)
      TM2=PAR(18)
      XLAT=PAR(19)
      TINT=PAR(20)
      XINT=PAR(21)
      CW11=0.0
      IF(TM2.GT.TM1)  CW11=XLAT/(TM2-TM1)
C**  IF(INFO(7).NE.-1) GO TO  333
      US=CWS*TM1
      UL=US+XLAT
      DTS=(RW*DX)/2.
      DTS1=1./DTS
      G2V3L = GRAV(NU)/VISC(NU)/VISC(NU)*SPC*SPC*SPC
      AG = SPC * WT
      NP = 21
      NX = 9
      GO TO (8,7,6,6) MODE
C**  GLAZING TRANSMITTANCE DETERMINED FROM OPTICAL PROPERTIES
```

```
C** AND ANGLE OF INCIDENCE OF SOLAR BEAM. (MODE 3 AND MODE 4)
  6   XKL = PAR(22)
      RI = PAR(23)
      RHOD = -1.
C** TRANSMITTANCE OF DIFFUSE AND REFLECTED SOLAR RADIATION IS
C** COMPUTED AT AN ANGLE OF INCIDENCE OF 60 DEGREES.
      TAL60=TALF(NC,60.,XKL,RI,AS,RHOD)
      NX = NX+1
      NP = NP+2
      IF (MODE.EQ.3) GO TO 8
C** AIR MASS FLOW RATE IN THE GAP DRIVEN BY DENSITY DIFFERENCES
C** (MODE 2 AND MODE 4)
  7   AV = PAR(NP+1)
      HTV = PAR(NP+2)
      NP = NP + 2
      NX = NX - 1
      BETA = AG/AV
      ARGUE = HTV*GRAV(NU)/(4.*BETA*BETA+2.)
      FLOFAC = SQRT(ARGUE)*3600.
  8   CONTINUE
      CALL TYPECK(1,INFO,NX,NP,0)
C** SET INITIAL GLAZING AND MEAN AIR GAP TEMPERATURES
      IF(TINT.GT.TM2) GO TO 100
      IF((TINT.LT.TM2) .AND. (TINT.GT.TM1)) GO TO 200
      UINT=CWS*TINT+XINT*XLAT
      GO TO 300
 200  UINT=US+(XINT*XLAT)
      GO TO 300
 100  UINT=US+XLAT+CWL*(TINT-TM2)
 300  UAV=UINT
      DO 400 I=1,N
      U(I)= UINT
      TT(I)=TINT
```

```
      XX(I)=XINT
400   CONTINUE
      PER=0.0
      XAV=XINT
      TAV=TINT
      XNC = FLOAT(NC)
      TM = (TT(1) + TG)/2.
 10   CONTINUE
      IF(INFO(7).GT.0)  GO TO 778
      DO 777 I=1,N
      USAV(I)=U(I)
      TSAV(I)=TT(I)
      XSAV(I)=XX(I)
777   CONTINUE
      PERSAV=PER
      GO TO 889
778   DO 888 I=1,N
      U(I)=USAV(I)
      TT(I)=TSAV(I)
      XX(I)=XSAV(I)
888   CONTINUE
      PER =PERSAV
889   CONTINUE
      IF (INFO(1).EQ.IUNIT) GO TO 11
      CALL TYPECK(6,INFO,0,0,0)
C**  COMPUTE THE ABSORBED SOLAR RADIATION
 11   CONTINUE
      IF (MODE.GT.2) GO TO 14
C**  TAU IS AN INPUT (MODE 1 AND MODE 2)
      TAU = XIN(8)
      HT = XIN(7)
      QS = TAU*AS*HT
      OUT(3) = QS * A
```

```
      GO TO 15
C**  TAU*ALPHA IS DETERMINED AS A FUNCTION OF THE ANGLE OF
C**  INCIDENCE OF THE SOLAR BEAM AND THE OPTICAL PROPERTIES
C**  OF THE GLAZINGS.  (MODE 3 AND MODE 4)
   14 QS = 0.
      OUT(3) = QS * A
      HT = XIN(7)
      HB = XIN(8)
      HD = HT - HB
      IF (HT .LT. 0.001) GO TO 15
      THT = XIN(9)
      TAUALF = TALF(NC,THT,XKL,RI,AS,RHOD)
      QS = TAUALF*HB + TAL60*HD
      OUT(3) = QS*A
   15 CONTINUE
C**  INPUT BUILDING AND ENVIRONMENT TEMPERATURES
C**  AND RESPECTIVE HEAT TRANSMISSION COEFFICIENTS
      TR = XIN(2)
      TA = XIN(3)
      VW = XIN(4)*WCNVT(NU)
      HTC3 = XIN(5)
      HTC5 = XIN(6)
C**  RADIATION HEAT TRANSFER COEFFICIENT BETWEEN WALL
C**  AND GLAZING, AND HEAT TRNSFER COEFFICIENT BETWEEN THE
C**  GLAZING AND THE ENVIRONMENT
      T1ABS = TT(1)+AB(NU)
      TAABS = TA + AB(NU)
      TGABS = TG+AB(NU)
      HTC2 = HR*(T1ABS*T1ABS+TGABS*TGABS)*(T1ABS+TGABS)
      IF (HTC3.GE.0.) GO TO 20
C**  HEAT TRANSMISSION COEFFICIENT BETWEEN GLAZING AND
C**  ENVIRONMENT COMPUTED FROM RELATION OF KLEIN.
```

```
      HW = 5.7 + 3.8*VW
      STF1 = SIGMA(NU)*(TGABS*TGABS+TAABS*TAABS)
     1*(TGABS+TAABS)
      STF1 = STF1/CNVT(NU)
      IF (NC.EQ.1) GO TO 19
      XN = XNC - 1.
      F = (1.-0.04*HW+0.0005*HW*HW)*(1.+0.091*XN)
      STF2 = 1./(EMG+0.05*XN*(1.-EMG))
      STF3 = ((2.*XN+F-1.)/EMG)-XN
      DT = TG - TA
      DT = AMAX1(ABS(DT),0.2)
      STF4 = (DT/(XN+F))**0.33
      STF5 = (XN*TGABS/C/STF4)+1./HW
      HTC3 = ((STF1/(STF2+STF3))+1./STF5)*CNVT(NU)
      GO TO 20
   19 CONTINUE
C**  HEAT TRANSMISSION COEFFICIENT BETWEEN GLAZING AND
C**  ENVIRONMENT COMPUTED FROM MCADAMS CORRELATION.
      HTC3 = (HW + STF1*EMG)*CNVT(NU)
   20 CONTINUE
      IGAM=INT(XIN(1)+SIGN(.1,XIN(1)))
      NCOUNT = 0
C**  DETERMINE GAP AIR TEMPERATURES, MASS FLOW RATE,
C**  AND HEAT TRANSFER COEFFICIENTS
   21 CONTINUE
      NCOUNT = NCOUNT + 1
      TMOLD = TM
      TMABS = TM + AB(NU)
      RHO = RHOREF(NU)/TMABS
      AIRK = CC1(NU) + CC2(NU)*TM
      IF (NCOUNT.GT.20) GO TO 50
      IF (IGAM) 23,22,24
C**  MASS FLOW RATE EQUALS ZERO
```

```
  22   HTC6 = 0.
       IGAM2 = 0
       AMDOT = 0.
       EM = 0.
       RM = 0.
       TS = TM
       DTBETA = ABS(TT(1)-TM)/TMABS
       IF(DTBETA .LT. 0.) DTBETA = -DTBETA
C**  NUSSELT RELATION IS FROM RANDALL
       GRSHOF = G2V3L*RHO*RHO*DTBETA
       NUSLT = 0.0965*((GRSHOF*PRNTL)**0.29)
       HTC4 = NUSLT*AIRK/SPC
       GO TO 28
C**  AIR IN GAP VENTED TO THE ENVIRONMENT
  23   TS = TA
       EM = 1
       RM = 0
       GO TO 25
C**  AIR IN GAP VENTED TO ROOM
  24   TS = TR
       EM = 0.
       RM = 1.
  25   IF (MODE.EQ.1.OR.MODE.EQ.3) GO TO 26
       DELTST = TST(NU)
       IF (IGAM2 .EQ. 1) DELTST = 0
       IF (TM.LE.TS+DELTST) GO TO 22
       IGAM2 = 1
C**  MASS FLOW DRIVEN BY BUOYANT FORCES
       DRHO = (TM-TS)/TMABS
       AMDOT = FLOFAC*RHO*AG*SQRT(DRHO)
       GO TO 27
C**  MASS FLOW RATE IS INPUT
  26   CONTINUE
```

```
      AMDOT = XIN(NX)
      IF (AMDOT.LE.0.) GO TO 22
   27 REYNLD = AMDOT/WT/VISC(NU)/3600.
      IF (REYNLD .GT. 2000.) GO TO 29
C**  NUSSELT CORRELATION FROM MERCER
      DHYD = 2.*AG/(SPC + WT)
      XSTR = HTL/DHYD/REYNLD/PRNTL
      NUSLT = (0.0606*XSTR**(-1.2))/(1.+0.0856*(XSTR**(-0.7))) + 4.9
      GO TO 30
   29 CONTINUE
C**  NUSSELT CORRELATION IS FROM KAYS
      NUSLT = 0.0158*(REYNLD**0.8)
      IF (NUSLT .LT. 5.385) NUSLT=5.385
   30 CONTINUE
      HTC4 = NUSLT*AIRK/SPC
      FTC1 = -(2.*HTC4*A/AMDOT/CP(NU))
      FTC3 = EXP(FTC1) - 1.
      HTC6 = FTC3*AMDOT*CP(NU)/A/(FTC3/FTC1 - 1.)
   28 CONTINUE
C**  DETERMINE AIR GAP AND GLAZING TEMPERATURES
      CTG=HTC2+HTC3+HTC4
      CTM=HTC4*2.+HTC6
      ARG1=HTC4*HTC4/CTM
      ARG2=TA*HTC3+TS*HTC4*HTC6/CTM
      ARG3=HTC2+ARG1
      ARG4=CTG-ARG1
      TG=(ARG2+TT(1)*ARG3)/ARG4
      TM=(TS*HTC6+(TT(1)+TG)*HTC4)/CTM
      DTMM = TM - TMOLD
      IF (ABS(DTMM).GT.0.01) GO TO 21
C**  OUTPUT ENERGY FLOWS
   50 TO = FTC3*(TS*2. - TT(1) - TG)/2. + TS
      QV=HTC6*(TM-TS)*A
```

```
      QRM=HTC5*(TT(N)-TR)*A
      OUT(7) = QV
      OUT(6) = HTC3*A*(TG-TA)
      OUT(5) = QRM
      OUT(4) = OUT(6) + QV*EM
      OUT(1) = QRM + QV*RM
      OUT(8) = AMDOT
C**  OUTPUT TEMPERATURES
      OUT(10)=TG
      OUT(9) = TO
C**  COMPUTE THE CHANGE IN TEMPERATURE OF THE WALL NODES
      DTS2=1./(HTC2+HTC4+(XWS/DX))
      DTS3=1./(HTC5+(XWS/DX))
      DELT1=DTS*MIN(DTS2,DTS3)
      NM=IFIX((DELT/DELT1)+1.)
      DELT1=DELT/NM
      IF(TIME.LT.(TIMEO+1.E-8)) GO TO 7500
      DO 5000 JJ=1,NM
      DO 800  I=1,N
      XK(I)=XX(I)*XWL+(1-XX(I))*XWS
  800 CONTINUE
      U(1)=U(1)+DTS1*DELT1*QS+DTS1*DELT1*((XK(2)*TT(2)XK(1)*TT(1))/
     1DX)+DTS1*DELT1*(TG-TT(1))*HTC2+DTS1*DELT1*(TM-TT(1))*HTC4
      DO 900 I=2,NM1
      U(I)=U(I)+(DELT1*DTS1/(DX*2.))*(XK(I-1)*TT(I-1)+XK(I+1)
     1*TT(I+1)-2.*XK(I)*TT(I))
      FFF=(DELT1*DTS1/(DX*2.))*(XK(I-1)*TT(I-1)+XK(I+1)
     1*TT(I+1)-2.*XK(I)*TT(I))
  900 CONTINUE
      U(N)=U(N)+DELT1*DTS1*(TR-TT(N))*HTC5+DELT1*DTS1
     1*((XK(NM1)*TT(NM1)-XK(N)*TT(N))/DX)
      DO 3000 I=1,N
      IF(U(I).GT.US) GO TO 2000
```

```
      TT(I)=(U(I)/CWS)
      XX(I)=0.0
      GO TO 3000
 2000 IF(U(I).LT.UL) GO TO 4000
      TT(I)=((U(I)-UL)/CWL)+TM2
      XX(I)=1.0
      GO TO 3000
 4000 TT(I)=TM1
      IF(TM1.LT.TM2) TT(I)=((U(I)-US)/CW11)+TM1
      XX(I)=(U(I)-US)/XLAT
 3000 CONTINUE
 5000 CONTINUE
      SUM=0.0
      DO 7000 I=1,N
      SUM=SUM+U(I)
 7000 CONTINUE
      UAV=SUM/FLOAT(N)
 7500 QSTORE=(UAV-UINT)*A*X*RW
      OUT(2)=QSTORE
C**  DE AV QUALITY
      X1=0.0DO 8000 I=1,N
      X1=X1+XX(I)
 8000 CONTINUE
      XAV=X1/FLOAT(N)
      OUT(11)=XAV
C**  FRAC OF T
      IPER=0.0
      IF(XAV.GT.0.) IPER=1
      PER=PER+DELT*FLOAT(IPER)
      OUT(12)=NM
      DO 9000 I=1,J=13+I
      OUT(J)=TT(I)
 9000 CONTINUE
```

```
      IF(TIME.LT. .001) GO TO 9500
      XPER=PER/TIME
      OUT(13)= XPER
9500 CONTINUE
      RETURN
      END
```

REFERENCES

1. Hale, D., Hoover M., and O'Neill, M., "Phase Change-Materials Handbook," NASA CR-61363, NASA George C.Marshall Space Flight Center, (1971).

2. Abhat, A., "Low Temperature Latent Heat Thermal Energy Storage : Heat Storage Materials," Solar Energy , Vol. 30, No. 4, pp. 313-332, (1983).

3. Lorch, H.G., "Latent Heat and Sensible Heat Storage for Solar Heating Systems," NSF/RANN/SE/GI27976/TR72/20, University of Pennsylvania, December (1972).

4. Altman, Manfred, et al., "Conservation and Better Utilization of Electric Power by Means of Thermal Energy Storage and Solar Heating-Final Summary Report," NSF/RANN/SE/GI/27976/PR73/5, University of Pennsylvania, July (1973).

5. Lane, G.A., et al., "Heat-of-Fusion Systems for Solar Energy Storage," Proceedings of Workshop on Solar Energy Storage Subsystems for Heating and Cooling of Buildings, pp. 43-55, Charlottesville, Virginia, (1975).

6. Denton, Jesse, C., "Phase Change Storage Systems Group Report," Proceedings of Workshop on Solar Energy Storage Subsystems for Heating and Cooling of Buildings, pp. 169, Charlottesville, Virginia, (1975).

7. Shelpuk, B., Joy, P., and Crouthamel, M., "Technical and Economic Feasibility of Thermal Storage-Final Report," COO/2591-76/1, RCA Advanced Technology Laboratories, Candem, N.J., (1976).

8. Bailey , J., et al., "A Solar Energy Subsystem Utilizing the Latent Heat of Fusion of Paraffin Hydrocarbons : A progress Report," Proceedings of Workshop on Solar Energy Storage Subsystems for Heating and Cooling of Buildings, NSF-RA-N-75-041, University of Virginia, (1975).

9. Bentilla, E.W., et al., "Research and Development Study on Thermal Control by use of Fusible Materials," Northrop Space Laboratories, NSL 65-16-1, Hawthorne, Calif., April (1966).

10. Belton, G., and Ajame, F., "Thermochemistry of Salt Hydrates," NSF/RANN/SE/GI 27976/TR/73/4, University of Pennsylvania, (1973).

11. Telkes M., "Thermal Storage for Solar Heating and Cooling," Proceedings of Workshop on Solar Energy Storage Subsystems for Heating and Cooling of Buildings, NSF-RA-N-75- 051, University of Virginia, (1975).

12. Bundy, F., Herrick, C., and Kosky, P., "The Status of Thermal Energy Storage," Report No. 76CRD041, General Electric Power Systems Laboratory, (1976).

13. Kauffman, K., and Pan, Y., "Thermal Energy Storage in Sodium Sulphate Decahydrate Mixtures," NSF/RANN/SE/GI/27976/TR72/11, University of Pennsylvania, (1972).

14. Chubb, T.A., "Analysis of Gas Dissociation Solar Thermal Power System," Solar Energy, Vol. 17, pp. 129-136, (1975).

15. Prengle, H.W., and Chi-Hua Sun, "Operational Chemical Storage Cycles for Utilization of Solar Energy to Produce Heat or Electric Power," Solar Energy,Vol. 18, pp. 561-567, (1976).

16. Williams, O.M., and Garden, P.O., "Ammonia Dissociation for Solar Thermochemical Absorbers," Energy Research, Vol. 3, pp. 129-142, (1979).

17. Klein S.A., et al., " TRNSYS, A Transient Simulation Program," University of Wisconsin-Madison , Version 12.2, (1988).

18. Mitchell, J.W., Beckman, W.A., and Pawelski, M.J., "Comparisons of Measured and Simulated Performance for CSU House I," American Society of Mechanical Engineers Paper 79-WA/SOL-35, (1979).

19. Beckman W.A., Klein S.A., and Duffie J.A.,"Solar Heating Design by the f-Chart Method," Wiley Interscience, New York, (1977).

20. F-Chart 5.6, Engineering Experimental Station Report 50, Solar Energy Laboratory, University of Wisconsin-Madison, (1988).

21. Balcomb, J.D., et al., "Passive Solar Design Handbook," Vol. 2, ASES, Boulder, CO, (1980).

22. Balcomb, J.D., et al., "Passive Solar Design Handbook," Vol. 3, ASES, Boulder, CO, (1982).

23. Monsen, W.A., "Design Methods for Building-Integrated Solar Heating Components," M.S. Thesis, University of Wisconsin-Madison, Solar Energy Laboratory, (1980).

24. Monsen, W.A., Klein, S.A., and Beckman, W.A., "Prediction of Direct Gain Solar Heating System Performance," Solar Energy, Vol. 27, No. 2, pp. 143-147, (1981).

25. Morrison, D.J., "Performance of Solar Heating Systems Utilizing Phase Change Energy Storage," M.S. Thesis, University of Wisconsin-Madison, Solar Energy Laboratory, (1976).

26. Morrison, D.J., and Abdel Khalik, S.I., "Effect of Phase-Change Energy Storage on the Performance of Air-Based and Liquid-Based Solar Heating Systems," Solar Energy, Vol. 20, pp. 57- 67, (1978).

27. Visser, H., "Energy Storage in Phase-Change Materials-Development of A Component Model Compatible with TRNSYS," Final report, contract No 2462-84-09 ED ISP NL, Delft Univ. of Technology, Department of a Applied Physics, Delft, (1986).

28. Jurinak, J.J., and Abdel Khalik, S.I., "Properties Optimization for Phase-Change Energy Storage in Air-Based Solar Heating Systems," Solar Energy, Vol 21, pp. 377-383, (1978).

29. Jurinak, J.J., "On the Performance of Air-Based Solar Heating Systems Utilizing Phase-Change Energy Storage,".M.S. Thesis, University of Wisconsin-Madison, Solar Energy Laboratory, (1979).

30. Telkes, M., "Trombe Wall with Phase-Change Storage Material," Proceedings of the 2nd National Passive Solar Conference, Philadelphia, Pennsylvania, March (1978).

31. Chahroudi, D., and Wellesley-Miller, S., "Thermocrete Heat Storage Materials : Applications and Performance Specifications," Proceedings of Joint Conf. ASIS and SES of Canada, Winnipeg, (1976).

32. Benard, C., Body, Y., and Zanoli, A., "Experimental Comparison of Latent and Sensible Heat Thermal Walls," Solar Energy, Vol. 34, No. 6, pp. 475-487, (1985).

33. Christensen, C.B., "Advanced Phase-Change Storage for Passive Solar Heating : Analysis of Materials and Configurations," Proceedings of the 8th National Passive Solar Conference, Sante Fe, New Mexico, September (1983).

34. Bourdeau, L., and Jaffrin, A., "Phase-Change Collector Wall Versus Water Collector Wall," ETS Report, Proceedings of the International Symposium on Solar Energy, Cairo, Egypt, June (1978).

35. Bourdeau, L.E., "Study of Two Passive Solar Systems Containing Phase-Change Material for Thermal Storage," Proceedings of the 5th National Passive Solar Conference, Amherst, MA, October (1980).

36. Askew, G.L., "Solar Heating Utilizing A Paraffin Phase-Change Material," Proceedings of the 2nd National Passive Solar Conference, Philadelphia, Pennsylvania, Maech (1978).

37. Collier, R.K., and Grimmer, D.P.,"The Experimental Evaluation of Phase-Change Material Building Walls Using Small Passive Test Boxes," Proceedings of the 3rd National Passive Solar Conference, San Jose, CA, January (1979).

38. Mitalas, G.P, and Arseneault, J.G., "FORTRAN IV Program to Calculate z-Transfer Functions for the Calculation of Transient Heat Transfer Through Walls and Roofs," National Research Council of Canada, DBR Computer Program No. 33, (1982).

39. ASHRAE Handbook of Fundamentals, American Society of Heating, Refrigerating and Air-Conditioning Engineers, INC., New York, (1977).

40. ASHRAE Handbook of Fundamentals, American Society of Heating, Refrigerating and Air-Conditioning Engineers, INC., New York, (1981).

41. Liu, B.Y.H., and Jordan, R.C., "The-Interrelationship and Characteristic Distribution of Direct, Diffuse and Total Solar Radiation," Solar Energy, Vol. IV, pp. 1-19, July (1960).

42. Boes, E.C., et al., "Distribution of Direct and Total Solar Radiation Availabilities for the U.S.A," Sandia Report SAND76-0411, August (1976).

43. Erbs, D.G., "Methods for Estimating the Diffuse Fraction of Hourly, Daily and Monthly Average Global Solar Radiation," M.S. Thesis, University of Wisconsin-Madison, Solar Energy Laboratory, (1980).

44. Knight, K.M., "Development and validation of a weather data generation model," M.S.Thesis, University of Wisconsin-Madison, Solar Energy Laboratory (1988).

45. Degelman, L.O., "A Weather Simulation Model for Building Energy Analysis," ASHRAE Transactions, Symposium on Weather Data, Seattle, WA, Annual Meeting, pp. 435-447, June (1976).

46. Personal Communication.

47. Hottel, H.C., and Whillier, A., Transactions of the Conference on the Use of Solar Energy, 2, Part I, 74, University of Arizona Press, (1958).

48. Rohsenow, W.M., Hartnett, J.P., Ganic, E.N., "Handbook of Heat Transfer Fundamentals," 2nd edition, New York, (1985).

49. Dittus, F.W., and Boelter, L.M.K., University of California (Berkeley), Pub. Eng., Vol. 2, pp. 443, (1930).

50. Hughes, P.J., Klein S.A., and Close, D.J., "Packed bed thermal storage models for solar air heating and cooling systems," Trans. ASME, Journal of Heat transfer, Vol. 98, pp. 336, (1976).

51. Ghoneim, A.A., "Comparison of Theoretical Models of Phase-Change and Sensible Heat Storage for Air and Water-Based Solar Heating Systems," Solar Energy, Vol. 42, No. 3, pp. 209-220, (1989).

52. Duffie, J.A., and Beckman, W.A., "Solar Engineering of Thermal Processes," Wiley Interscience, New York, (1980).

53. ASHRAE, Standard 93-77,"Methods of Testing to Determine the Thermal Performance of Solar Collectors," American Society of Heating, Refrigerating and Air Conditioning Engineers, New York, (1977).

54. Blackwell, J.H., "A Transient Flow Method for Determination of Thermal Constants of insulating Materials in Bulk," Journal of Applied Physics, Vol. 25, No. 2, (1954).

55. Holman, J.P.,"Heat Transfer," McGraw-Hill Book Company, New York, (1976).

56. van Koppen, C.W., et al., "The Actual Benefits of Thermally Stratified Storage in a Small and a Medium Size Solar," Proceedings ISES, Atlanta, (1979).

57. Veltkamp, W.B., and van Koppen, C.W., "Optimization of the Flows in a Solar Heating System," Report WPS3-82.09.R335, September (1982).

58. Wuestling, M.D., "Investigation of Promising Control Alternatives for Solar Water Heating Systems," M.S. Thesis, University of Wisconsin-Madison, Solar Energy Laboratory, (1983).

59. Much, J.J., "Residential Water Heating, Fuel Consumption, Economics and Public Policy," RAND Report R 1498, (1974).

60. Zollner, A., "A Performance Prediction Methodology for Integral Collector Storage Solar Domestic Hot Water Systems," M.S.Thesis, University of Wisconsin-Madison, Solar Energy Laboratory, (1984).

61. Phillips, W.F., and Dave, R.N.,"Effects of Stratification on the Performance of Liquid-Based Solar Heating Systems," Solar energy, Vol. 29, No. 2, pp. 111-120, (1980).

62. Cole, R.L., and Bellinger, J.O., "National Thermal Stratification in Tanks," Argonne National Laboratory, 82-7, February (1982).

63. Copsey, A.B., "A Modification of the F-Chart Method for Solar Domestic Hot Water Systems with Stratified Storage," M.S. Thesis, University of Wisconsin-Madison, Solar Energy Laboratory, (1984).

64. Fanney, A.H., and Klein S.A., "Performance of Solar Domestic Hot Water Systems at the National Bureau of Standards-Measurements and Predictions," Trans. ASME, Journal of Solar Energy Engineering, Vol. 105, August (1983).

65. Duffie, J.A., and Mitchell, J.W., "F-Chart : Predictions and measurements," Trans. ASME, Journal of Solar Energy Engineering, Vol. 105, pp. 3-9, February (1983).

66. Klein, S.A., et al., TRNSYS User's Manual, University of Wisconsin-Madison, Engineering Experiment Station Report 38-12, April (1988).

67. Utzinger, D.M., "Analysis of Building Components Related to Direct Solar Heating of Buildings," M.S. Thesis, University of Wisconsin-Madison, Solar Energy Laboratory, (1979).

68 McAdams, W.C., "Heat Transmission," 3rd edition, New York, McGraw-Hill Book Company (1954).

69. Klein, S.A., "Calculation of Collector Loss Coefficients," Solar Energy, Vol. 17, pp. 79-80, (1975).

70. Trombe, F., et al., "Concrete Walls to Collect and Hold Heat," Solar Age, Vol. 2, No. 8, pp. 13-19, August (1977).

71. Randall, K.R., Mitchell, J.W., and El-Wakil, M.M., "Natural Convection Heat Transfer Characteristics of Flat Plate Enclosures," Journal.of Heat Transfer, Vol. 101, pp. 120-125, February (1979).

72. Mercer, et al., "Laminar Forced Convection in the Entrance Region Between Parallel Flat Plates," Journal of Heat Transfer, Vol. 89, pp. 251-257 (1967).

73. Erbs, D.G., Klein, S.A., and Beckman, W.A., "Estimation of Degree-Days and Ambient Temperature Bin Data from Monthly-Average Temperatures," ASHRAE Journal, June (1983).

, TRNSYS User's Manual, University o
ent Station Report 87-12, April (1988)

d Analysis of Building Components Related
S. Thesis, University of Wisconsin-M

Heat Transfer, 2nd edition, Ne

diance in Liquid Layers Containing Scatterers."

Chapter: Wells to Collect and Hold W